CELL BIOLOGY AND GENE EXPRESSION PROFILING DURING THE EARLY BIOTROPHIC INVASION BY THE RICE BLAST FUNGUS *MAGNAPORTHE ORYZAE*

by

PRASANNA KANKANALA

B.S., St. Ann's college for women, India, 1998
B.S., Kansas State University, 2002

AN ABSTRACT OF A DISSERTATION

submitted in partial fulfillment of the requirements for the degree

DOCTOR OF PHILOSOPHY

Department of Plant Pathology
College of Agriculture

KANSAS STATE UNIVERSITY
Manhattan, Kansas

2007

Abstract

Rice blast is a major fungal disease on rice, caused by the hemibiotrophic filamentous ascomycete fungus, *Magnaporthe oryzae*. This disease accounts for 157 million tons of grain loss annually. The fungus produces a specialized cell called appressorium to penetrate the host surface barrier and enter inside. It produces intracellular Invasive Hyphae (IH) that grow form cell to cell to colonize the host. The mechanisms of appressorium formation and host penetration have been studied in detail but the host colonization strategies remain largely unknown. We applied live-cell imaging to characterize spatial and temporal development of IH and plant responses inside successively-invaded rice cells. Early loading experiments with the endocytotic tracker, FM4-64, showed dynamic plant membranes around IH. These hyphae showed remarkable plasticity and recruited plant cell components. IH exhibited pseudohyphal growth and were sealed in plant membrane, termed the Extra-Invasive Hyphal Membrane (EIHM). The fungus spent up to 12 hours in the first cell, often tightly packing it with IH. IH that moved into neighboring cells were biotrophic, although they were initially thinner and grew more rapidly. IH in neighboring cells were wrapped in EIHM with distinct membrane caps at the hyphal tips. Time-lapse imaging showed IH scanning plant cell walls before crossing them, and transmission electron microscopy showed crossing occurring at pit fields. This and additional evidence strongly suggest that IH co-opt plasmodesmata for cell-to-cell movement. Our studies have revealed insights into a novel hemibiotrophic strategy employed by the blast fungus. Few genes have been previously characterized that impact the biotrophic IH. To understand the molecular basis of the biotrophic infection strategy we employed Laser Microdissection (LM) technology to isolate and purify the IH at this early growth stage. We compared the gene expression of these samples with axenically-grown mycelium using *M. oryzae* whole genome microarrays. We identified several hundreds of infection specific genes. We have shown that LM technology can be used to isolate homogenous cells from the infected rice tissues to study the underlying molecular mechanisms of signaling during disease formation. These studies will be very critical to understand the host-pathogen interactions to eventually develop durable management strategies.

CELL BIOLOGY AND GENE EXPRESSION PROFILING DURING THE EARLY BIOTROPHIC INVASION BY THE RICE BLAST FUNGUS *MAGNAPORTHE ORYZAE*

by

PRASANNA KANKANALA

B.S., St. Ann's college for women, India, 1998
B.S., Kansas State University, 2002

A DISSERTATION

submitted in partial fulfillment of the requirements for the degree

DOCTOR OF PHILOSOPHY

Department of Plant Pathology
College of Agriculture

KANSAS STATE UNIVERSITY
Manhattan, Kansas

2007

Approved by:

Major Professor
Dr. Barbara Valent

Abstract

Rice blast is a major fungal disease on rice, caused by the hemibiotrophic filamentous ascomycete fungus, *Magnaporthe oryzae*. This disease accounts for 157 million tons of grain loss annually. The fungus produces a specialized cell called appressorium to penetrate the host surface barrier and enter inside. It produces intracellular Invasive Hyphae (IH) that grow form cell to cell to colonize the host. The mechanisms of appressorium formation and host penetration have been studied in detail but the host colonization strategies remain largely unknown. We applied live-cell imaging to characterize spatial and temporal development of IH and plant responses inside successively-invaded rice cells. Early loading experiments with the endocytotic tracker, FM4-64, showed dynamic plant membranes around IH. These hyphae showed remarkable plasticity and recruited plant cell components. IH exhibited pseudohyphal growth and were sealed in plant membrane, termed the Extra-Invasive Hyphal Membrane (EIHM). The fungus spent up to 12 hours in the first cell, often tightly packing it with IH. IH that moved into neighboring cells were biotrophic, although they were initially thinner and grew more rapidly. IH in neighboring cells were wrapped in EIHM with distinct membrane caps at the hyphal tips. Time-lapse imaging showed IH scanning plant cell walls before crossing them, and transmission electron microscopy showed crossing occurring at pit fields. This and additional evidence strongly suggest that IH co-opt plasmodesmata for cell-to-cell movement. Our studies have revealed insights into a novel hemibiotrophic strategy employed by the blast fungus. Few genes have been previously characterized that impact the biotrophic IH. To understand the molecular basis of the biotrophic infection strategy we employed Laser Microdissection (LM) technology to isolate and purify the IH at this early growth stage. We compared the gene expression of these samples with axenically-grown mycelium using *M. oryzae* whole genome microarrays. We identified several hundreds of infection specific genes. We have shown that LM technology can be used to isolate homogenous cells from the infected rice tissues to study the underlying molecular mechanisms of signaling during disease formation. These studies will be very critical to understand the host-pathogen interactions to eventually develop durable management strategies.

Table of Contents

List of Figures

List of Tables

Acknowledgements

It is an honour to express my sincere gratitude to all the important people in my life on this happy occasion of completing the Ph.D. program at Kansas State University. I owe this success to Dr. Barbara Valent, my major advisor. She taught me to be humble, openminded and focused by her example. I am very greatful to her as these lessons apply are not only in my professional life but also in my personal life. She molded me into a scientist with her passion for science and wisdom. Her conviction that it is important to be happy in our personal lives in order to be successful in our professional lives gave everyone in the lab the space needed to grow both personally and professionally. I am indeed indebted to her for the faith she reposed in me and the guidance she gave me. I would like to express my sincere thanks to my advisory committee, Dr. Jan Leach, Dr. Beth Montelone and Dr. Xiaoyan Tang. Their critical evaluations helped me all along the program. I am greatful for their mentoring and support. A special vote of thanks goes to Dr. Wayne Geyer, my outside committee chair, who accepted the responsibility at a very short notice. Unfortunately, he met with an accident and hurt his knee few weeks before the defense. Inspite of the physical ailment he supported me to finish my defense on time.

The Valent lab group has taught me many valuable lessons on a daily basis. I am greatful to the whole group for making the learning process exciting and smooth. Melinda Dalby was very patient in teaching me good lab practices. I am very thankful for her mentoring and friendship. I would like to thank the department of Plant Pathology for the support during my course of the program. A special thanks also goes to Dr. Forrest Chumley for his encouragement all along.

Dr. Kirk Czymmek and Dr. Philline Wangemann spent a considerable amount of time to teach me microscopy. I express my gratitude to them for their guidance. I would like to thank the rice blast community who encouraged this work with enthusiasm. I would like to thank Alvin and Rosalee sarachek for their generosity to fund my scientific travel to the 4th International Rice Blast Conference held in Changsha, China in October 2007.

I take this opportunity to thank all my teachers since my childhood who helped me shape my personality. I sincerely thank all my friends whose loving support was always motivating. I thank Deepthi Dhara, Sangeetha Reddy, Vijay Pradeep, Anuradha, Lalitha Sudhakar, Sudhakar

Nalam, Nanda Gopal, Raghuram, Sairam Jabba, Nandi Nagaraj, and the Sai family for their love and encouragement. The young adults of the Sri Sathya Sai Organization were very motivating and I am very thankful for their support. I extend my heartfelt gratitude to Mr. Sai Krishna Mudulodu for his guidance and friendship. Mr. Nirat Bhatt, Dr.Bharat Patel and Mrs. Bharti Patel helped me during my undergraduate program at K-State in all aspects including financial support. They provided me a home away from home. I wouldn't have completed my B.S. degree without their helping hand. I express my sincere thanks to them. I would like to thank my brother, Mr. Sreenath Reddy, and sister-in-law, Mrs. Sumani Reddy for their encouragement all along.

I express my humble and heartfelt gratitude to my parents without whom I would have never accomplished this goal. They themselves not being educated beyond middle school and high school, wanted to make sure that their children would get the best education possible. They made several sacrifices to achieve this goal. To send us to the best possible private school in town they raised the required funds by selling the wedding ring. Thus began the saga of my academic career and their sacrifices over a couple decades made this day possible. I am greatful to God for giving me the precious gift of such loving parents.

Finally, last but not the least, I offer my loving gratitude to Bhagawan Sri Sathya Sai Baba, who is my guru and guide. His pure, unconditional love has been my support during all the ups and downs of my life.

Dedication

With love and humility, I dedicate this work to my Mother, Father and Bhagawan Sri Sathya Sai Baba.

CHAPTER 1 - Literature Review

Introduction

The Rice blast fungus, *Magnaporthe oryae*, is an important pathogen on rice. The blast disease is the most explosive and damaging disease on rice leading to heavy grain losses (Zeigler et al., 1994), thus posing a threat to global food security. Rice blast has invaded all the rice growing regions of the world. This pathosystem has been developed as a model system to study plant pathogen interactions with real world significance. The genomes of rice as well as the fungus are sequenced (Dean et al., 2005; Project, 2005), thus empowering us to study the molecular mechanisms of interactions at a rapid pace.

Rice:

Rice, *Oryza sativa*, is an important cereal crop feeding over 50% of world population. It has been cultivated over 9000 years by humans. Among the different *Oryza* species, *Oryza sativa* and *Oryza glaberrima* are cultivated. The former originated in the humid tropics of Asia and the latter in West Africa (http://www.fao.org/rice2004/en/aboutrice.htm). *O. sativa and O. glaberrima* belongs to the family Poaceae and subfamily Pooideae. These are diploid with 24 chromosomes (2n = 24). Rice is grown in a variety of environmental conditions including hot, humid, flooded, dry lands and saline, alkaline and acidic soils. Rice supplies 23% of the calories used for human consumption. Rice is staple food for 17 countries in Asia and Pacific, 9 countries in North and South America and 8 countries in Africa. (http://www.fao.org/rice2004/en/f-sheet/factsheet3.pdf). According to the FAO (Food and Agriculture Organization of United Nations) around 150 million hectares of land are used for rice cultivation producing around 600 million tons of paddy rice. The total milled rice amounts to, around 400 million tons. Developing countries account to 95% of this total production with China and India contributing to more than half of this output. The annual growth rate of rice production has decreased over the last couple of decades raising serious concerns about world food security. The International Food Policy

Research Institute has estimated that the rice production must increase 38% by 2030 to be able to meet the food demands of the world [(G. Moore, 1995), http://www.fao.org/rice2004/en/press.htm]. More than 50 % of the population suffering from chronic hunger (840 million) are dependent on rice for their nutritional and financial needs.

Rice has become a model cereal crop for plant research due to several reasons. It has a relatively small genome size (430 Mb) when compared with sorghum (750 Mb), maize (2500 Mb), barley (5000 Mb) or wheat (15,000Mb) (The Rice Chromosome 10 Sequencing, 2003). Rice shares collinearity with the other major cereal crops, maize sorghum, and wheat (G. Moore, 1995). The genome has mostly single copy DNA (McCouch, 1998). In addition, rice has a well established transformation system. These features have shaped rice into a model system to study evolutionary relationships as well as host pathogen interactions.

Some of the common diseases of rice are bacterial blight, bacterial leaf streak, blast, smut and seedling blight, amongst others (C.A.Hollier, 2007). Among the bacterial, fungal, viral and other parasitic attacks on rice, fungi are most devastating. The major fungal disease is the rice blast disease caused by *Magnaporthe oryzae* [previously *Magnaporthe grisea,* (Couch and Kohn, 2002)]. Rice blast causes 11% to 13% crop loss annually which amounts to loss of 157 million tones of rice (http://www.riceblast.org/StatementIntent.htm). Resistant cultivars and fungicides are used to control this disease. The relatively rapid appearance of virulent forms of fungus in the field limits utility of currently available resistance genes, and thus it is an ongoing race for coming up with new sources of resistance. Fungicide application is a limiting factor owing to the environmental conditions and the high costs of fungicides for poor farmers. The future demands developing environmental friendly fungicides and increased sources of host resistance for efficient disease management.

Blast Fungus: Magnaporthe oryzae

The fungus *Magnaporthe oryzae* (Couch and Kohn, 2002) is a hemi-biotrophic filamentous ascomycete fungus and includes the devastating rice blast pathogen (Kawasaki,

2004) as well as economically important pathogens on wheat (Urashima et al., 2004) and other cereals and grasses (Farman, 2002; Zellerhoff et al., 2006). Hemi-biotrophy is defined as the pathogen lifestyle that is initiated through biotrophic infection and later switching to necrotrophic growth. The biotrophic infection is defined as the pathogen lifestyle where it invades living plant cells and necrotrophic infection is defined as the lifestyle where the pathogen kills the host cells ahead of its infection and then invades them. The blast fungus was first described by Soong Ying-Shin in the 17th century (Ou, 1985). Today blast is found in all rice growing regions and has been identified in over 85 countries (Greer and Webster, 2001). Blast fungus has been long known to infect all the above ground parts of the plant. The most fatal form of the disease occurs when it infects the neck/panicle, which will fail to set seed (Ou, 1985). Recently this fungus was shown to infect roots like a classical root pathogen, forming hyphapodia in the laboratory (Sesma and Osbourn, 2004). However, the occurrence of *M. oryzae* as a root pathogen in nature has not yet been demonstrated. The sources of inoculum can be spores, crop residue or secondary hosts (Teng, 1994; Greer and Webster, 2001).

Rice Blast life cycle:

The blast fungus initiates disease cycle when the pyriformed, three-celled, asexual spore, the conidium, lands on a compatible host. The spore germinates to form a germ tube under optimal humidity. Usually the germ tube arises from the lower or upper cell, but rarely it can also arise from the middle cell. Free water is enough to trigger this germination process. Appressorium initiation begins when the tip of the germ tube forms a terminal hook. The nucleus in the cell which gives rise to the germ tube undergoes a mitotic division. One daughter nucleus stays in the conidial cell while other ends up in the developing appressorium. Appressorium formation requires completion of mitosis, nuclear migration, and death of the conidium in that order. The fungal nucleus migrates into the germ tubes and undergoes mitosis at 4-6 hours post inoculation (hpi). Around 8 hpi one of the daughter nuclei moves into the incipient appressorium and the other nucleus returns to the conidium. The three nuclei in the conidium disintegrate at 12-15 hpi and undergo cell death. The autophagic cell death is coupled with the completion of mitosis. Prevention of mitosis arrests spore death and impairs the penetration process.

Autophagic death of the spore is essential for the appressorial penetration (Veneault-Fourrey et al., 2006). Δ*MgAPT8*, which is impaired in autophagy, rendered the fungus nonpathogenic (Veneault-Fourrey et al., 2006). Appressorial formation is an elaborate process that begins when the tips of germ tubes swell and bend to become flat against leaf surface. This phenomenon is called 'hooking' which indicates recognition of the host (Howard and Valent, 1996). After initiation, the apex expands into a dome-shaped cell. During the initial stages of appressorium formation, the cell wall lying against the host cuticle is specialized and lacks chitin. This layer is much thinner compared to the other areas of the appressorial wall and single layered. As the appressorium develops the cell wall becomes thinner at this host interface. Appressorium formation is completed by deposition of one additional homogeneous melanin layer (~100nm thick) in between the plasma membrane and the wall. This layer extends all around the appressorium except the future penetration site which lacks a cell wall (previously region with thinner wall layer against the host cuticle). This wall less region, called the appressorium pore, is surrounded by an 'O ring', which seals the appressorium to the host surface tightly. Melanin is visible as dark grey color under bright field optics in a fully matured appressorium. The melanin is composed of polymerized dihydroxynaphthalene produced by the pentaketide biosynthetic pathway. Melanin formation is critical for generation of enormous turgor pressure required to mechanically breach the plant cell wall. The turgor pressure in these appressoria which is around 80 times atmospheric pressure, is the highest known turgor pressure reported in a living organism. Although the mechanical pressure plays a major role in host penetration, role for enzymatic activity cannot be completely excluded. Just before the host wall penetration, a cell wall layer, called the pore wall overlay, is deposited at the appressorial pore. It later becomes double layered. The appressorium also has numerous glycogen reserves, lipid bodies, and smooth membrane cisternae apart from the normal cell organelles. The penetration pegs develop through the wall overlay and have vesicles at the apex. The cytoplasm of a penetration peg initially contains abundant actin microfilaments and lacks recognizable cytoplasmic organelles, including ribosomes. This is called the zone of exclusion. This zone of exclusion was continuous with a similar appearing region in the apressorium. The diameter of the peg was 0.7 μm and the length upto 10 μm on cellophane membranes. The tip of the peg was distinctly different from the growing tips of germ tubes and somatic hyphae (Howard and Valent, 1996). Upon reaching the epidermal cell lumen, the penetration peg expands to form a narrow filamentous primary hypha.

The peg then becomes a conduit for moving the nucleus and cytoplasmic contents from the appressorium into the growing primary hypha. In the compatible interaction, primary hyphae differentiate into thicker, bulbous invasive hyphae (IH) that fill the first-invaded cell and then move into neighboring cells (Heath et al., 1990). The fungus colonizes the host to form eye-shaped sporulating lesions, completing its life cycle (Figure 1).

Several factors influencing the disease cycle:

Germination:

Spores of the blast fungus can germinate at wide temperature ranges (20-30^{o}C) in a thin film of water. There are reports that the germination rate increases at high temperature. After 10 hours (hrs) of infection the germination rate was shown to be 100% at 25^{o}C irrespective of the light conditions (Kyu, 1994). The germination process begins in 3 hrs on wet leaves. Dry leaves delay the process. Thus leaf wetness is important for the germination process (Teng, 1994).

Appressorium formation:

The optimal temperature for appressorium formation might vary depending on the physiological races of the fungus. Kim et al. (1994) have shown that the appressorium formation begins 4 to 6 hrs after germination and reaches 60 to 80% by 15 hpi at 25^{o}C $\pm$ 1^{o}C (Kyu, 1994). Spore germination and appressorium formation is more effective when plants are treated with fertilizers high in nitrogen or potassium (Teng, 1994).

Colonization, symptom development and sporulation:

Fungal penetration is less efficient in plants with high silica levels (Teng, 1994). Hyphal growth in seedlings exposed to higher temperatures (29/21^{o}C) was higher than in seedlings exposed to lower temperatures (23/15^{o}C). This also correlated to the delayed appearance of

symptoms on the plant. Although symptoms can appear at as low as 15^{o}C, the optimal temperature for symptom development is 26^{o}C (Kyu, 1994). In temperate ecosystems the fungus completes its lifecycle in one week and the secondary cycle takes 8-11days. Conidia can range from several hundreds to several hundred thousands in a lesion depending on the age, size, lesion type and the weather conditions (Kyu, 1994). Relative humidity of $\geq$89% favors sporulation (Greer and Webster, 2001).

Biology of the fungus *in planta*:

Several studies have been done to understand the preinfection process, which includes conidial germination, appressorium formation as well as host penetration mediated by penetration pegs (Bourett and Howard, 1990; Bourett and Howard, 1992; Howard and Valent, 1996; Talbot, 2003). Few studies concentrated on *in planta* fungal growth. Heath et al., (1990) studied the interactions between the blast fungus and several hosts (rice, goosegrass and weeping lovegrass). They reported a varied range of cytological features that marked susceptibility, partial resistance and complete resistance (Heath et al., 1990). They reported that the penetration peg which grew into primary hypha (20 μm) was usually thinner than the hyphae that developed later. The relatively thicker hyphae were called secondary hyphae. This study reported that this fungal dimorphism was critical for the disease. If the primary hyphae fail to expand into secondary hyphae, it corresponds to fungal death. The thin hyphae do not divide but try to grow straight into mesophyll cells in few instances. However, they cannot spread and form a lesion. Thus it was suggested that this change in hyphal morphology was critical and signifies a key fungal-plant interaction that decides the fate of the fungal and plant cell (Heath et al., 1990).

Ultrastructural analysis was done by Heath et al. (1990) to study the cell biology of the IH *in planta.* They studied the interactions of the blast fungal strain, 4091-5-8 (Valent and Chumley, 1991), in both compatible (weeping lovegrass) and less compatible (goosegrass) hosts. In the compatible reaction, around 25% of the appressoria failed to penetrate and in the less compatible reaction (goosegrass) around 80% failed to form appressoria (Heath et al., 1990). In

weeping lovegrass after 22 hpi, appressoria formed primary hyphae 5 μm long and 2 μm wide. These hyphae were reported to have plant plasma membrane surrounding them. The cytoplasms of invaded cells did not differ much from those of uninfected cells. At 46 hpi, the epidermal cell contained branched septate hyphae with dense cytoplasm. The plant cytoplasm was disorganized. The hyphae that invaded the underlying mesophyll cells had less dense cytoplasm compared to hyphae in the epidermal cells. The cell wall did not show any signs of damage at the point where the vegetative hyphae entered and exited the host cells. The plant cytoplasm appeared to be disorganizing in some cells while in others it appeared normal. The fungus was surrounded by the plant plasma membrane (Heath et al., 1992). In the less compatible reaction with goosegrass, out of the 13 appressoria observed, only three had penetrated. One of the three appressoria formed hyphae in the epidermal cell while the other two formed only thin primary hyphae after 46 hpi. The other appressoria failed to penetrate the cell wall. The plant cell wall had increased electron opaque granules in the middle lamella and in the extracellular material at the junctions between the epidermal and underlying mesophyll cells. In the two cases where the appressoria formed the primary hyphae, they were short (< 5 μm) and had very little fungal cytoplasm. The plant cytoplasm was disorganized in these cells. In one instance there was accumulation of electron-opaque granules adjacent to the penetration pegs in the plant cell wall (Heath et al., 1992).

In an independent study of a compatible reaction between the fungus and rice, the invading hyphae was in direct contact with the host cytoplasm in Transmission Electron Microscopy (TEM) indicating the plant plasma membrane was breached (Koga and Horino, 1984b; Koga, 1989). In some cases fibrillar structures were seen at the surface of the invading hyphae. This was in contrast to the observation by Heath et al (1992) discussed earlier. In the ultrastructural studies of panicle blast, the appressoria, penetration pegs, primary hyphae and invaded hyphae had similar biology to that observed in leaves and leaf sheaths. It was observed that the invaded hyphae that colonized the sclerenchyma cells penetrated through pit-pairs where the cell wall was usually thin. Often the hyphae were septate where they penetrated the cell wall. Occasionally woronin bodies were seen at these septa (Koga, 1994b). This study also suggested that the fungus might develop more rapidly in the young panicles compared to the leaves and leaf sheaths because it can spread faster through the thin walled pit-pairs. There was no blockage of

the vascular tissue observed in this study. The epidermal and parenchymal cells appeared alive for a little while after the fungal invasion suggesting that the fungus does not secrete toxins which kill the cells ahead of time.

During a major resistance (*R*) gene-mediated incompatible interaction, invaded plant cells lost membrane integrity and ability to plasmolyze, and showed cytoplasmic granulation and autofluorescence (Koga and Horino, 1984a; Peng and Shishiyama, 1989; Koga, 1994a; Koga et al., 2004). In the incompatible reaction, at 24 hpi, the plasma membrane of epidermal cells of rice leaf sheaths formed lomasome-like structures by invagination. By 48 hpi, the epidermal cells had swollen endoplasmic reticula, and degenerated mitochondria. At 72 hpi several vesicles of varying sizes were observed in the highly resistant variety (Koga, 1989). In the incompatible reaction on rice leaves, invaded hyphae were found in epidermal cells, necrotic paraenchymatous cells and stomatal chambers. The fungal hyphae were not healthy in these cells. They had swollen mitochondria and granulation. On the other hand in the compatible interactions, the hyphae were rich in lipid granules, cytoplasmic matrix and other cell organelles (Koga et al., 1982). Extensive cytological studies of blast disease have shown that the initial plant cell invasion is biotrophic, because invaded cells appeared healthy and retained ability to plasmolyze (Koga et al., 2004). Understanding the mechanisms by which blast IH invade living rice cells is critical for understanding disease mechanisms as well as mechanisms of *R* gene-mediated resistance that rice breeders manipulate in attempts to control this disease (Jia et al., 2004; Kawasaki, 2004). Knowledge of the nature of the interface between blast IH and rice is important for future studies to understand how pathogen effectors are secreted inside plant cells.

Fungi employ different strategies to derive nutrients from the host cells. Obligate biotrophs maintain the host cells alive either till they finish the life cycle and sporulate or till they establish themselves in the hosts. These pathogens can be intercellular (*Cladosporium fulvum*), subcuticular (*Venturia inaequalis*), inter- and intracellular (*Claviceps purpurea, Ustilgo maydis,* monokaryotic rust fungi), extracellular with haustoria within the epidermal cells (powdery mildews), or intercellular with haustoria within parenchyma cells (dikaryotic rust fungi and downy mildews). On the other hand necrotrophic fungi derive their nutrients from the host by killing the plant cells and then feeding on them as saprophytes (*Cochliobolus heterostrophus*).

Hemibiotrophic fungi have an initial biotrophic phase and later switch to necrotrophic growth (*Colletotrichum spp., Phytophthora infestens, Magnaporthe oryzae*) (Mendgen and Hahn, 2002).

During the biotrophic phase of fungal pathogenesis, the plant-biotroph interface is very critical and it is believed to serve the dual purpose of the interface for nutrient uptake as well as the interface for the fungus to secrete the effectors into the host cells. Effectors are pathogen molecules (virulance factors) that are delivered into the host to enhance microbial fitness (Jones and Dangl, 2006). Several studies have focused on understanding the host-pathogen interface. The haustoria of obligate biotrophs enter the cell lumen and remain intercellular. They are surrounded by extrahaustorial membrane. The extrahaustorial membranes are induced by the pathogen and the composition is different from the plant plasma membrane (O'Connell and Panstruga, 2006). In powdery mildews this membrane is thicker than the plasma membrane. In the rusts, *Uromyces appendiculatus* and *Puccinia coronata*, this membrane has less sterol content than the host plasma membranes (O'Connell and Panstruga, 2006). Live cell confocal imaging in Arabidopsis epidermal cells infected with *E.cichoracearum* showed that the extra haustorial membrane excluded eight different gfp-tagged plasmamembrane marker proteins (Koh et al., 2005).

Haustoria are surrounded by an interfacial extrahaustorial matrix between the fungal cell wall and the extrahaustorial membrane. This interfacial matrix is present around the intracellular filamentous hyphae and haustoria of most biotrophs and mycorrhizal fungi except *Magnaporthe oryzae* and few *Colletotrichum* species (Heath et al., 1992; Wharton et al., 2001; O'Connell et al., 2004).The composition of the matrix varies greatly among different fungi. In rust fungi components of primary plant cell wall, for example pectins, xyloglucan, arabinogalactan proteins, were found in the matrix while in powdery mildews none of the plant cell wall components were detected. Several fungal proteins like the glycoprotein elicitor in *Puccinia graminis tritici*, Uf-RTP1p of *Uromyces fabae*, CIH1p of *Colletotrichum lindamuthianum* were identified in the interfacial matrix. In the maize smut fungus, *Ustilago maydis*, α-glucosidase (*gas1*) played a role in the formation of the matrix (O'Connell and Panstruga, 2006). Mutants that failed to produce *gas1* were arrested in the host epidermis indicating that the proper

glycosylation of fungal cell wall or the matrix proteins was important for the proper interface development in maize smut.

For dikaryotic rusts and powdery mildews, annular "neckband" structures attach the plant plasma membrane to the haustorial neck, and produce a specialized matrix compartment that is separate from the plant apoplast (O'Connell and Panstruga, 2006). In contrast to biotrophic haustorial fungi, hemibiotrophic *Colletotrichum* species produce biotrophic IH that either lack an interfacial matix (Latunde-Dada, 2001; Wharton et al., 2001; O'Connell et al., 2004) or contain a simplified matrix without a neckband (O'Connell et al., 1985; O'Connell and Panstruga, 2006).

In contrast to biotrophic hyphae, necrotrophic hyphae are associated with death of plant cells ahead of the fungal growth front, and they lack a specialized interface in the plant cell. This is best illustrated for the hemibiotrophic pathogens in *Colletotrichum* spp., which undergo 2-stage infection cycles that begin with intracellular biotrophic hyphae and then switch to necrotrophic hyphae (Latunde-Dada, 2001; Wharton et al., 2001; O'Connell et al., 2004). *Colletotrichum* spp. initially undergo cell invasion by biotrophic intracellular infection vesicles and enlarged biotrophic primary hyphae, both of which invaginate the host plasma membrane. Depending on the *Colletotrichum* spp. investigated, biotrophic invasion involves one or a few plant cells. Then biotrophic primary hyphae differentiate into narrow, filamentous secondary hyphae that lack invaginated host plasma membrane and kill host cells before invasion. Necrotrophic hyphae are typically thinner and grow in the host cell walls or in the lumens of dead host cells. Unlike biotrophic hyphae, necrotrophic hyphae do not constrict when they cross the host cell wall. Additionally, host walls show signs of enzymatic digestion in the presence of necrotrophic hyphae. Mutational analyses support the occurrence of distinct biotrophic and necrotrophic phases for *Colletotrichum* spp., because pathogen genes have been identified that have a role in switching from biotrophy to necrotrophy (Latunde-Dada, 2001; Wharton et al., 2001; O'Connell et al., 2004). In contrast, distinct biotrophic and necrotrophic phases have not been documented for the blast fungus, and despite extensive screening for nonpathogenic mutants in *M. oryzae*, no genes that block the predicted switch have been discovered (Talbot, 2003).

There is growing documentation of interactions occurring at the biotroph-plant cytoplasm interface. For example, TEM with high-pressure frozen and freeze-substituted (HPF/FS) samples provided excellent detail in the interfacial region for downy mildew *Hyaloperonospora parasitica* on leaves of *Arabidopsis thaliana* (Mims et al., 2004). The extrahaustorial matrix and extrahaustorial membrane (EHM) were highly irregular in outline, and numerous vesicles were either near by or incorporated in the EHM. Another TEM study provided evidence that plant endocytosis occurred at the biotroph-plant interface based on immunolocalization of clathrin on tubular coated pits on the EHM surrounding haustoria of the monokaryotic cowpea rust, *Uromyces vignae* (Stark-Urnau and Mendgen, 1995). Koh et al. (2005) used live-cell confocal microscopy to study the powdery mildew fungus *Erysiphe cichoracearum* in epidermal cells of *Arabidopsis thaliana*. They used Arabidopsis plants engineered to tag various organelles with green fluorescent protein (GFP), and reported very active host plasma membrane dynamics, both near and distal to the penetration site, in infected epidermal cells. In an interesting example of a pathogen preparing its host cell before invasion, Koh et al. (2005) reported that the epidermal plasma membrane showed pouch-like invaginations underneath the developing appressoria before penetration occurred. Haustoria subsequently grew into these membrane pouches. A dramatic case of a fungus controlling plant cell processes before entering the plant cell has been reported for a symbiotic arbuscular mycorrhizal fungus on *Medicago truncatula* (Genre et al., 2005). To reach the root cortex and form intracellular arbuscles (analogous to haustoria), the fungus produces an appressorium that controls host nuclear movement, cytoskeletal elements and endoplasmic reticulum to build a prepenetration apparatus inside root epidermal cells. This elaborate structure appears to be involved in building an apoplastic compartment that the fungus uses to cross the epidermal cell. These examples illustrate the way that biotrophic hyphae co-opt normal plant cell processes, and thus suggest potential functions for biotrophic effectors that are secreted inside the plant cell (O'Connell and Panstruga, 2006).

Fungal strategies to colonize the host:

Mechanisms used by biotrophic fungi, including the blast fungus, for moving from one cell to the next are not understood, although there are reports that this process involves localized

cell wall degradation and mechanical pressure (Heath et al., 1992; Xu and Mendgen, 1997; Martinez et al., 1999). Among plant pathogens known to move from one living cell to another, only viruses have been extensively studied. Viruses manipulate plasmodesmata for their cell-to-cell movement (Lazarowitz and Beachy, 1999; Zambryski and Crawford, 2000).

Plasmodesmata are the plasma membrane-lined channels that cross plant cell walls and connect the cytoplasms of plant cells into a symplastic network. Plasmodesmata are delimited by the plasma membrane on the outside and enclose the central desmotubule made up of the appressed endoplasmic reticulum. Cytoplasmic sleeve is the space between the desmotubule and the plasma membrane and is the major conduit for transport of molecules and proteins between cells. Interconnections can be seen between both the membranes by means of globular particles and elongated spokes. Actin filaments have also been reported along the length of the plasmodesmata. The ends of the plasmodesmata, also called the necks, are usually constricted. Transport through the plasmodesmata can be either the non-targeted or targeted type. Non-targeted movement is usually passive by diffusion. The movement of particles depends on the aperture size, biochemical properties of the molecules and the protein availability itself. Growth hormones, minerals, amino acids and sugars are some of the cargo that is transported by diffusion. Targeted transport is an active process that has been extensively studied with viral movement proteins. The mRNA of maize *knotted1* gene was also reported to traffic through plasmodesmata. Targeted proteins traffic between cells when other proteins of the same size fail to, apparently by increasing the 'size exclusion limit' of the plasmodesmata (Zambryski and Crawford, 2000).

Viruses produce movement proteins (MP) that increase the size exclusion limit of plasmodesmata without noticeable structural changes (Zambryski and Crawford, 2000). MPs act as molecular chaperones and assist single stranded viral nucleic acids to move through plasmodesmata. For some viruses, movement of intact virions or subviral particles through plasmodesmata is associated with the production of tubules ~30 to 50 nm in diameter that extend out from the plant cell wall (Ward et al., 1997; Lazarowitz and Beachy, 1999). Mechanisms that biotrophic intracellular hyphae use to move from cell to cell must take into account the much larger diameter of these hyphae relative to virus particles that spread through plasmodesmata.

Molecular basis of the biology:

Understanding the molecular basis of the biology of the biotrophic hyphae is an important step towards disease control management. Few genes that impact biotrophic growth of the blast fungus have been identified, because extensive mutational analyses have mainly identified genes with a role in appressorium structure and function (Talbot, 2003). The exciting breakthrough in the field of molecular plant microbe interactions has been the identification of effector proteins. Effector proteins are secreted by the pathogen into the host cell to manipulate the plant regulatory pathways (van't Slot and W.Knogge, 2002). In cases where the plant has a resistance gene that recognizes the effector, the recognition triggers defense responses and arrests the pathogen growth. This is called the gene-for-gene resistance model. The rice blast system follows this where the interaction of the host resistance (*R*) gene with the corresponding avirulence (*AVR*) gene confers resistance to the host. This interaction is very specific to a given *R* gene. The absence of the corresponding *R* gene or the *AVR* gene renders the fungus virulent (Jia et al., 2000). As in bacterial pathosystems (Desveaux et al., 2006), blast effector genes that are likely to be secreted inside living host cells have been identified by their avirulence activity in conferring recognition and resistance mediated by major rice *R* genes (Kawasaki, 2004). A few *R* genes and *AVR* genes have been cloned (Sweigard et al., 1995; Farman et al., 2002; Böhnert et al., 2004) and, in one case, the rice *R* gene *Pi-ta* and its corresponding *AVR-Pita* gene from the fungus were cloned and their interaction characterized (Bryan et al., 2000; Orbach et al., 2000). AVR-Pita protein appears to interact directly with Pi-ta and transient expression of this avirulence/effector protein in the cytoplasm of rice cells with Pi-ta triggers hypersensitive resistance (Jia et al., 2000). This suggests that the fungus delivers AVR-Pita protein into the cytoplasm of the rice cell. Although AVR-Pita appears to function as a protease inside rice cells, its role in the invasion process is not yet understood. To understand how AVR-Pita and other blast effectors function in promoting rice blast disease, it is first necessary to understand how the fungus co-opts normal plant cell processes for successful colonization of host tissue.

Identifying the fungal effectors has been a challenge since it has been difficult to enrich the biomass of the biotrophic hyphae in the conventional infection methods like spray inoculations and drop inoculations. Several studies have focused on identifying infection-specific genes in the rice blast system using cDNA libraries and more recently whole genome microarray experiments. In the search for infection specific genes in *M. oryzae*, Takano et al. (2003) developed two cDNA libraries from mycelia grown in liquid cultures and conidia germinated for 8 hrs on an appressorium-inducing surface. Microarrays were constructed using 3500 cDNA clones. RNA from mycelia, conidia and appressoria from conidia germinated on inductive surfaces were used to study the gene expression pattern. This study identified 48 appressorium-specific genes.

Efficient nitrogen metabolism in fungi is considered to allow the fungus to adapt in different environmental condition including infection of the host plants. Donofrio et al. (2006) did a genome-wide analysis of gene expression of *M. oryzae* under nitrogen starvation conditions. They identified 520 genes that were differentially up-regulated under nitrogen deprived conditions. However it is debated if the nitrogen starvation condition mimics the *in planta* environment. Jantasuriyarat et al. (2005) used an EST (Expressed Sequence Tags) sequencing approach to identify the molecular basis for defense responses. They studied resistant, partially resistant and susceptible interactions at 6 hpi and 24 hpi. The two time points represent the early stages of infection when the germ tubes were formed and when the appressorial penetration occured on the leaves at the early infection stages when no macroscopic symptoms were visible. They identified 68,920 EST sequences, but most of them represented rice gene expression. Only 4 sequences showed similarity to blast fungus. Kim et al. (2001) did EST analysis of infected rice leaves at 84 and 120 hpi when the blast symptoms were visible. They identified 24.6% fungal sequences with matches in the NCBI database. In a different study Rauyaree et al. (2001) identified 359 novel EST's by analyzing the cDNA libraries of rice leaves infected with *M. oryzae* at 48 hpi.

In all these studies the majority of the genes identified were rice genes. The fungal genes identified were mostly either appressorial specific or *in planta* genes at later stages of infection. In order to study the genes involved in establishing the biotrophic phase, the leaf sheath assays

were used. Mosquera et al. (2007) optimized this assay to enrich the fungus up to 20% at 36 hpi enabling gene expression analysis using whole genome microarray hybridizations. This study identified around 1700 infection-specific genes which included the two known *AVR* up-regulated genes, *PWL2* and *AVR-Pita*. The fungus fails to infect at 5 to 20% of the infection sites even in a susceptible interaction. Thus using whole plant tissues in the leaf sheath assay still has heterogenous plant and fungal samples. An interesting phenomenon of the fungus is to manipulate and redeploy the plant cellular components to serve its needs (O'Connell and Panstruga, 2006). In order to study the changes in the plant cell gene expression in both cells that are infected as well as those surrounding the infected cells, we need an efficient way to isolate individual cell types. In order to purify the synchronous hyphal types and map the temporal and spatial gene expression patterns, we optimized the Laser Microdissection process.

Laser microdissections:

Laser Microdissection (LM) technology has given the paramount ability to study the basis of biology / biological processes at the cellular and the organelle level (Nelson et al., 2006). This technology allows cutting and manipulating single cells / cellular components with a laser coupled with a microscope. Although this technology was around for several years in the field of animal research, it is relatively new in the arena of plant research. Plants have tough cell walls posing a challenge for cutting by the laser. Recently improved laser technology and tissue processing protocols have extended this technology to plant tissues (Nelson et al., 2006). The advantage of this technology over other types of tissue harvesting methods like fluorescence activated cell sorting, hand microdissections, cell fractionation and the like is that LM allows one to harvest any type of tissue from any plant species that can be seen with light microscopy. The current LM technology can be classified into two major types based on how the cells are harvested. They are Laser cutting and Laser Capture Microdissection (LCM) (Nelson et al., 2006).

LCM technology, also called the “melt-stick-pull off” technology, was developed at NIH (Nelson et al., 2006). In this method, an infrared laser is used to excite a proprietary dye in the

ethyl-vinyl-acetate (EVA) film that sits above the cells of interest. When excited, the film melts and sticks to the target cells. The cells are harvested when the film is peeled away. This technology is licensed to the Arcturus Biosciences.

Laser cutting technology involves separating the target cells from the tissue section with the UV laser and harvesting the cells. Several methods have been developed and patented for collecting these cells. These include Laser Pressure Catapulting (LPC), Leica Microsystems laser Dissection (LMD), Molecular Machines and Industries (MMI). LMD technology was developed by Leica and the sections are in an inverted position. After cutting, the cells are ejected downwards into a collection tube beneath the sample. MMI technology uses a membrane frame to cover the glass slide thus protecting the samples from any kind of contamination. The isolation caps rest on these membranes to help collect the cells. LPC is a P.A.L.M. (Position Ablation Laser Microdissection) Microlaser System technology, which is a Carl Zeiss company. This technology uses the Laser Microdissecction and Pressure Catapulting (LMPC,) combining Laser Microbeam Microdissection (LMM) and LPC. This technology employs a 337 nm nitrogen laser to cut out the cells. After cutting the laser is defocused and the cut cells are pressure catapulted into a cap held above the sample. The cells in the cap are later spun down into the tubes for further processing.

The amount of target sample required for analysis depends on the type of cells/tissues and the downstream application. Whole transcriptome profiling using microarray experiments requires several micrograms of RNA, which demands more material compared with RT-PCRs experiments or protein and metabolite analyses. Typically plant and animal cells contain 10 to 100 pg of total RNA per cell. Thus microarray analysis requires linear amplification of RNA. There are a couple of RNA linear amplification kits available in the market that enable us to amplify RNA from picograms to micrograms thus facilitating microarray studies.

The major challenge for LM is the sample processing protocol that yields good quality material for downstream analysis (DNA/RNA/Proteins). There are two major categories of fixatives, namely coagulative fixatives and cross-linking fixatives (Nakazono et al., 2003). The coagulating fixatives such as alcohol and acetone denature proteins and form a network of the

cell contents. The cross-linking fixatives like aldehydes chemically cross link cellular proteins and lipids and maintain good histological preservation compared to the coagulating fixatives. The quantity and quality of RNA produced by these two groups of fixatives in plants were compared (Nakazono et al., 2003). Maize coleoptile samples were fixed with 37 to 40 % formaldehyde/glacial acetic acid/95% ethyl alcohol (10%:5%:5%: v/v) (FAA), a cross-linking fixative, and with 75% ethanol / 25% acetic acid (EA), a coagulating fixative. The samples fixed with FAA had better morphological preservation compared to the coagulating fixative. RNA samples extracted from EA-fixed samples were of higher quality than the RNA samples from FAA-fixed samples and the same result was obtained in the RT-PCR experiments in which the FAA-fixed samples had degraded RNA compared to the EA-fixed samples. Another fixative that is used commonly in LM protocols is 100% Acetone. Several groups have used this fixative and successfully extracted RNA for constructing cDNA libraries (Asano et al., 2002) as well as transcriptome analysis (Tang et al., 2006).

Cryosections as well as paraffin-embedded sections can be used for LM. RNA yields from cryosections are of higher quality and quantity when compared with RNA yields from paraffin embedded samples (personal communication with Carl Zeiss technical experts). However, Ramsay et al. (2004) reported that the transcript analyses from giant cells of tomato roots were better using paraffin-embedding sections compared to cryo-preservation. A paraffin embedding protocol has been used to process plant tissues for LM to extract RNA for RT-PCRs (Kerk et al., 2003; Ramsay et al., 2004; Murata and Luca, 2005; Sanders et al., 2005; Jiang et al., 2006; Nelson et al., 2006). For downstream analyses that demand more starting material (microarray hybridizations and cDNA library construction) larger quantities of starting material are needed. Cryopreservation is preferred for these experiments (Asano et al., 2002; Nakazono et al., 2003; Tang et al., 2006). In one study, RNA was extracted from 150 rice phloem cells which were cryoembedded by Asano *et al*. Two rounds of T7 based linear amplification was done to amplify the RNA. Double stranded cDNA was generated and amplified by PCR yielding 1µg of cDNA. These cDNA fragments were sequenced and analysed for transcription profiling of the phloem cells. In another study, RNA extracted from >10,000 cryofixed maize coleoptile cells was amplified and used successfully for microarray hybridization and transcript analysis (Nakazono et al., 2003). Approximately 40 ng RNA was obtained from 10,000 cells. T7 based

linear amplification was done twice to amplify the RNA >60,000 fold. This enabled gene expression profiling by microarray hybridizations.

More recently this technology was extended to study plant pathogen interactions. A microwave based paraffin embedding protocol was recently developed and used to study *in planta* gene expression profiling of *Colletotrichum graminicola* infecting maize stalks (Tang et al., 2006). Ice cold 100% acetone was used for fixing the samples followed by paraffin embedding. The fixation and the paraffin embedding were accelerated by heating in a microwave. Cells corresponding to approximately 1 mm^2 (~ 800 cells) were catapulted. RNA was extracted and subjected to two rounds of linear amplification using a kit from Epicentre Biotechnologies Inc. The amplification yielded 5 to 10 µg aRNA (amplified RNA) from ~0.5 ng starting RNA. Global gene expression profiling was done using microarrays. They found 437 fungal genes that were significantly upregulated and 370 genes that were significantly downregulated during infection when compared with in-vitro germinated conidia.

Transcription profiling of the syncytia induced by the soybean cyst nematode *Heterodera glycines* in soybean roots was studied using laser microdissections (Ithal et al., 2007). Samples were fixed in 3:1 ethanol/glacial acetic acid and paraffin embedded. A minimum of 100 syncytia were used for each biological replicate. RNA was extracted followed by two rounds of T7 based linear amplification yielding 20 µg cRNA. Gene expression profiling with microarrays suggested local downregulation of jasmonic acid biosynthesis, and local suppression in plant defense mechanisms. The results identified components of signal transduction pathways governing the growing syncytia and its functions. Thus laser microdissections have been used successfully not only to isolate and purify specific cell types for gene expression profiling but also to study plant-microbe interactions.

The blast fungus is defined as a hemibiotroph, but the switch between the biotrophic and necrotrophic stages of the life cycle was not defined earlier. We set out to understand the cell biology and gene expression profiling of the blast fungus *in planta* during the early biotrophic stage of infection which is critical for disease establishment. We defined the type of hemibiotrophy that occurs in the rice leaf sheath epidermal cells and studied the process of

fungal cell-to-cell movement. We resolved the previous controversy about the presence/absence of an intact plant membrane around the fungus growing *in planta*. To understand the molecular basis of the biology we isolated and purified the fungus from infected tissues using LM technology. We did gene expression profiling using microarray analyses. Our results promise the potential of applying LM technology to study plant-microbe interactions.

References:

Asano, T., Masumura, T., Kusano, H., Kikuchi, S., Kurita, A., Shimada, H., and Kadowaki, K.-i. (2002). Construction of a specialized cDNA library from plant cells isolated by laser capture microdissection: toward comprehensive analysis of the genes expressed in the rice phloem. The Plant Journal **32,** 401-408.

Böhnert, H.U., Fudal, I., Dioh, W., Tharreau, D., Notteghem, J.-L., and Lebrun, M.-H. (2004). A putative polyketide synthase/peptide synthetase from *Magnaporthe grisea* signals pathogen attack to resistant rice. Plant Cell **16,** 2499-2513.

Bourett, T.M., and Howard, R.J. (1990). *In vitro* development of penetration structures in the rice blast fungus *Magnaporthe grisea*. Canadian Journal of Botany **68,** 329-342.

Bourett, T.M., and Howard, R.J. (1992). Actin in penetration pegs of the fungal rice blast pathogen, *Magnaporthe grisea*. Protoplasma **168,** 20-26.

C.A.Hollier, D.E.G., M.C.Rush, R.K.Webster,collators. (2007). Common names of plant diseases. In APSnet Database.

Couch, B.C., and Kohn, L.M. (2002). A multilocus gene genealogy concordant with host preference indicates segregation of a new species, *Magnaporthe oryzae*, from *M. grisea*. Mycologia **94,** 683-693.

Dean, R.A., Talbot, N.J., Ebbole, D.J., Farman, M.L., Mitchell, T.K., Orbach, M.J., Thon, M., Kulkarni, R., Xu, J.-R., Pan, H., Read, N.D., Lee, Y.-H., Carbone, I., Brown, D., Oh, Y.Y., Donofrio, N., Jeong, J.S., Soanes, D.M., Djonovic, S., Kolomiets, E., Renmeyer, C., Li, W., Harding, M., Kim, S., Lebrun, M.H., Bohnert, H., Coughlan, S., Butler, J., Calvo, S., Li-Jun, M., Nicol, R., Purcell, S., Nusbaum, C., Galagan,

J.E., and Birren, B.W. (2005). The genome sequence of the rice blast fungus *Magnaporthe grisea*. Nature **434,** 980-986.

Desveaux, D., Singer, A.U., and Dangl, J.L. (2006). Type III effector proteins: doppelgangers of bacterial virulence. Current Opinion in Plant Biology **9,** 376-382.

Donofrio, N.M., Oh, Y., Lundy, R., Pan, H., Brown, D.E., Jeong, J.S., Coughlan, S., Mitchell, T.K., and Dean, R.A. (2006). Global gene expression during nitrogen starvation in the rice blast fungus, *Magnaporthe grisea*. Fungal Genetics and Biology **43,** 605-617.

Farman, M.L. (2002). *Pyricularia grisea* isolates causing gray leaf spot on perennial ryegrass (*Lolium perenne*) in the United States: Relationship to *P. grisea* isolates from other host plants. Phytopathology **92,** 245-254.

Farman, M.L., Eto, Y., Nakao, T., Tosa, Y., Nakayashiki, H., Mayama, S., and Leong, S.A. (2002). Analysis of the structure of the *AVR-CO39* avirulence locus in virulent rice-Infecting isolates of *Magnaporthe grisea*. Molecular Plant Microbe Interactions **15,** 6-16.

G. Moore, K.M.D., Z.Wang and M.D.Gale. (1995). Cereal genome evolution: Grasses, line up and form a circle. Current Biology **5,** 737-739.

Genre, A., Chabaud, M., Timmers, T., Bonfante, P., and Barker, D.G. (2005). Arbuscular mycorrhizal fungi elicit a novel intracellular apparatus in M*edicago truncatula* root epidermal cells before infection. The Plant Cell **17,** 3489-3499.

Greer, C.A., and Webster, R.K. (2001). Occurrence, distribution, epidemiology, cultivar reaction, and management of rice blast disease in California. Plant Disease **85,** 1096-1102.

Heath, M.C., Valent, B., Howard, R.J., and Chumley, F.G. (1990). Interactions of two strains of *Magnaporthe grisea* with rice, goosegrass, and weeping lovegrass. Canadian Journal of Botany **68,** 1627-1637.

Heath, M.C., Howard, R.J., Valent, B., and Chumley, F.G. (1992). Ultrastructural interactions of one strain of *Magnaporthe grisea* with goosegrass and weeping lovegrass. Canadian Journal of Botany **70,** 779-787.

Howard, R.J., and Valent, B. (1996). Breaking and entering: Host penetration by the fungal rice blast pathogen *Magnaporthe grisea*. Annual Review of Microbiology **50,** 491-512.

Ithal, N., Recknor, J., Nettleton, D., Maier, T., Baum, T.J., and Mitchum, M.G. (2007). Developmental transcript profiling of cyst nematode feeding cells in Soybean roots. Molecular Plant Microbe Interactions **20,** 510-525.

Jantasuriyarat, C., Gowda, M., Haller, K., Hatfield, J., Lu, G., Stahlberg, E., Zhou, B., Li, H., Kim, H., Yu, Y., Dean, R.A., Wing, R.A., Soderlund, C., and Wang, G.-L. (2005). Large-scale identification of expressed sequence tags involved in rice and rice blast fungus interaction. Plant Physiol. **138,** 105-115.

Jia, Y., McAdams, S.A., Bryan, G.T., Hershey, H.P., and Valent, B. (2000). Direct interaction of resistance gene and avirulence gene products confers rice blast resistance. The EMBO Journal **19,** 4004-4014.

Jia, Y., Wang, Z., Fjellstrom, R.G., Moldenhauer, K.A.K., Azam, M.A., Correll, J., Lee, F.N., Xia, Y., and Rutger, J.N. (2004). Rice *Pi-ta* gene confers resistance to the major pathotypes of the rice blast fungus in the United States Phytopathology **94,** 296-301.

Jiang, K., Zhang, S., Lee, S., George, T., Kim, K., Huang, H., Chilcott, C., Zhu, T., and Feldman, J.L. (2006). Transcription profile analyses identify genes and pathways central to root cap functions in Maize. Plant Molecular Biology **60**.

Jones, J.D.G., and Dangl, J.L. (2006). The plant immune system. Nature **444,** 323-329.

Kawasaki, S. (2004). Proceedings of the 3rd International Rice Blast Conference:
Rice Blast: Interaction with rice and control. (Dordrecht, The Netherlands: Kluwer Academic Publishers).

Kerk, N.M., Ceserani, T., Tausta, S.L., Sussex, I.M., and Nelson, T.M. (2003). Laser capture microdissection of cells from plant tissues. Plant Physiology **132,** 27-35.

Kim, S., Il-Pyung, A., and Lee, Y.-H. (2001). Analysis of genes expressed during Rice-*Magnaporthe grisea* interactions. Molecular Plant-Microbe Interactions **14,** 1340-1346.

Koga, H. (1989). Histopathology of resistant and susceptible rice plants inoculated with *Pyricularia oryzae* Cavara. JARQ **23,** 8-15.

Koga, H. (1994a). Hypersensitive death, autofluorescence, and ultrastrctural changes in cells of leaf sheaths of susceptible and resistant near-isogenic lines of rice (*Pi-z*^{t}) in relation to penetration and growth of *Pyricularia oryzae*. Canadian Journal of Botany **72,** 1463-1477.

Koga, H. (1994b). Electron microscopy of early infection processes in the panicle neck of rice inoculated with *Pyricularia oryzae*. Ann. Phytopathol. Soc. Japan **60,** 89-98.

Koga, H., and Horino, O. (1984a). Electron microscopical observation of rice leaves infected with *Pyricularia oryzae* Cav. in compatible and incompatible combinations. III. Resistance expression and loss of capability for plasmolysis in inner epidermal cells of leaf-sheath. Annals of the Phytopathological Society of Japan **50,** 353-360.

Koga, H., and Horino, O. (1984b). Electron microscopical observation of rice leaves infected with *Pyricularia oryzae* Cav. in compatible and incompatible combinations. IV. The interface between invading hypae and host cytoplasm in epidermal cells of leaf-sheath. Annals of the Phytopathological Society of Japan **50,** 375-378.

Koga, H., Kobayashi, T., and Horino, O. (1982). Electron microscopical observation of rice leaves infected with Pyricularia oryzae Cav. in compatible and incompatible combinations I. Fine structures of invaded hyphae in host cells. Ann. Phytopathol. Soc. Japan **48,** 281-289.

Koga, H., Dohi, K., Nakayachi, O., and Mori, M. (2004). A novel inoculation method of *Magnaporthe grisea* for cytological observation of the infection process using intact leaf sheaths of rice plants. Physiological and Molecular Plant Pathology **64,** 67-72.

Koh, S., Andre, A., Edwards, H., Ehrhardt, D., and Somerville, S. (2005). *Arabidopsis thaliana* subcellular responses to compatible *Erysiphe cichoracearum* infections. The Plant Journal **44,** 516-529.

Kyu, K.C. (1994). Blast management in high input, high yield potential, temperate rice ecosystems. (Wallingford, Oxon, UK: CAB International and IRRI).

Latunde-Dada, A.O. (2001). *Colletotrichum*: tales of forcible entry, stealth, transient confinement and breakout. Molecular Plant Pathology **2,** 187-198.

Lazarowitz, S.G., and Beachy, R.N. (1999). Viral movement proteins as probes for intracellular and intercellular trafficking in plants. The Plant Cell **11,** 535-548.

Martinez, C., Roux, C., and Dargent, R. (1999). Biotrophic development of *Sporisorium reilianum f. sp. zeae* in vegetative shoot apex of maize. Phytopathology **89,** 247-253.

McCouch, S. (1998). Toward a plant genomics initiative: Thoughts on the value of cross-species and cross-genera comparisons in the grasses **95,** 1983-1985.

Mendgen, K., and Hahn, M. (2002). Plant infection and the establishment of fungal biotrophy. Trends in Plant Science.

Mims, C.W., Richardson, E.A., Holt III, B.F., and Dangl, J.L. (2004). Ultrastructure of the host-pathogen interface in *Arabidopsis thaliana* leaves infected by the downy mildew *Hyaloperonospora parasitica*. Canadian Journal of Botany **82,** 1001-1008.

Mosquera, G., Coughlan, S., and Valent, B. (2007). Analysis of the interaction transcriptome of biotrophic invasion by the rice blast fungus, *Magnaporthe oryzae*. Submitted.

Murata, J., and Luca, V.D. (2005). Localization of tabersonine 16-hydroxylase and 16-OH tabersonine-16-O-methyltransferase to leaf epidermal cells defines them as a major site of precursor biosynthesis in the vindoline pathway in *Catharanthus roseus*. Plant Journal **44,** 581-594.

Nakazono, M., Qiu, F., Borsuk, L.A., and Schnable, P.S. (2003). Laser-Capture Microdissection, a tool for the global analysis of gene expression in specific plant cell types: Identification of genes expressed differentially in epidermal cells or vascular tissues of Maize. Plant Cell **15,** 583-596.

Nelson, T., Tausta, S.L., Gandotra, N., and Liu, T. (2006). Laser Microdissection of plant tissue: What you see is what you get. Annual Review of Plant Biology **57,** 181-201.

O'Connell, R.J., and Panstruga, R. (2006). Tête à tête inside a plant cell: establishing compatibility between plants and biotrophic fungi and oomycetes. New Phytologist **171,** 699-718.

O'Connell, R.J., Bailey, J.A., and Richmond, D.V. (1985). Cytology and physiology of infection of *Phaseolus vulgaris* by *Colletotrichum lindemethianum*. Physiological Plant Pathology **27,** 75-98.

O'Connell, R.J., Herbert, C., Sreenivasaprasad, S., Khatib, M., Esquerré-Tugayé, M.-T., and Dumas, B. (2004). A novel *Arabidopsis-Colletotrichum* pathosystem for the molecular dissection of plant-fungal interactions. Molecular Plant Microbe Interactions **17,** 272-282.

Ou, S.H. (1985). Rice diseases. (Kew, Surrey: Commonwealth mycological institute).

Peng, Y.-L., and Shishiyama, J. (1989). Timing of a cellular reaction in rice cultivars associated with differing degrees of resistance to *Pyricularia oryzae*. Canadian Journal of Botany **67,** 2704-2710.

Project, T.I.R.G.S. (2005). The map-based sequence of the rice genome. Nature **436,** 793-800.

Ramsay, K., Wang, Z., and Jones, M.G.K. (2004). Using laser capture microdissection to study gene expression in early stages of giant cells induced by root-knot nematodes. Molecular Plant Pathology **5,** 587-592.

Rauyaree, P., Choi, W., Fang, E., Blackmon, B., and Dean, R.A. (2001). Genes expressed during early stages of rice infection with the rice blast fungus *Magnaporthe grisea*. Molecular Plant Pathology **2,** 347-354.

Sanders, M.P., Bui, Q.A., Le, H.B., and Goldberg, B.R. (2005). Differentiation and degeneration of cells that play a major role in tobacco anther dehiscence. Sexual Plant Reproduction **17,** 219-241.

Sesma, A., and Osbourn, A.E. (2004). The rice blast leaf pathogen undergoes developmental processes typical of root-infecting fungi. Nature **431,** 582-586.

Stark-Urnau, M., and Mendgen, K. (1995). Sequential deposition of plant glycoproteins and polysaccharides at the host-parasite interface of *Uromyces vignae* and *Vigna sinensis*: Evidence for endocytosis and secretion. Protoplasma **186,** 1-11.

Sweigard, J.A., Carroll, A.M., Kang, S., Farrall, L., Chumley, F.G., and Valent, B. (1995). Identification, cloning, and characterization of *PWL2*, a gene for host species specificity in the rice blast fungus. The Plant Cell **7,** 1221-1233.

Takano, Y., Choi, W., Mitchell, T.K., Okuno, T., and Dean, R.A. (2003). Large scale parallel analysis of gene expression during infection-related morphogenesis of *Magnaporthe grisea*. Molecular Plant Pathology **4,** 337-346.

Talbot, N.J. (2003). On the trail of a cereal killer: exploring the biology of *Magnaporthe grisea*. Annual Review of Microbiology **57,** 177-202.

Tang, W., Coughlan, S., Crane, E., Beatty, M., and Duvick, J. (2006). The application of laser capture microdissection to In Planta gene expression profiling of the maize anthracnose stalk rot fungus *Colletotrichum graminicola*. Molecular Plant-Microbe Interactions **19,** 1240-1250.

Teng, P.S. (1994). The epidemiological basis for blast management. (Wallingford, Oxon, Uk: CAB International and IRRI).

The Rice Chromosome 10 Sequencing. (2003). In-depth view of structure, activity, and evolution of rice chromosome 10. Science **300,** 1566-1569.

Urashima, A.S., Lavorent, N.A., Goulart, A.C.P., and Mehta, Y.R. (2004). Resistance spectra of wheat cultivars and virulence diversity of *Magnaporthe grisea* isolates in Brazil. Fitopathologia Brasileira **29,** 511-518.

Valent, B., and Chumley, F.G. (1991). Molecular genetic analysis of the rice blast fungus, *Magnaporthe grisea*. Annual Review of Phytopathology **29,** 443-467.

van't Slot, K.A.E., and W.Knogge. (2002). A dual role for microbial pathogen-derived effector proteins in plant diseases and resistance. . Critical Reviews in Plant Sciences **21,** 229-271.

Veneault-Fourrey, C., Barooah, M., Egan, M., Wakley, G., and Talbot, N.J. (2006). Autophagic fungal cell death is necessary for infection by the rice blast fungus. Science **312,** 580-583.

Ward, B.M., Medville, R., Lazarowitz, S.G., and Turgeon, R. (1997). The geminivirus BL1 movement protein is associated with endoplasmic reticulum-derived tubules in developing phloem cells. Journal of Virology **71,** 3726-3733.

Wharton, P.S., Julian, A.M., and O'Connell, R.J. (2001). Ultrastructure of the infection of *Sorghum bicolor* by *Colletotrichum sublineolum*. Phytopathology **91,** 149-158.

Xu, H., and Mendgen, K. (1997). Targeted cell wall degradation at the penetration site of cowpea rust basidiosporelings Molecular Plant Microbe Interactions **10,** 87-94.

Zambryski, P., and Crawford, K. (2000). Plasmodesmata: Gatekeepers for cell-to-cell transport of developmental signals in plants. Annu. Rev. Cell Dev. Biol. **16,** 393-421.

Zeigler, R.S., Leong, S.A., and Teng, P.S. (1994). Rice blast disease. (Wallingford, Oxon OX10 8DE, UK: CAB International).

Zellerhoff, N., Jarosch, B., Groenewald, J.Z., Crous, P.W., and Schaffrath, U. (2006). Nonhost resistance of barley is successfully manifested against *Magnaporthe grisea* and a closely related *Pennisetum*-infecting linage but is overcome by Magnaporthe oryzae. Molecular Plant Microbe Interactions **19,** 1014-1022.

Figure 1.1 Disease life cycle of M. oryzae

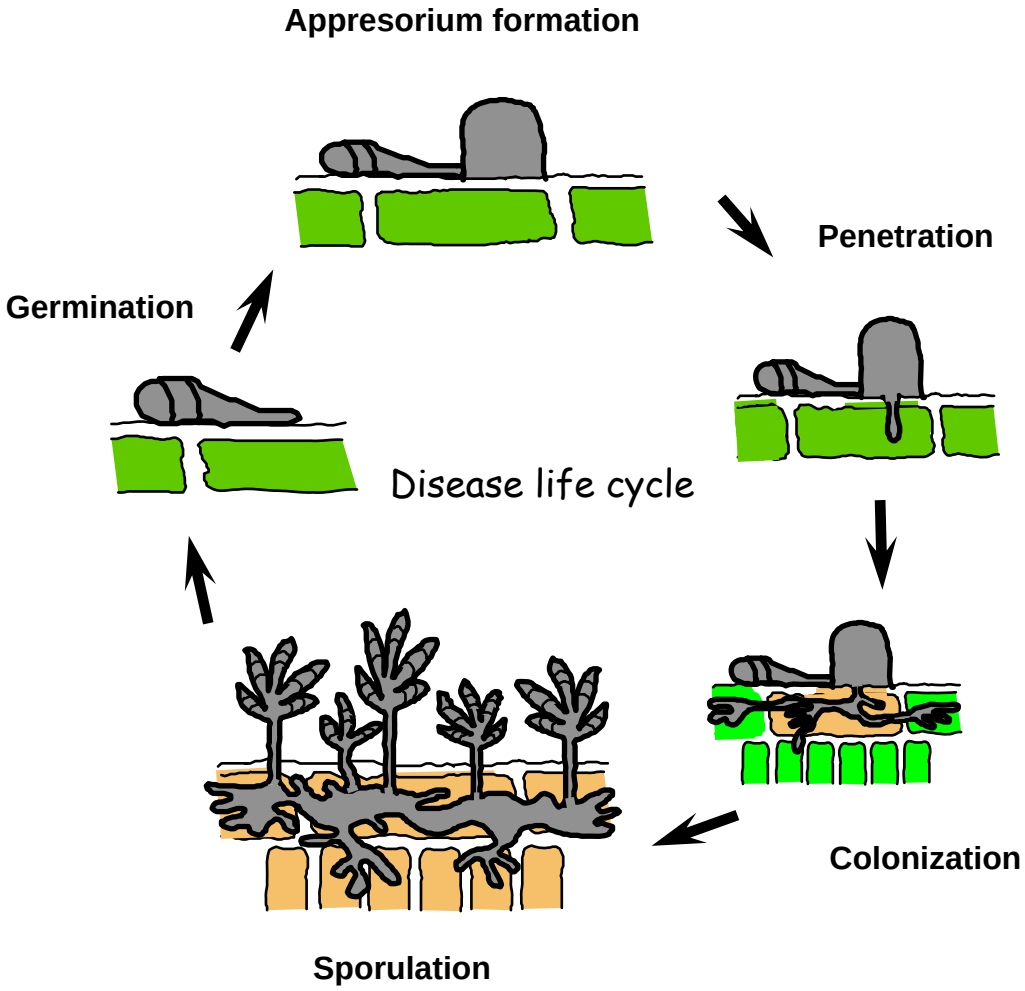
Appresorium formation
Penetration
Germination
Disease life cycle
Colonization
Sporulation

CHAPTER 2 - Roles for Rice Membrane Dynamics and Plasmodesmata during Biotrophic Invasion by the Blast Fungus

Abstract

Rice blast disease is caused by the hemibiotrophic fungus *Magnaporthe oryzae*, which invades living plant cells using intracellular invasive hyphae (IH) that grow from one cell to the next. Cellular and molecular processes by which this occurs are not understood. We applied live-cell imaging to characterize spatial and temporal development of IH and plant responses inside successively-invaded rice cells. Loading experiments with the endocytotic tracker, FM4-64, showed dynamic plant membranes around IH. IH were sealed in plant membrane, termed Extra-Invasive Hyphal Membrane (EIHM), which showed multiple connections to peripheral rice cell membranes. The IH switched between pseudohyphal and filamentous growth. Successive cell invasions were biotrophic, although each invaded cell appeared to have lost viability when the fungus moved into adjacent cells. EIHM formed distinct membrane caps at the tips of IH that initially grew in neighboring cells. Time-lapse imaging showed IH scanning plant cell walls before crossing, and transmission electron microscopy showed IH preferentially contacting or crossing cell walls at pit fields. This and additional evidence strongly suggest that IH co-opt plasmodesmata for cell-to-cell movement. Analysis of biotrophic blast invasion will significantly contribute to understanding normal plant processes and allow characterization of secreted fungal effectors that impact these processes.

Introduction:

The hemibiotrophic ascomyceteous fungus *Magnaporthe oryzae*, the causal agent of rice blast disease leads to severe crop losses annually. Rice blast is the major fungal disease on rice. So far, genetic control is the major form of control applied for this disease. In the arms race for survival, the fungus mutates itself to adapt to the host resistance. While the hunt for more resistance genes is an ongoing challenge, it is important to understand the biology of the fungal growth and colonization strategies to understand the disease cycle.

(Hemi) biotrophic pathogens have evolved to co-adapt with host cells and maintain them alive while deriving nutrition. The interface between the fungus and the host has been extensively studied in several biotrophic fungi. Apart from serving as the gateway for nutrient uptake, this interface plays a critical role in secreting effectors into the plant cell to manipulate the cell signaling and machinery (O'Connell and Panstruga, 2006). The well studied blast effector, avirulence gene product of *Avr-Pita*, was shown to directly interact with the corresponding rice resistance (*R*) gene product in transient bombardment assays (Jia et al., 2000). They suggested that the avirulence gene product has to be secreted into the host for this interaction to take place.

The initial invaded rice cells in a susceptible interaction retain the ability to plasmoyze, indicating their viability (Koga et al., 2004). In an *R*-gene mediated resistance interaction, the invaded cells fail to plasmolyze and show granulation and autofluorescence (Peng and Shishiyama, 1989; Koga, 1994; Koga et al., 2004). Understanding the mechanisms by which blast IH invade living rice cells is critical for understanding disease mechanisms as well as mechanisms of *R* gene-mediated resistance that rice breeders manipulate in attempts to control this disease (Jia et al., 2004; Kawasaki, 2004). The current literature contained contradictory reports on the nature of the IH-plant cytoplasm interface in rice blast disease. One report presented experimental evidence suggesting that IH were separated from host cytoplasm by invaginated plasma membrane (PM) and another report presented evidence suggesting that blast IH breached the plant PM and grew directly within the rice cytoplasm (Koga and Horino, 1984a;

Heath et al., 1992). Understanding the nature of the interface between blast IH and rice is critical for future studies to understand how pathogen effectors are secreted inside plant cells.

In this study, we investigated the nature of the fungus-plant interface and cell-to-cell invasion in the fully susceptible interaction characteristic of rice blast disease in the field. We studied biotrophic blast invasion using live-cell fluorescence and confocal microscopy with fluorescent probes that identify particular plant and fungal components. This microscopic analysis involved >950 independent infection sites using 4 different fluorescent probes. Key results were confirmed using TEM with HPF/FS samples, which provided improved preservation of membranes compared to conventional chemical fixation methods (Bourett et al., 1999; Mims et al., 2004). We documented an amazing degree of plasticity in the intracellular biotrophic IH responsible for rice blast disease. We demonstrated that differentiation of primary hyphae into bulbous IH included an event that sealed IH inside a tightly-fitted plant-derived Extra-Invasive Hyphal Membrane (EIHM), which prevented apoplastically-applied FM4-64 from reaching the fungal PM. Bulbous IH exhibited pseudohyphal growth and they searched for locations to cross cell walls into neighboring cells. At certain locations, IH swelled and crossed the wall using highly constricted IH pegs that became primary hyphae-like "filamentous IH" inside the next cell. The filamentous IH enlarged into bulbous IH and this biotrophic invasion process was repeated in successive rice cells. EIHM encasing filamentous IH had distinctive "membrane caps" that were not seen on bulbous IH. Blast IH lacked a uniform interfacial matrix, although rare patches of complex plant cellular components occurred between the EIHM and IH wall. Plant membrane dynamics were dramatically affected in the vicinity of the fungus. We present evidence suggesting that IH utilize plasmodesmata for moving into the next live cell. This would require IH to constrict at least 100-fold to approach the diameter of a plasmodesma (~30-50 nm; Cook et al., 1997). Understanding the cellular strategies used for biotrophic plant cell invasion in a pathosystem in which genetic analysis and genome resources are available for both the fungus (Dean et al., 2005) and rice (International Rice Genome Sequencing Project, 2005), will allow elucidation of plant cellular mechanisms as well as mechanisms critical for this important fungal-plant interaction.

Results

Intracellular IH, but not Primary Hyphae, Are Sealed Within Host Membrane

We produced a fungal strain, KV1, with constitutive, cytoplasmic expression of enhanced yellow fluorescent protein (EYFP), and visualized its invasion of rice leaf sheath epidermal cells. This rice tissue is optically clear and relatively flat, which facilitates live-cell imaging (Koga et al., 2004). To assess if major *R* gene-mediated specificity is maintained in leaf sheaths under our assay conditions, we compared compatible and incompatible interactions mediated by the *Pi-ta* resistance gene. KV1, which expresses avirulence gene *AVR-Pita*, is compatible with rice variety YT16 (*pi-ta*$^{-}$) and incompatible with rice variety Yashiro-mochi (*Pi-ta*). We assayed ability of invaded plant cells to plasmolyze as an indicator of membrane integrity and cell viability (Koga et al., 2004; O'Connell et al., 2004). As expected from other studies (Koga and Horino, 1984a; Koga et al. 2004), KV1-invaded host cells of susceptible YT16 plasmolyzed at 27 hours post inoculation (hpi), and most invaded host cells (98%) of resistant Yashiro-mochi failed to plasmolyze at this same stage of invasion (Table 1). Retention of *Pi-ta* mediated resistance specificity in infected leaf sheath pieces suggested that cellular studies of disease development in this system will be relevant to leaf cell invasion, which is responsible for much devastation in the field.

Our approach to understanding detailed cell biological events in the compatible interaction was to first investigate if IH were surrounded by rice membrane inside the first-invaded epidermal cell. Membranes surrounding haustoria in other pathogen systems lacked normal plant PM proteins because they failed to label with chimeric, fluorescent PM proteins (Koh et al., 2005; O'Connell and Panstruga, 2006). Considering the possibility of such failure, we first attempted to label plant PM in infected rice sheath cells with the membrane-selective dyes, Hexyl-Rhodamine B (RB) and FM4-64. The RB dye is passively taken up by cells and integrated into all internal membranes, including the endoplasmic reticulum. FM4-64 inserts in PM and diffuses laterally into contiguous membranes. The dye moves into internal cellular membranes only through an active, time-dependent endocytotic process, finally reaching vacuolar membranes. In other plants, FM4-64 failed to label the endoplasmic reticulum and

nuclear membranes (Bolte et al., 2004). In the rice sheath cells, RB labeled the lace-like network characteristic of endoplasmic reticulum and FM4-64 did not (Figure 1A-B). Both FM4-64 and RB staining showed membrane aggregation near the site of appressorial penetration (Figure 1A-B) as has been documented previously in other host-pathogen systems (O'Connell and Panstruga 2006). The diffuse staining pattern of RB around and inside IH sharply contrasted the FM4-64 fluorescence closely outlining the IH. Therefore, endoplasmic reticulum and other rice cell membranes aggregated around IH, but remained outside a tightly-fitting, FM4-64-labeled membrane surrounding IH.

We recorded confocal images of 80 FM4-64-stained sheath epidermal cells with IH developing at 27 hpi. These images reflect the expected dimorphism of thin, filamentous primary hyphae and bulbous IH (Figure 1B-E). Alternative fates of the primary hyphae are illustrated in two contiguous cells in Figure 1B. The primary hypha in the upper rice cell showed co-localization of EYFP and FM4-64 fluorescence (yellow color), and was presumed alive. The primary hypha in the lower rice cell lacked EYFP fluorescence and was apparently dead. At this time period, primary hyphae lack EYFP expression in 50% (n=80) of the infection sites surveyed. This suggested that primary hyphae were dispensable once IH were established inside the rice cell.

Both primary hyphae and IH internalized the endoplasmic reticulum dye RB (data not shown). However, there was a major difference in the FM4-64 staining patterns for these two hyphal types. While living primary hyphae (expressing EYFP) were brightly fluorescent due to internal FM4-64 staining, IH were closely outlined by a thin layer of FM4-64 fluorescence and lacked internal FM4-64 fluorescence. This is clearly illustrated by separation of the EYFP and FM4-64 channels (Figure 1C-E) for the upper sheath cell in Figure 1B. The lack of internal FM4-64 fluorescence inside IH was especially obvious in the IH septal and vacuolar membranes, which were expected to accumulate the dye (Atkinson et al., 2002). Thus, primary hyphae internalized FM4-64, but IH did not.

One explanation for the failure of IH to internalize FM4-64 would be if they were enveloped by a plant membrane that prevented the dye from reaching the fungal PM.

Alternatively, IH inside the rice cell may lack endocytotic capabilities. In support of the first explanation, the septal PM of IH never labeled with FM4-64. One would predict that if FM4-64 inserted in the fungal PM, it would label septal PM by lateral diffusion without the need for endocytosis (Atkinson et al., 2002). In addition, several lines of evidence make the latter alternative unlikely: (1) Spores and germ tubes of the fungus on the plant surface internalize FM4-64 by endocytosis (Atkinson et al., 2002; and unpublished results); (2) Rare IH inside susceptible rice tissues had internalized FM4-64, showing that at least some IH were capable of taking up the dye (In these cases, IH with internal FM4-64-staining showed diminished EYFP fluorescence, suggesting that they were unhealthy or dying.); and (3) Invasive-like hyphae formed in dialysis membranes (Bourett and Howard, 1990) internalized FM4-64 within 20 minutes, confirming that similar hyphae formed *in vitro* undergo endocytosis (Figures 1F-H). Taken together, the results suggested that healthy IH inside plant cells were sealed within a plant membrane that blocked access of fungal membranes to FM4-64 uptake. We named this plant membrane the Extra-Invasive Hyphal Membrane (EIHM). FM4-64-staining showed connections between the EIHM and rice membranes across the cell (Figure 1I).

To confirm the presence of EIHM surrounding IH, we performed TEM with similarly infected sheath samples prepared by HPF/FS. The TEM images confirmed that IH were encased in a membrane outside the fungal cell wall (Figure 1J-K). Taken together, our results settled a long-standing question (Koga and Horino, 1984a; Heath et al., 1992) by demonstrating that IH were tightly encased in host membrane as they grew within host epidermal cells.

Enhanced Rice Membrane Dynamics in Cells with IH

FM4-64 is generally used as an endocytosis marker during early stages of loading the dye (Bolte et al, 2004). We performed experiments to visualize the time course of dye uptake in infected sheath epidermal cells. Apparently due to the sheath cuticle, the time course of dye incorporation is not uniform for all plant cells. Epidermal cells near stomata and cells near some appressoria were the first to internalize the dye. Therefore, the time course of dye uptake in a

particular cell depends on the location of that cell relative to points of dye entry across the plant cuticle.

We visualized FM4-64 uptake in individual cells at early stages before internal plant cellular membranes were loaded with dye by identifying epidermal cells in which neither the EIHM nor the entire PM were stained. In the example in Figure 2A-B, only portions of the PM were stained with the dye (Supplemental Movies 1 and 2). In addition, at this early stage, the dye had not yet loaded into internal rice membranes. Confocal imaging showed that numerous FM4-64-labeled membrane tubules extended from the labeled PM towards IH. Figure 2A and Supplemental Movie 1 shows a membrane tubule that was separate from the plant PM. After 4 minutes, this tubule appeared to be rounding up, as if forming a round vesicle (Figure 2B, Supplemental Movie 2). Tubular and round vesicles were abundant in cells with IH, but not in uninvaded cells. Based on their FM4-64 staining characteristics, these vesicles appeared to be endocytotic compartments derived from the rice PM. These early stage FM4-64 internalization studies showed enhanced vesicular activity in the vicinity of the fungus.

Microscopy of infected cells that were saturated with FM4-64 showed the dynamic nature of other host membranes around the growing IH. At this later stage of dye loading, internal rice membranes, including vacuolar membranes were stained. Images of an infected cell taken 90 min apart showed different membrane connections between the EIHM and peripheral rice membranes (Figure 2C-D, Supplemental Movies 3 and 4). Membranes in the rice cell moved to surround the IH during this time period, as shown in the Supplemental Movies. The position of the vacuole also appeared to have shifted as indicated by arrows in Figure 2C-D. The FM4-64 patterns were distinct from the diffuse RB patterns showing endoplasmic reticulum surrounding IH (Figure 2E). This comparison confirmed that host endoplasmic reticulum surrounded the developing IH, but generally remained outside the EIHM.

TEM analysis showed that the EIHM was generally closely appressed to the fungal cell wall with no apparent matrix material separating the plant membrane from the fungal wall (Figure 1J). However, the EIHM sometimes exhibited irregular localized elaborations, and some of these elaborations contained fibrillar (Figures 1J and 2F), electron transparent (Figure 2G) or

electron opaque (data not shown) material inside. In two independent examples, the EIHM appeared to enclose extensive cellular components, including endoplasmic reticulum-like membranes inside the EIHM and in direct contact with the fungal cell wall (Figure 2F). We conclude that blast IH lack a defined, uniform interfacial matrix between the IH wall and the EIHM. However, diverse cellular materials were sometimes incorporated inside this interfacial zone.

Biotrophic Invasion Continues in Neighboring Rice Cells

The IH in the second- and later-invaded rice cells differed in behavior, and often in appearance, from the IH in the first-invaded cell. After penetrating the host cell at 24 hpi, IH grew in the first-invaded cell for 8 to 12 hrs, often filling it up. A time-dependent switch occurred during this period, since IH tended to spread into neighboring cells between 32 and 36 hpi no matter how quickly, or how completely, the first cell had been filled with fungus. The initial hyphae that formed after internal cell wall penetrations were thin and filamentous (filamentous IH) compared to bulbous IH in the first-invaded cell (Table 2, Figure 3). The filamentous IH enlarged into IH that we will continue to refer to as bulbous IH, although they generally appeared less bulbous than IH in first-invaded cells. Bulbous IH in subsequently invaded-cells grew more rapidly from one cell to the next, requiring only 2-3 hrs to move into neighboring cells.

Fungal strains that expressed a histone::GFP fusion protein for labeling nuclei initially showed no nuclear fluorescence within IH growing in neighboring cells (Figure 2H-K). Apparently, IH could show significant growth before a nucleus moved from IH in the previous rice cell. Filamentous IH in neighboring cells were seen to thicken up, branch and undergo pseudohyphal-like budding (Supplemental Movie 5). A similar phenomenon was observed early in the infection process when primary hyphae penetrated into the first-invaded host cell (data not shown). Primary hyphae were thin and anucleate. Nuclei entered primary hyphae around the time that they differentiated into IH.

We assessed biotrophic invasion of successively-invaded cells using a plasmolysis assay. Compatible rice cells containing IH plasmolyzed at 27 hpi, suggesting the cell's PM was intact and functional at this point (Figure 4A; Table 1). These first-invaded plant cells failed to plasmolyze after 32 hpi, indicating that the PM was no longer intact. This suggested that a host cell was no longer viable by the time the fungus exited it. Neighboring rice cells that were penetrated, even by multiple hyphae, were initially able to undergo plasmolysis (Figure 4B). The plasmolyzing protoplast always shrank around the IH ($n>125$) and did not retract along the hyphae from their site of entry into the cell (Figure 4A-B; Table 1). This is consistent with FM4-64 labeling studies in suggesting the fungus was sealed inside the plant PM.

To quantify the level of plasmolysis during successive cell invasions, we observed the ability to plasmolyze in the first-, the second-, and the third- or fourth- invaded plant cells. In this analysis, we focused on plant cells containing IH that had not yet exited the cell. Seventy to 90% ($n>110$ at each time point) of these invaded plant cells plasmolyzed (Figure 4C). Cells that failed to plasmolyze had generally reached the late cell colonization stage just before the fungus moved on into neighboring cells. These results were therefore consistent with our previous finding that plant cells no longer plasmolyzed around the time the fungus moved into the next cell. Plasmolysis patterns observed in this study were consistent with our previous observations (Table 1) that IH were always enclosed within the shrinking protoplast. Together, the plasmolysis experiments indicated that the blast fungus sequentially invades living rice cells.

FM4-64 uptake studies showed that IH growing in neighboring cells were sheathed in EIHM. An unusual feature of the EIHM surrounding the filamentous IH that had just entered neighboring rice cells was the prominent dome-shaped cap at the hyphal tips (Figure 4D-E, Table 2). The caps were clearly visible with differential interference contrast (DIC) microscopy before these IH had grown half-way across the cell (Figure 4D). FM4-64 loading studies confirmed that the caps represented EIHM that extended ahead of the hyphal tips (Figure 4E). Three-dimensional optical sectioning of the entire cell in Figure 4D showed 6 filamentous IH invading neighbors, including the 3 shown. All six had membrane caps. Similarly, the IH in Figure 4E had produced 12 filamentous IH, including the 5 shown. All 12 had membrane caps. We used laser scanning confocal microscopy to examine filamentous IH from seven additional

cells. In total, membrane caps were visible for 45 out of 50 filamentous IH (90%) that had grown less than half-way across the second cell. Membrane caps were also seen at the tips of the filamentous primary hyphae inside first-invaded cells (data not shown). However, differentiated bulbous IH uniformly lacked membrane caps. Therefore, membrane caps were a structural feature of the plant membrane surrounding primary hyphae and filamentous IH before they differentiated into bulbous IH.

As with the bulbous IH in first-invaded cells, IH in second-, third- and fourth-invaded plant cells failed to internalize FM4-64. We conclude that these hyphae are also enveloped by plant membrane that blocks dye from reaching fungal membranes. Therefore, filamentous and bulbous IH inside neighboring plant cells were biotrophic. During this study, we did not observe rice cell death ahead of the fungus, nor did we see fungus growing into non-plasmolyzing cells. Our results are consistent with an extended biotrophic invasion strategy in rice blast disease.

IH Appear to Exploit Plasmodesmata for Cell-to-Cell Movement

Time-lapse confocal imaging (Figure 5A-D, Supplemental Movie 5) demonstrated that the IH often exhibit budding, pseudohyphal-like growth instead of typical filamentous tip growth (Gancedo, 2001). IH appeared to search for specific locations to cross the plant cell wall. This sometimes took the form of a hyphal tip repeatedly touching the wall and moving away (arrowhead in Figure 5A-D, Supplemental Movie 5). Often hyphae that reached the cell wall grew along it for a period before crossing. Two IH that had traveled for at least 5 μm along the wall before crossing are indicated (stars in Figure 5A-D). Finally, some IH grew along the wall for extended periods without crossing, suggesting they had not found favorable conditions to cross. These results suggested that the fungus sought out specific locations to cross the plant cell wall.

At certain locations, IH stopped scanning and swelled slightly before sending a highly constricted hypha across the wall (arrow, Figure 5 A-D). These constricted hyphae developed

from apically-expanding IH in a similar manner to development of penetration pegs from appressoria. Therefore, we refer to these specialized hyphae as IH pegs. The IH peg expanded and grew as filamentous IH in the new cell. Although it had previously been reported that IH constrict when they move across walls (Czymmek et al., 2002; Rodrigues et al., 2003), live-cell imaging showed the extreme degree of this constriction (Figure 5E). Due to this level of constriction and the searching behavior of IH, we hypothesized that they sought out plasmodesmata, which are clustered in pit field regions of the wall (Zambryski and Crawford, 2000).

In order to investigate potential associations between IH and plasmodesmata, we performed ultrastructural analysis on infected rice sheath cells. IH and plasmodesmata in sheath tissues were visualized using TEM with HPF/FS samples. Approximately 25 invaded cells were sampled in one study of infected tissue at 36 hpi. Twelve of these cells contained IH that had either touched or moved across the host cell wall. We used semi-thick (250nm) tissue sections in order to observe any fine connections between IH and the rice cell walls. Plasmodesmata were seen at nine out of 10 locations in which the fungus had direct physical contact with the wall. For example, a section that just grazed the tip of an IH showed fine interconnections between the IH and a pit field (Figure 6A). Another IH showed fine interconnections with the plant wall at a pit field (Figure 6B). In this view a few interconnections were seen outside the visible pit field where the IH was further away from the wall. Yet another IH was closely pressed against the cell wall at a pit field region (Figure 6C). We failed to see plasmodesmata at only one of the 10 contact locations in this analysis. Therefore, this TEM analysis of infected tissue at 36 hpi, and similar results from infected tissue at 48 hpi (data not shown), showed that close associations between IH and the plant cell wall generally occurred at pit fields.

The TEM analysis on infected tissue at 36 hpi showed 2 events where an IH had crossed the cell wall. In both cases IH had crossed the cell wall adjacent to a normal-appearing plasmodesma (Figure 6D). These micrographs strongly suggested that blast IH crossed the plant cell wall at pit fields. The IH crossing the wall was ~10-fold larger in diameter than the plasmodesmatal channel beside it. The region in the cell wall traversed by the IH appeared well defined, without signs of mechanical or enzymatic damage.

Guard cells lack functional plasmodesmata (Zambryski and Crawford, 2000; Oparka and Roberts, 2001). If the fungus uses functional plasmodesmata to cross the plant cell wall, it should not be able to move into guard cells. To test this prediction, we visualized IH at later infection stages (48 to 72 hpi) to ensure that the fungus had ample time and opportunity to grow into guard cells. Fungus failed to enter guard cells at 98 out of 100 infection sites in which it had heavily colonized the surrounding cells. At the 2 remaining sites, a browning response made it difficult to see if there was fungus inside the guard cells. Figure 7A illustrates how IH can tightly pack a subsidiary cell without moving into the guard cell. These results are consistent with the hypothesis that the fungus uses functional plasmodesmata to cross the plant cell wall.

We attempted to co-localize a plasmodesmatal-specific fluorescent protein with IH crossing the wall. We performed transient plant expression assays with particle bombardment transformation in attempts to express GFP-labeled Tobacco Mosaic Virus movement protein (TMV-MP) (Oparka et al., 1997) in rice cells with growing IH. Fluorescently-labeled TMV-MP labeled punctae characteristic of plasmodesmata in transformed rice leaf sheath cells, but it failed to move into neighboring rice cells. In five independent experiments, we failed to observe epidermal cells that contained both IH and fluorescent TMV-MP. We did observe IH growing in rice cells undergoing transient expression of cytoplasmic GFP, suggesting that wounding due to microprojectile bombardment was not inhibiting growth of the fungus in the transformed cells.

Transient expression assays with the fluorescent TMV-MP confirmed that brighter fluorescent spots in plant cell walls stained with FM4-64 corresponded to pit fields. We predicted this because PMs of adjacent cells are continuous through plasmodesmata. The fluorescence of the TMV-MP co-localized with these FM4-64 punctae (Figure 7B-D). Several other examples of the FM4-64 staining pattern in the cell walls can be seen in Supplemental Movies 1-4. In confocal studies of FM4-64-stained tissues, we documented examples in which the EIHM had connections with pit fields. This is illustrated by an image of a late stage IH (36 hpi) that had filled the first-invaded rice cell (Figure 7E). Only the FM4-64 fluorescence is shown in order to highlight the EIHM around the IH and other plant membranes. Note that this apparently healthy IH was expressing EYFP (data not shown), and that it had not internalized

FM4-64. For the left hyphae contacting the plant wall in Figure 7E, the EIHM had 2 connections that tethered the IH to FM4-64-stained spots at the wall. For the IH contacting the plant wall on the right (Figure 7E), the EIHM was continuous with FM4-64 stained membranes that appeared to cross the wall into the next cell. Plasmodesmata are the only known locations where membranes, both PM and endoplasmic reticulum, cross from one plant cell to the next. Therefore, this confocal image associates IH with plasmodesmata.

Taken together, the searching behavior of IH, the extreme constriction of IH crossing the wall, the TEM experiments that showed the fungus contacts the cell wall preferentially at pit fields, and TEM images of IH moving across the wall at pit fields, strongly suggested the fungus uses plasmodesmata for its cell-to-cell movement. This hypothesis is also supported by the failure of IH to enter guard cells and by additional confocal imaging of the EIHM connections to FM4-64-labeled regions in the host cell wall.

In a second strategy to label the plasmodesmata in the infected plant cell with GFP, we transformed the fungus to secrete TMV-MP::GFP fusion protein inside the invaded rice cell. We constructed vectors for expressing translational fusions of TMV-MP and GFP with the fungal P27 ribosomal protein promoter. One construct included the Avr-Pita signal peptide for secretion and one lacked the signal peptide. We recovered 50 transformants for each vector, but none of them expressed GFP either in cytoplasmic or secreted forms. Fungal transformants with the background vector that lacked the TMV-MP expressed GFP. To determine if the TMV-MP and the GFP fragments were intact in the fungal genome in the transformants, we did PCR with genomic DNA from 5 independent transformants. All the transformants had the expected 1.6 Kb band (Figure 8) indicating that the lack of GFP expression was not due to deletions. Apparently, the fungus was not able to produce the chimeric viral movement protein.

Crossing Internal Plant Walls Does Not Require High Turgor Pressure

Some aspects of the biology of the hyphal pegs used by IH to cross internal plant cell walls appeared similar to the biology of penetration pegs produced by appressoria to cross the

plant cuticle and outer epidermal wall (Howard and Valent, 1996). In both cases, apically-expanding (swollen) hyphal cells produce highly constricted hyphae that cross the wall. These constricted hyphae expand into thin filamentous hyphae that grow for a short period before differentiating into bulbous IH (Table 2). We have shown that in both cases, the thin hyphae that grow immediately after wall crossings have distinctive membrane caps (Figure 4D and E; data not shown).

Appressoria produce and focus high turgor pressures to force penetration pegs through the outer plant surface (Howard and Valent, 1996). To test whether high turgor pressure might be involved in crossing internal plant walls, we observed tissue colonization by a melanin biosynthesis mutant incapable of building high pressure. The *alb*$^{-}$ mutant CP721, which is defective in the polyketide synthase responsible for the first step in melanin biosynthesis (Howard and Valent, 1996), was inoculated onto lightly wounded inner leaf sheath tissue. The mutant produced unmelanized appressoria on the abraded sheath cuticle, some of which penetrated into epidermal cells. The mutant produced IH that colonized the first-invaded host cell and then moved into neighboring cells in a manner indistinguishable from wild type (Figure 7F). Further, the mutant still exhibited characteristic swelling before crossing internal cell walls (Figure 7G). We conclude that, although the fungus may require some pressure produced by the swollen fungal cells to cross internal plant cell walls, it does not require the extremely high melanin-derived turgor pressures required by appressoria to pierce the outer plant surface.

Later Infection Stages and Leaf Colonization

To determine if the health of the fungus was maintained in the initially-invaded cells as later cells were filling with fungus, we checked for EYFP expression and for propidium iodide uptake (Figure 9). Propidium iodide is internalized only in fungal hyphae with damaged membranes. Very few fungal hyphae in developing lesions stained red due to uptake of propidium iodide. The rarity of colocalization of propidium iodide and EYFP fluorescence confirmed that cells that were taking up propidium iodide had generally lost EYFP expression, and were presumably not viable. This image shows the variation in shapes of bulbous IH *in*

planta. The IH continued to swell and constrict during crossing of normal appearing plant cell walls. Unlike primary hyphae in the first-invaded cells, filamentous IH maintained viability as the lesion developed. This produced an interconnected hyphal network that showed high levels of EYFP expression by IH throughout the colonized tissue, even though the only actively growing IH were at lesion margins. Sporulation began in the first-invaded cells days after they filled with IH.

We determined if the biotrophic invasion strategy we described in the leaf sheath assay occurred in rice leaves. The easiest feature of biotrophic invasion to visualize in green leaves was the swelling of the IH and hyphal constriction through the plant cell walls. Extensive fungal growth was seen in rice leaf tissue at 72 hpi (Figure 10). A higher magnification confocal image of a densely invaded area of the leaf showed extensive hyphal swelling and constriction (Figire 10). In a related study of leaf infection, Berruyer et al. (2006) reported the fungal growth front always preceded symptom development even at later stages of leaf colonization. Together, these results suggested that the blast fungus uses an extended biotrophic invasion strategy in leaves as well as in leaf sheaths.

Discussion

Rice Membrane Dynamics and Biotrophic Blast Invasion

This analysis of biotrophic rice blast invasion has revealed new features of cellular mechanisms resulting in disease. We have characterized three distinct types of hyphae (Table 2) that play a role in biotrophic invasion: (1) filamentous primary hyphae in the first-invaded plant cell; (2) bulbous IH in first- and in subsequently-invaded plant cells; and (3) filamentous IH that initially grow in successively-invaded cells (Table 2). Primary hyphae, first described by Heath et al. (1990), grew in lumens of first-invaded cells after pressure-based appressorial penetration (Howard and Valent, 1996; Talbot, 2003). Filamentous IH were produced in lumens of successively-invaded rice cells following an internal wall penetration event that did not require high pressures (Figure 7F-G). Both primary hyphae and filamentous IH differentiated into bulbous IH. Primary hyphae resembled filamentous IH in diameter and in formation directly

from highly constricted hyphal pegs that crossed the plant cell wall. Both primary hyphae and filamentous IH initially grew without nuclei, which must move across the hyphal pegs. Both were coated in plant membrane featuring distinctive membrane caps. On the other hand, primary hyphae differed from filamentous and bulbous IH in their accessibility to FM4-64 within the plant cell. That is, primary hyphae internalized FM4-64, whereas filamentous and bulbous IH did not. This suggested that primary hyphae differed from IH in their relationship to the host PM and their availability to the plant apoplast. Primary hyphae also differed from filamentous and bulbous IH in that they often lost viability after IH were established inside the host cell. Filamentous and bulbous IH remained viable as fungus spread to new rice cells in the developing lesion (Figure 9). These hyphal types, plus the more constricted penetration pegs and IH pegs that crossed the cell wall barriers, documented remarkable hyphal plasticity in the blast fungus as it successively colonized rice cells.

We clearly demonstrated that the specialized biotrophic IH of the rice blast fungus were sealed in a plant membrane, the EIHM, as they colonized living plant cells. Previously published discrepancies on the presence of a plant membrane surrounding blast IH may have been due to challenges in preserving membranes with conventional chemical fixatives used for TEM in these studies (Koga and Horino, 1984a; Heath et al., 1992). Even though the HPF/FS TEM used in our study is better for preserving membranes, artifactual breaks in membranes still occur (Bourett et al., 1999). Therefore, TEM images alone could not prove that the EIHM was continuous around IH, especially for extensive IH formed in the later stages of cell colonization. Our live-cell microscopy and FM4-64 dye loading experiments provided a unique perspective on this issue (Figures 1, 4E and 7E). The failure of IH to internalize FM4-64 suggested that the dye was not reaching the fungal PM because the fungus was sealed inside an EIHM that blocked passage of the dye. Interestingly, once IH developed, they were shielded from FM4-64 uptake even as they passed through cell walls. Thus, it appeared that the mechanism used by the fungus to cross plant cell walls maintained integrity of the EIHM.

During plasmolysis, blast IH were always included within the shrinking plant protoplast, and the plant PM did not pull away from the IH wall (Table 1 and Figure 4A and B). This suggests that there is a seal between the plant PM and blast IH cell wall near the point the hypha

entered the PM, and/or that there is a tight connection between the EIHM and the IH wall. Inclusion of IH inside the plasmolyzing protoplast together with shielding of IH from apoplastically applied FM4-64 suggest that blast IH might be sealed inside the plant protoplast by a structure analogous to neckbands in biotrophic rusts and powdery mildews. Compared to other fungi that produce biotrophic intracellular hyphae, the relationship between blast IH and the rice PM during plasmolysis most closely resembled the relationship between intracellular hyphae of the monokaryotic parasitic stage of the cowpea rust fungus *Uromyces vignae* and the cowpea PM (Heath et al., 1997). Events during plasmolysis in rice blast disease differed from plasmolysis events seen with the hemibiotophic *Colletotrichum* spp. (O'Connell et al., 1985; O'Connell and Panstruga, 2006), where the plant PM withdrew from biotrophic hyphae during plasmolysis.

We describe unique features of the blast EIHM. First, numerous FM4-64-stained connections were seen between the EIHM and rice membranes at the cell periphery (Figure 1I; Figure 2C-D and Figure 7E). These EIHM-membrane connections were seen to change over time (Figure 2C-D). Second, prominent membrane caps were seen at the tips of primary hyphae and filamentous IH (Figure 4D-E). Membrane caps were no longer visible after these hyphae differentiated to bulbous IH. Similar structural features have not been described for other membranes encasing biotrophic intracellular hyphae or haustoria, and their roles are yet to be explored.

Although there is no uniform, organized interfacial matrix between the EIHM and the IH cell wall, localized elaborations containing electron-opaque, electron-transparent, and fibrillar materials were observed. Rare dramatic EIHM elaborations contained diverse cellular components, including endoplasmic reticulum-like membranes, against the fungal cell wall (Figure 2F). This was the case even though comparison of the RB and FM4-64 staining patterns in infected cells (Figure 1A and B, 2E) showed that rice endoplasmic reticulum generally remained outside the tight-fitting EIHM. Our TEM images showing the patchy nature of the EIHM-IH interface are consistent with findings in previously reported studies of the blast fungus-plant cell interface. Koga and Horino, (1984a) presented micrographs of IH with associated fibrillar material similar to the endoplasmic reticulum-like membranes we report,

although they did not see EIHM in these images. Heath et al. (1992) reported that the cell walls of intracellular blast hyphae were closely surrounded by invaginated plant PM except for areas of localized elaborations or electron-opaque patches inside the membrane.

Our early dye-loading experiments with FM4-64 documented tubular and round vesicles proliferating near developing IH, suggesting that these are part of the endocytotic compartment of host cells (Figure 2A-B). Future studies will include determining if endocytosis inhibitors block the formation of these plant vesicles. Inhibitors that specifically block plant and not fungal endocytosis would be most valuable in order to separate effects on the host from effects on the pathogen. Endocytotic vesicles might also be identified by immunolocalization of plant clathrin molecules with vesicles within invaded host cells (Stark-Urnau and Mendgen, 1995). The plant vesicular activity we report may function in nutrient uptake by the IH. Vesicular fusion would also provide a mechanism for internalization of plant cell components within the EIHM (Figure 2F).

The mechanism for origin of the EIHM, or of any plant membrane encasing biotrophic hyphal structures, is not known. It has generally been assumed that the plant membranes that surround biotrophic fungal structures are produced by invagination of plant PM (O'Connell and Panstruga, 2006). Koh et al. (2005) showed that the EHM surrounding haustoria of the powdery mildew fungus in Arabidopsis was clearly differentiated from the PM by the absence of eight GFP-labeled PM proteins. They suggested two possibilities for origin of the EHM: Invagination of the PM with some mechanism for excluding normal PM proteins; or *de novo* membrane assembly by targeted vesicle trafficking. In the first scenario, lipids added to the PM by exocytosis around the cell periphery would allow increased PM capacity for invagination around growing haustoria. In the second scenario, lipids would be added directly to the EHM by specialized vesicular activity.

The extremely large surface area of EIHM that coats blast IH (Figure 1D and 7E), the extensive connections between the EIHM and peripheral rice membranes, and the curious membrane caps and inclusions raise the intriguing question of how the EIHM is constructed as IH grow. The large membrane surface area, especially around late-stage IH (Figure 7E), might

suggest that *de novo* lipid biosynthesis is involved. However, reports in the literature that lipid biosynthesis inhibitors made the plant more susceptible to blast disease suggested that *de novo* lipid biosynthesis is not required for disease development (Koga, 1994). Our working hypothesis is that the EIHM is being assembled *de novo* from redeployed plant membranes, and that this assembly occurs by fusion of the dynamic plant membrane tubules and round vesicles around the expanding EIHM. We propose that the fungus re-directs membrane trafficking in the plant cell in order to supply membrane components for building the EIHM. Transgenic rice expressing fluorescent markers specifically labeling the plant PM and endocytotic compartments will provide important tools for understanding the source of the EIHM.

Knowledge that blast IH are wrapped in EIHM means that AVR-Pita, and other rice blast effectors must be delivered across the EIHM to reach the rice cytoplasm. We have recently shown that the fungus secretes the AVR-Pita avirulence protein (Orbach et al., 2000) into the membrane caps (Figure 4D-E) at the tips of both primary hyphae and filamentous IH . The next step is to demonstrate delivery of AVR-Pita protein across the EIHM into the rice cytoplasm. Studies of the delivery of fungal effectors into the host cytoplasm are in early times for all fungal and oomycete systems. Demonstration of secretion of a rust haustorial protein into the infected plant cell has been reported (Kemen et al., 2005), and a specialized secretion signal appears to play a role in secretion of oomycete avirulence proteins into plant cells (Kamoun, 2006). Nothing is yet known of the fungal mechanisms for secretion inside living plant cells. Understanding these mechanisms is a critical area for future disease research.

Hemibiotrophy in the Rice Blast System

In this study of a highly aggressive pathogen on rice, sequentially invaded epidermal cells were initially alive as determined by their ability to plasmolyze. All forms of IH were sealed in EIHM (Figure 1C-E, 4D-E and 7E), and they underwent swelling and constriction (IH pegs) as they moved through internal cell walls. We did not observe death of plant cells ahead of the growing front of the fungus as would be expected for necrotrophic hyphae. Berruyer et al. (2006) used the EYFP-labeled strain KV1 to follow macroscopic lesion development in rice

leaves, and they reported that the fungal growth front always preceded visible symptom development. We suggest that there is no distinct switch from biotrophy to necrotrophy for rice blast disease, at least in the highly compatible interaction we studied. From these findings, rice blast defines a novel paradigm for hemibiotrophic plant infection; one in which each successive plant cell invasion is biotrophic, but individual invaded cells are no longer viable by the time the fungus moves into the next cell. We suggest a defining feature of biotrophic invasion by the blast fungus is repeated movement through plasmodesmata into living host cells.

TEM analysis showed an apparent lack of damage at the sites where IH pegs crossed internal cell walls during biotrophic invasion (Figure 6D). This suggested that extensive enzymatic digestion of the plant cell wall is not involved in biotrophic invasion. Still, the blast fungus is capable of producing an array of plant cell wall degrading enzymes such as cellulases and xylanases (Dean et al., 2005), and cytological studies report extensive degradation of plant cell walls in heavily invaded tissue and at later time periods (Rodrigues et al., 2003). There are numerous reports that blast invasion involved extensive destruction of mesophyll cells (Heath et al., 1990; Rodrigues et al., 2003), suggesting that necrotrophic hyphae might play some role in colonization. Blast necrotrophic hyphae might produce plant cell wall degrading enzymes for recovering remaining nutrients from plant cell walls in tissue that had already undergone biotrophic invasion. Defining exactly when biotrophic hyphae switch to necrotrophic growth remains for future studies.

Although different strains of the *M. oryzae* are specialized for specific grass species (Couch and Kohn, 2002), strains can be found that exhibit a continuum of symptoms on particular hosts. In nature, symptoms can range from no visible macroscopic symptoms, to larger brown necrotic spots that fail to sporulate, to sporulating lesions of different sizes (Heath et al., 1990; Valent et al., 1991). An extended biotrophic invasion strategy may be characteristic of the most susceptible interactions in the field. Perhaps less compatible interactions (resulting in smaller sporulating or non-sporulating lesions) featured in some studies may involve a more necrotrophic growth strategy (Rodrigues et al., 2003; Zellerhoff et al., 2006).

Roles for Plasmodesmata during Biotrophic Blast Invasion

Although it is well known that viruses spread from cell to cell using plasmodesmata (Wolf et al., 1989; Oparka et al., 1997; Lazarowitz and Beachy, 1999; Zambryski and Crawford, 2000), movement of an intact, relatively large-sized eukaryotic organism like *M. oryzae* through plasmodesmata would require extraordinary constriction of the organism, significant plasticity in plasmodesmata, extensive modification of plasmodesmata, or a combination of these factors. However, several lines of evidence support our hypothesis that blast IH use plasmodesmata for their cell-to-cell movement: (1) Blast IH searched for particular locations to cross the plant cell wall, and indeed, some IH apparently failed to find such suitable locations; (2) Live-cell confocal imaging showed connections between EIHM and membranes at pit fields as well as extreme constriction of IH as they crossed the wall; and (3) HPF/FS TEM analyses found that IH preferentially contacted the plant cell wall at pit fields (Figure 6A-C), and documented IH crossing cell walls at pit fields (Figure 6D). Together, these results strongly suggested that IH search out plasmodesmata for crossing to the next cell.

Demonstration that the fungus did not move into guard cells from neighboring cells was highly suggestive that functional plasmodesmata are required for fungal cell-to-cell movement, because plasmodesmata degenerate as guard cells mature (Oparka and Roberts, 2001). However, the unique physiological properties of guard cells might make them unattractive for IH invasion. We found support in the literature that IH are able to grow inside a guard cell if it is penetrated by an appressorium (Heath et al., 1992; Koga, 1994a). Heath et al. (1992) described an infection site in which an appressorium had penetrated into a stomatal guard cell and formed a normal-appearing hypha that had grown to fill the cell. Koga (1994a) reported TEM analysis of the blast fungus invading rice panicle neck cells. This publication includes a micrograph (Figure 4 in Koga, 1994a) showing an appressorium that had developed over the guard cells of a stomate. One of these guard cells contained an apparently healthy IH. Although it wasn't possible to confirm that this IH had entered the guard cell from the appressorium above it, this was likely to be the case. This image clearly showed that IH are capable of growing inside rice guard cells. Other micrographs from this paper (Koga, 1994a) were consistent with our results in showing subsidiary cells that contained IH, but the IH had not moved into adjacent guard cells. From

these combined studies, it appeared that IH were able to colonize guard cells through appressorial penetration, but not by moving from neighboring cells. Failure of IH to cross guard cell walls is consistent with the hypothesis that functional plasmodesmata are required for crossing internal cell walls.

Attempts to co-localize IH crossing the plant cell wall with plasmodesmata-specific markers have proven challenging. Plasmodesmata are commonly localized in plant cell walls by visualization of plasmodesmata-associated callose, which is involved in controlling the plasmodesmatal pore size in response to wounding (Lazarowitz and Beachy, 1999; Zambryski and Crawford, 2000). These studies involve either staining callose with aniline blue or immunolocalizations with callose antibodies (Oparka and Roberts, 2001). We were unable to visualize plasmodesmata-associated callose with aniline blue due to innate autofluorescence in the rice sheath cell walls (data not shown). The next step would be to use callose-specific antibodies to localize plasmodesmata. However, co-localization of callose and IH crossing plant walls may be ambiguous, because callose is a frequent component of collars, appositions or extrahaustorial matrices surrounding fungal hyphae at cell wall penetration sites (Mims et al., 2004; O'Connell and Panstruga 2006). Labeled plasmodesmatal proteins would provide a more specific probe for identifying plasmodesmata. Although pit fields in rice sheath cells were clearly labeled with fluorescently labeled TMV-MP using a microparticle bombardment transient expression assay, we were unable to find fungus growing in cells expressing TMV-MP. Our attempts to make the fungus secrete the TMV-MP into infected cells also did not yield positive results. Future experiments will involve generating stable transgenic rice expressing fluorescent chimeric proteins that will label plasmodesmata in cells with growing IH.

There are literature reports that fungi move through pit pairs, pit field regions in plant tissues with thickened secondary walls. Koga (1994a) reported that the blast fungus invaded sclerenchyma cells of rice panicle neck tissue through pit-pairs, where the cell wall is relatively thin due to lack of secondary wall deposition. Two reports on cytological analyses of another pathogen, *Fusarium graminearum* infecting wheat spikes and stems, showed fungus moving into neighboring cells through pit pairs (Guenther and Trail, 2005; Jansen et al., 2005). *F. graminearum* is reported not to have a biotrophic stage (Jansen et al., 2005), and this fungus may

have simply chosen the thinnest location to cross thick secondary cell walls. Never-the-less, these published reports suggest that fungi seek out and use pit fields for cell-to-cell movement, even though they do not mention the possibility that the fungus specifically uses plasmodesmata in these pit pairs.

Alternative mechanisms are possible if indeed the fungus is using plasmodesmata for its cell-to-cell movement. From the TEM analysis, we estimated that IH (>5 μm in diameter) were constricted at least 10-fold, to ~0.5 μm in diameter, at the point they had crossed the cell wall (Figure 6D). One possibility is that IH use precisely controlled degradation of the pit field cell wall to produce a channel for their movement. The resulting channel should be large enough to accommodate passage of an IH peg of this size. For this hypothesis, localized wall degradation would be facilitated by the unique structure of the plant cell wall in pit fields (Orfila and Knox, 2000). However, the appearance of an apparently normal plasmodesma next to crossing IH (Figure 6D) is inconsistent with extensive degradation of pit field walls, because wall surrounding at least one plasmodesma survived during this crossing event.

Another possibility is that IH might manipulate individual plasmodesma to move into neighboring cells. From our TEM analysis, diameters of IH crossing the wall are at least 10-fold larger than diameters of plasmodesmata (30 to 50 nm). Thus for an IH to fit through the plasmodesmatal channel would require further constriction of the initial IH peg beyond what we visualized, and/or dilation of the plasmodesmatal channel. It is possible that IH pegs that first penetrated the wall were thinner than the mature IH pegs seen in the TEM images, and that they expanded the diameter of the opening after they passed through. It is known that appressorial penetration pegs are highly specialized for crossing physical plant barriers, because they initially lack normal cytoplasmic organelles and they contain abundant actin microfilaments (Bourett and Howard, 1992). After penetration, the cytoplasm, nucleus and organelles of the fungus pass through the penetration peg into primary hyphae growing in the cell lumen (Howard and Valent, 1996). It is conceivable that IH pegs involved in crossing internal walls have a unique biological structure that facilitates their initial movement through plasmodesmata.

Neither hypothesis for how IH might be using pit fields/plasmodesmata has considered the complex components comprising functional plasmodesmata, including PM, desmotubule, protein and cytoskeletal components. Our results show that the cell about to be entered is alive, with intact PM (plasmolyzes), and that the IH remains encased in EIHM. In Figure 7E, the EIHM appeared continuous with a plant membrane that passed through the cell wall. These biological features make it seem less likely that the IH merely degrades pit field walls or empties the plasmodesmatal channel. Any mechanism that the fungus employed to move through plasmodesmata would necessarily involve manipulation of the PM, endoplasmic reticulum and proteins in these structures.

The blast biotrophic growth strategy in first-invaded cells clearly differed from its biotrophic strategy in subsequently-invaded cells. Plant cells use plasmodesmata to communicate with each other when under abiotic or biotic stresses (Lazarowitz and Beachy, 1999; Zambryski and Crawford, 2000). It is a reasonable prediction that the blast fungus might control plant signalling through plasmodesmata. The fungus might also prevent the invaded cell from alerting its neighbors by suppressing defenses in them. Biotrophic pathogens that produce haustoria are apoplastic. Hemibiotrophs like *Colletotrichum* spp. have a biotrophic phase confined to one or a few host cells. The blast fungus differs from these biotrophs in its sequential intracellular biotrophic invasion strategy. Thus, the blast fungus might have to manipulate the plant processes it needs for biotrophic invasion in the host cells ahead of its growing front. Potential fungal control of plasmodesmatal signaling represents a novel area of plant disease research.

Understanding effector function requires identification and functional analysis of candidate blast effectors. We have performed microarray analysis and identified novel genes that are only expressed by biotrophic IH *in planta* (Mosquera, Coughlan and Valent, unpublished results). Proteins encoded by these genes are highly enriched for secreted proteins and therefore represent a rich source of blast effector candidates. Targeted gene disruptions are being used to identify functions for these putative effectors. We expect that rice blast effectors are involved in suppressing host defense responses, as has been shown in bacterial pathosystems (Desveaux et al., 2006). Blast effectors may also be redirecting the plant membrane trafficking system for

building the EIHM and for feeding. In addition, our research suggested novel biological functions for effectors in rice blast disease. We suggest that the fungus is manipulating the structure and function of plasmodesmata for its own cell-to-cell movement and for controlling plant cellular communication. As with studies of viral movement proteins (Wolf et al., 1989; Lazarowitz and Beachy, 1999), identifying fungal molecules that impact plasmodesmatal function may contribute to basic understanding of the structure and function of plasmodesmata in general and their role in plant signaling.

Materials and Methods

Fungal Strains, DNA Manipulation and Fungal Transformation

M. oryzae strains 0-137 (Orbach et al., 2000) and 0-135 (Valent et al., 1991) were isolated from rice in field plots at the China National Rice Research Institute in Hangzhou, Zhejiang, China in 1985. Since collection, these field isolates have been stored dehydrated and frozen at -20^{o}C such that they maintain full pathogenicity characteristic of aggressive field isolates (Valent et al., 1991). Guy11, a field isolate from rice in French Guiana was obtained from J.L. Notteghem (CIRAD, Montpellier, France). We generated strain KV1 by transformation of O-137 with pBV13 using a protoplast transformation protocol described previously (Sweigard et al., 1995). Plasmid pBV13 was produced by insertion of the *EYFP* (Enhanced Yellow Fluorescent Protein) gene from pEYFP (cat# 6004-1, BD Biosciences Clontech, Palo Alto, CA) into the *M. oryzae* vector pSM324 as described by Bourett et al.(Bourett et al., 2002). This vector contains a bialaphos resistance gene for selection and the constitutive promoter from the *M. oryzae* ribosomal protein 27 gene. The melanin biosynthesis mutant CP721 (*alb1-22*) contains a spontaneous mutation in the *ALB1* gene in field isolate O-135. To produce fungal strains with GFP-labeled nuclei, we transformed Guy11 with pAM1293 from Dr. Marc Orbach (Univ. of AZ). This plasmid was made by cloning the *ccg-1*::histone H1::GFP fragment from pMF280 (Freitag et al., 2004) and the hygromycin resistance gene from pCB1004 into pAM1145 (Kellner et al., 2005).

Infection and Plasmolysis Assays

Rice varieties YT-16 and Yashiro-mochi were grown as described (Berruyer et al., 2006). Leaf sheath assays have been used extensively for microscopy (Koga and Horino, 1984b; Koga et al., 2004). We used 3 to 4 week old plants. Leaf sheaths from intermediate-aged leaves were cut into strips approximately 9 cm long. Fungal spores were harvested at a concentration of 10^5 spores/ml (unless otherwise noted) in 0.25% gelatin (Type B from bovine skin, Sigma G-6650). Inoculum was introduced into the hollow space enclosed by the sides of the leaf sheaths above the mid-vein. Inoculated sheaths were supported horizontally in a Petri dish containing wet filter paper such that the spores settled on the mid-vein regions. When ready for microscopy, the sheaths were hand-trimmed to remove the sides and expose the epidermal layer above the mid-vein (Figure 11). Lower mid-vein cells were then removed to produce sections 3 to 4 cell layers thick. To observe plasmolysis, trimmed sheath tissue sections were mounted on microscope slides and observed directly in 0.75 M sucrose solution.

For infection with the *alb*$^-$ mutant CP721, sides of the sheath were trimmed to expose the inner epidermal layer. This surface was wounded by rubbing 0.5mm zirconia/silicon beads (cat no # 11079105z, Biospec Products, Inc) on the inner sheath cuticle with a Q-tip. Spore inoculum was placed on the wounded surface. Fungus that grew on this tissue was re-isolated to confirm that it still had the melanin-deficient phenotype.

Leaf drop inoculation assays were performed as described (Jia et al., 2003; Berruyer et al., 2006). Leaves from rice variety YT-16 were cut into 7 to 8 cm pieces and placed in Petri dishes with wet filter paper to maintain high humidity. Twenty µl droplets of spore inoculum at a concentration of $1x10^4$ spores/ml were applied to the leaf pieces. Confocal imaging was performed 75 hpi.

Microscopy

Confocal microscopy: Hand-trimmed leaf sheath pieces were placed in a single-well Lab-Tek II chambered #1.5 cover glass system. Confocal images were acquired using a 63X C-Apochromat (NA 1.2) water immersion objective lens on a Zeiss Axiovert 200M microscope equipped with a Zeiss LSM 510 META system. All spectral data for dual-labeled samples were collected with simultaneous 488 nm (EYFP) and 543 nm (FM4-64) excitation using the 30 mW argon and 1 mW helium:neon lasers, respectively. Spectral scans were acquired using a 10.7 nm window from 510-610 nm. Reference spectra were acquired and used for linear unmixing to cleanly separate the overlapping EYFP and FM4-64 signals. Alternatively, samples labeled only with EYFP were imaged using 488 nm excitation with a 530 nm long pass filter and DIC transmitted light. In leaf assays, chloroplasts were visualized using 543 nm excitation with a 560 nm long pass filter. All images are confocal except where mentioned otherwise.

Differential Interference Contrast Microscopy: DIC imaging was done using a Zeiss Axioplan 2 IE Mot microscope. Cells were observed with a 63X C-Apochromat (NA 1.2) water immersion objective lens. Images were acquired using a Zeiss AxioCam HRc camera and analyzed with Zeiss Axiovision® Digital Image Processing Software, Version 3.1.

Transmission Electron Microscopy: TEM was adapted from a published protocol (Bourett et al., 1999). Tissue discs were excised from infected sheaths at 24, 36 or 48 hpi using a 1.2 mm diameter biopsy punch, transferred to a 1-hexadecene-filled 1.2 mm-400 μm HPF flat specimen carrier and then frozen using a Leica EMPACT high-pressure freezer. Frozen samples were placed in a Leica EM AFS and freeze-substituted at -90°C for 3 days in 4% OsO_4 in acetone, warmed slowly to room temperature, rinsed 3X in acetone, and embedded in Embed-812 resin. Sections were stained with lead citrate and uranyl acetate and imaged on a Zeiss CEM 902 transmission electron microscope equipped with a Megaview II digital camera (Soft Imaging System, Boulder, CO).

Tissue Staining Protocols

FM4-64 Staining: An aqueous 17 mM stock solution (Bolte et al., 2004) of FM4-64 (Cat # 13320, Invitrogen, Carlsbad, CA) was made and stored at -20^{o}C. Trimmed leaf sheaths and inoculated dialysis membranes were incubated in a 10 µM aqueous working solution for 30 to 120 minutes. Images in Figure 1B-E were stained differently. A stock solution was made at the concentration of 1 mg/ml in DMSO. Trimmed leaf sheath samples were incubated for 2 to 3 hrs in a working solution of 4 µg/ml in water.

Rhodamine B Staining: A stock solution of 10 µg/ml of the hexyl ester of Rhodamine B (Cat # R648MP, Invitrogen, Carlsbad, CA) was made in water and stored in 20 µl aliquots at -20^{0}C. Trimmed infected leaf sheaths were incubated in a 1 µg/ml working solution in 1x PBS for 30 minutes at 4^{0}C, followed by 30 minutes at room temperature. The pieces were mounted into chambered slides with a drop of stain solution and imaged.

Propidium Iodide Staining: Propidium iodide was purchased as a solution of 1 mg/ml dye in water (Cat # P3566, Invitrogen, Carlsbad, CA). An aqueous working solution of 100 µg/ml in 1xPBS was used for staining the tissues. Trimmed infected sheaths were incubated in dye solution for 15 minutes, followed by microscopy.

In vitro Formation of Invasive-like Hyphae

Conidia of strain KV1 were harvested from 10 day-old oatmeal agar cultures (Valent et al., 1991) in sterile distilled water and diluted to 1.0 x 10^5 spores/ml. Droplets of conidial suspensions were placed on 5x5 mm pieces of sterile, single-layered dialysis membrane in Petri dishes with moist filter papers. They were incubated at room temperature for 30 to 50 hours (Bourett and Howard, 1990). Some dialysis membrane pieces were moved to 2YEG (2 gm yeast extract, 2 gm glucose per liter) nutrient agar plates after 35 hours so that the invasive-like hyphae continued to grow.

Transient Expression in Rice

The gene encoding Tobacco Mosaic Virus 30K movement protein was amplified by PCR from vector pGreen0229, obtained from Dr. Karl Oparka at the University of Edinburgh. The gene was inserted into a pUC18-based vector that had been engineered for expression with the maize ubiquitin promoter and an in-frame translational fusion to the sgfp-tyg (Heim et al., 1995) reporter gene. This construct was introduced into leaf sheaths with the aid of a particle inflow gun (Finer et al., 1992). Fifty mg of M10 tungsten particles (Sylvania Inc.) were suspended in 500 µl of water and 25 µl aliquots were coated with 5 µl of DNA (2.4 µg/µl). Particles were vortexed, left at room temperature for one minute, and mixed with 25 µl of 2.5 M $CaCl^2$ and 10 µl of 0.1 M spermidine. The particle suspension was vortexed and incubated on ice for 4 minutes, and 50 µl of the supernatant was discarded. The remaining mixture was vortexed. Leaf sheath tissues were placed in a Petri dish with wet filter papers and bombarded with 2 µl of the suspension at 60 psi pressure and 28 in. Hg vacuum. This low pressure is important because high pressures in microprojectile bombardment experiments affect plasmodesmatal function (Zambryski and Crawford, 2000).

Sub-cloning the TMV-MP into Fungal GFP Expression Vectors

The gene encoding the Tobacco Mosaic Virus 30K Movement Protein (TMV-MP) was amplified by PCR from vector pGreen0229 with flanking BamH1 site. This site was used to sub clone the fragment into the vector pBV126 and pBV134 to generate pBV157 and pBV158 respectively. The vectors pBV126 and pBV134 contained RP27::EGFP::β tubulin terminator fragment and a RP27::Avr-Pita signal peptide::EGFP:: β tubulin terminator fragment respectively. The vectors contained the hygromycin antibiotic selection marker to screen the fungal transformants. Hygromycin inhibits protein synthesis both in prokaryotic and eukaryotic cells. The hygromycin resistance gene, Hygromycin phosphotransferase (*HPT*), encodes a kinase which blocks hygromycin activity by phosphorylation (http://www.hygromycin.com/). For *M. oryzae*, 200µg/ml concentration of the antibiotic was used for selecting resistant colonies. The bacterial selection marker was the antibiotic kanaycin resistance. Kanamycin causes frameshift mutations in bacteria by shifting the reading frame by one codon. The translational effects are usually lethal (http://www.kanamycin.com). The vectors were pBV157 and pBV158were

transformed into the agrobacterium strain Agl1 (Khang et al., 2005) to generate the strains BV161 and BV164.

Polymerase Chain Reactions for Gene Replacement Constructs

PCR reactions were done with the Takara Ex-Taq™ Polymerase (Product # TAK RR001A,B,C Takara, WI). The reaction mixture contained 5 µl 10X buffer, 4 µl dNTP mixture, 0.25 µl Ex-Taq, 2 µl template, and 1 µl of each primer at a concentration of 10 mM in a reaction volume of 50 µl. The thermocycler program was set to an initial denaturation of 1 min. The lid temperature was set to 95^{o}C. The cycle with denaturation at 95^{o}C for 30 sec, annealing at 58^{o}C for 1min, extension at 72^{o}C was repeated 30 times followed by a final extension of 5 minutes. The forward primer bound to the 5' end of TMV-MP (GCGCGGATCCATGGCTCTAGTTG) and the reverse primer (CAAGCTGCTCTAGCATTCGCCATTG) was complimentary to the 3' end of the terminator.

Agrobacterium Mediated Fungal Transformations

The agrobacterium clones BV161 and BV164 were grown in minimal medium for 44 hrs. One hundred microlitres of this culture was used to inoculate 100 µl of induction media containing acetosyringone and kanamycin. Acetosyringone is the inducer for the transfer of T-DNA into fungal spores of strain 0-137. The agrobacterium cultures were induced for 6 hrs at 28^{o}C at 250 rpm. A spore suspension from the fungal strain O-137 was prepared at a concentration of 10^{6} spores/ml. 100 µl of this spore suspension was mixed with 100 µl of the induced agrobacterium cultures and spread onto Whatman® sterile membrane filters (Cat# 7141 104, 0.45µm pore size) on cocultivation medium plates. The plates were kept in the dark at 28^{o}C for 36 hrs. The filters were then moved to TB3 (3 g yeast extract, 3 g casaminoacids, 20% sucrose) plates with cefatoxim (200 µg/ml) and hygromycin (200µg/ml). Cefatoxim is toxic to agrobacterium cultures. This is added to clean the fungal cultures from bacterial growth. These plates were wrapped in aluminum foil and placed in the fungal growth chamber at 24^{o}C. After two days, a significant amount of agrobacterium was growing on the filter papers. With the aid

of a pipet tip, the agro cultures were spread onto the plate. On the fifth day, the plates were observed under the stereomicroscope for fungal growth. Mycelia grew out from the edges of the filter paper. The filter papers were discarded and the plates were returned to the 24^{o}C fungal chamber. Distinct fungal colonies were seen growing on the plates. On the seventh day the colonies were transferred to the second round of selection plates. Following growth, the transformants were purified by isolation of cultures dericed frin single conidiophores.

DNA extractions for PCR

Fungal mycelia were scrapped from 1 cm^2 cultures growing either on oatmeal with the flat end of sterile wooden tooth picks. Care was taken to avoid agar in the collected material. This mycelial mat was suspended in 500 µl of extraction buffer (100 mM Tris – HCl - pH 8.0, 10 mM EDTA - pH 8.0, 1 M KCl) in 1.5ml tubes. The mycelia were ground using WING2. WING2 is a hand held grinder that fits a disposable plastic pestle at its tip. The tip pestle fits into the 1.5 ml tubes and helps grinds the mycelium. The WING2 was set to high and ground for 30 seconds. The tubes were centrifuged at 5,000 rpm at room temperature for 10 minutes. The supernatant was transferred into fresh 1.5 ml tubes containing 300 µl isopropyl alcohol (Cat # A416-500, Fisher Scientific) at -20^{o}C. The tubes were inverted several times to allow the alcohol precipitation of the DNA and centrifuged at 4^{o}C for 15 minutes at 13,000 rpm to pellet the DNA. The pellet was washed with 800 µl of 70% ethanol (-20^{o}C) and centrifuged at 4^{o}C for 5 min at 13,000 rpm. Ethanol was discarded taking care that the DNA pellet remained at the bottom of the tube. The tubes were air dried for 15 to 20 minutes and the DNA pellet was resuspended in 20 µl double distilled water.

References:

Atkinson, H.A., Daniels, A., and Read, N.D. (2002). Live-cell imaging of endocytosis during conidial germination in the rice blast fungus, *Magnaporthe grisea*. Fungal Genetics and Biology **37,** 233-244.

Berruyer, R., Poussier, S., Kankanala, P., Mosquera, G., and Valent, B. (2006). Quantitative and qualitative influence of inoculation methods on *in planta* growth of rice blast fungus. Phytopathology **96,** 346-355.

Berruyer, R., Khang, C.H., Kankanala, P., Kang, S., and Valent, B. (Unpublished results).

Bolte, S., Talbot, C., Boutte, Y., Catrice, O., Read, N.D., and Satiat-Jeunemaitre, B. (2004). FM-dyes as experimental probes for dissecting vesicle trafficking in living plant cells. Journal of Microscopy **214,** 159-173.

Bourett, T.M., and Howard, R.J. (1990). *In vitro* development of penetration structures in the rice blast fungus *Magnaporthe grisea*. Canadian Journal of Botany **68,** 329-342.

Bourett, T.M., and Howard, R.J. (1992). Actin in penetration pegs of the fungal rice blast pathogen, *Magnaporthe grisea*. Protoplasma **168,** 20-26.

Bourett, T.M., Czymmek, K.J., and Howard, R.J. (1999). Ultrastructure of chloroplast protuberances in rice leaves preserved by high-pressure freezing. Planta **208,** 472-479.

Bourett, T.M., Sweigard, J.A., Czymmek, K.J., Carroll, A., and Howard, R.J. (2002). Reef coral fluorescent proteins for visulaizing fungal pathogens. Fungal Genetics and Biology **37,** 211-220.

Couch, B.C., and Kohn, L.M. (2002). A multilocus gene genealogy concordant with host preference indicates segregation of a new species, *Magnaporthe oryzae*, from *M. grisea*. Mycologia **94,** 683-693.

Dean, R.A., Talbot, N.J., Ebbole, D.J., Farman, M.L., Mitchell, T.K., Orbach, M.J., Thon, M., Kulkarni, R., Xu, J.-R., Pan, H., Read, N.D., Lee, Y.-H., Carbone, I., Brown, D., Oh, Y.Y., Donofrio, N., Jeong, J.S., Soanes, D.M., Djonovic, S., Kolomiets, E., Renmeyer, C., Li, W., Harding, M., Kim, S., Lebrun, M.H., Bohnert, H., Coughlan, S., Butler, J., Calvo, S., Li-Jun, M., Nicol, R., Purcell, S., Nusbaum, C., Galagan, J.E., and Birren, B.W. (2005). The genome sequence of the rice blast fungus *Magnaporthe grisea*. Nature **434,** 980-986.

Desveaux, D., Singer, A.U., and Dangl, J.L. (2006). Type III effector proteins: doppelgangers of bacterial virulence. Current Opinion in Plant Biology **9,** 376-382.

Finer, J.J., Vain, P., Jones, M.W., and McMullen, M.D. (1992). Development of the particle inflow gun for DNA delivery to plant cells. Plant Cell Reports **11,** 323-328.

Freitag, M., Hickey, P.C., Raju, N.B., Selker, E.U., and Read, N.D. (2004). GFP as a tool to analyze the organization, dynamics and function of nuclei and microtubules in *Neurospora crassa*. Fungal Genetics and Biology **41,** 897-910.

Guenther, J.C., and Trail, F. (2005). The development and differentiation of *Gibberella zeae* (anamorph: *Fusarium graminearum*) during colonization of wheat. Mycologia **97,** 229-237.

Heath, M.C., Nimchuk, Z.L., and Xu, H. (1997). Plant nuclear migrations as indicators of critical interactions between resistant or susceptible cowpea epidermal cells and invasion hyphae of the cowpea rust fungus. New Phytologist **135,** 689-700.

Heath, M.C., Valent, B., Howard, R.J., and Chumley, F.G. (1990). Interactions of two strains of *Magnaporthe grisea* with rice, goosegrass, and weeping lovegrass. Canadian Journal of Botany **68,** 1627-1637.

Heath, M.C., Howard, R.J., Valent, B., and Chumley, F.G. (1992). Ultrastructural interactions of one strain of *Magnaporthe grisea* with goosegrass and weeping lovegrass. Canadian Journal of Botany **70,** 779-787.

Heim, R., Cubitt, A.B., and Tsien, R.Y. (1995). Improved green fluorescence. Nature **373,** 663-664.

Howard, R.J., and Valent, B. (1996). Breaking and Entering: Host penetration by the fungal rice blast pathogen *Magnaporthe grisea*. Annual Review of Microbiology **50,** 491-512.

Jansen, C., von Wettstein, D., Schäfer, W., Kogel, K.-H., Felk, A., and Maier, F.J. (2005). Infection patterns in barley and wheat spikes inoculated with wild-type and trichodiene synthase gene disrupted Fusarium graminearum. Proceedings of the National Academy of Sciences U.S.A. **102,** 16892-16897.

Jia, Y., Valent, B., and Lee, F.N. (2003). Determination of host responses to *Magnaporthe grisea* on detached rice leaves using a spot inoculation method. Plant Disease **87,** 129-133.

Jia, Y., McAdams, S.A., Bryan, G.T., Hershey, H.P., and Valent, B. (2000). Direct interaction of resistance gene and avirulence gene products confers rice blast resistance. The EMBO Journal **19,** 4004-4014.

Kamoun, S. (2006). A catalogue of the effector secretome of plant pathogenic oomycetes Annual Review of Phytopathology **44,** 41-60.

Kellner, E.M., Orsborn, K.I., Siegel, E.M., Mandel, M.A., Orbach, M.J., and Galgiani, J.N. (2005). *Coccidioides posadasii* contains a single 1,3-{beta}-glucan synthase gene that appears to be essential for growth. Eukaryotic Cell **4,** 111-120.

Kemen, E., Kemen, A.C., Rafiqi, M., Hempel, U., Mendgen, K., Hahn, M., and Voegele, R.T. (2005). Identification of a protein from rust fungi transferred from haustoria into infected plant cells. Molecular Plant Microbe Interactions **18,** 1130-1139.

Khang, C.H., Park, S.-Y., Lee, Y.-H., and Kang, S. (2005). A dual selection based, targeted gene replacement tool for *Magnaporthe grisea* and *Fusarium oxysporum*. Fungal Genetics and Biology **42,** 483-492.

Koga, H. (1994). Hypersensitive death, autofluorescence, and ultrastrctural changes in cells of leaf sheaths of susceptible and resistant near-isogenic lines of rice (*Pi-z*^{t}) in relation to penetration and growth of *Pyricularia oryzae*. Canadian Journal of Botany **72,** 1463-1477.

Koga, H., and Horino, O. (1984a). Electron microscopical observation of rice leaves infected with *Pyricularia oryzae* Cav. in compatible and incompatible combinations. IV. The interface between invading hyphae and host cytoplasm in epidermal cells of leaf-sheath. Annals of the Phytopathological Society of Japan **50,** 375-378.

Koga, H., and Horino, O. (1984b). Electron microscopical observation of rice leaves infected with *Pyricularia oryzae* Cav. in compatible and incompatible combinations. III. Resistance expression and loss of capability for plasmolysis in inner epidermal cells of leaf-sheath. Annals of the Phytopathological Society of Japan **50,** 353-360.

Koga, H., Dohi, K., Nakayachi, O., and Mori, M. (2004). A novel inoculation method of *Magnaporthe grisea* for cytological observation of the infection process using intact leaf sheaths of rice plants. Physiological and Molecular Plant Pathology **64,** 67-72.

Koh, S., Andre, A., Edwards, H., Ehrhardt, D., and Somerville, S. (2005). *Arabidopsis thaliana* subcellular responses to compatible *Erysiphe cichoracearum* infections. The Plant Journal **44,** 516-529.

Lazarowitz, S.G., and Beachy, R.N. (1999). Viral movement proteins as probes for intracellular and intercellular trafficking in plants. The Plant Cell **11,** 535-548.

Mims, C.W., Richardson, E.A., Holt III, B.F., and Dangl, J.L. (2004). Ultrastructure of the host-pathogen interface in *Arabidopsis thaliana* leaves infected by the downy mildew *Hyaloperonospora parasitica*. Canadian Journal of Botany **82,** 1001-1008.

O'Connell, R.J., and Panstruga, R. (2006). Tête à tête inside a plant cell: estabilishing compatibility between plants and biotrophic fungi and oomycetes. New Phytologist **171,** 699-718.

O'Connell, R.J., Bailey, J.A., and Richmond, D.V. (1985). Cytology and physiology of infection of *Phaseolus vulgaris* by *Colletotrichum lindemethianum*. Physiological Plant Pathology **27,** 75-98.

O'Connell, R.J., Herbert, C., Sreenivasaprasad, S., Khatib, M., Esquerré-Tugayé, M.-T., and Dumas, B. (2004). A novel *Arabidopsis*-*Colletotrichum* pathosystem for the molecular dissection of plant-fungal interactions. Molecular Plant Microbe Interactions **17,** 272-282.

Oparka, K.J., and Roberts, A.G. (2001). Plasmodesmata: A not so open-and-shut case. Plant Physiology **125,** 123-126.

Oparka, K.J., Prior, D.A.M., Santa Cruz, S., Padgett, H.S., and Beachy, R.N. (1997). Gating of epidermal plasmodesmata is restricted to the leading edge of expanding infection sites of tobacco mosaic virus (TMV). The Plant Journal **12,** 781-789.

Orbach, M.J., Farrall, L., Sweigard, J.A., Chumley, F.G., and Valent, B. (2000). The fungal avirulence gene *AVR-Pita* determines efficacy for the rice blast resistance gene *Pi-ta*. Plant Cell **12,** 2019-2032.

Orfila, C., and Knox, J.P. (2000). Spatial regulation of pectic polysaccharides in relation to pit fields in cell walls of tomato fruit pericarp. Plant Physiology **122,** 775-781.

Peng, Y.-L., and Shishiyama, J. (1989). Timing of a cellular reaction in rice cultivars associated with differing degrees of resistance to *Pyricularia oryzae*. Canadian Journal of Botany **67,** 2704-2710.

Rodrigues, F.A., Benhamou, N., Datnoff, L.E., Jones, J.B., and Belanger, R.R. (2003). Ultrastructural and cytological aspects of silicon-mediated rice blast resistance. Phytopathology **93,** 535-546.

Stark-Urnau, M., and Mendgen, K. (1995). Sequential deposition of plant glycoproteins and polysaccharides at the host-parasite interface of *Uromyces vignae* and *Vigna sinensis*: Evidence for endocytosis and secretion. Protoplasma **186,** 1-11.

Sweigard, J.A., Carroll, A.M., Kang, S., Farrall, L., Chumley, F.G., and Valent, B. (1995). Identification, cloning, and characterization of *PWL2*, a gene for host species specificity in the rice blast fungus. The Plant Cell **7,** 1221-1233.

Talbot, N.J. (2003). On the trail of a cereal killer: exploring the biology of *Magnaporthe grisea*. Annual Review of Microbiology **57,** 177-202.

Valent, B., Farrall, L., and Chumley, F.G. (1991). *Magnaporthe grisea* genes for pathogenicity and virulence identified through a series of backcrosses. Genetics **127,** 87-101.

Wolf, S., Deom, C.M., Beachy, R.N., and Lucas, W.J. (1989). Movement protein of tobacco mosaic virus modifies plasmodesmata size exclusion limit. Science **246,** 377-379.

Zambryski, P., and Crawford, K. (2000). Plasmodesmata: Gatekeepers for cell-to-cell transport of developmental signals in plants. Annu. Rev. Cell Dev. Biol. **16,** 393-421.

Zellerhoff, N., Jarosch, B., Groenewald, J.Z., Crous, P.W., and Schaffrath, U. (2006). Nonhost resistance of barley is successfully manifested against *Magnaporthe grisea* and a closely related *Pennisetum*-infecting linage but is overcome by Magnaporthe oryzae. Molecular Plant Microbe Interactions **19,** 1014-1022.

Figure 2.1 Live-Cell imaging of *M. oryzae* **IH and Rice Cell Membranes**

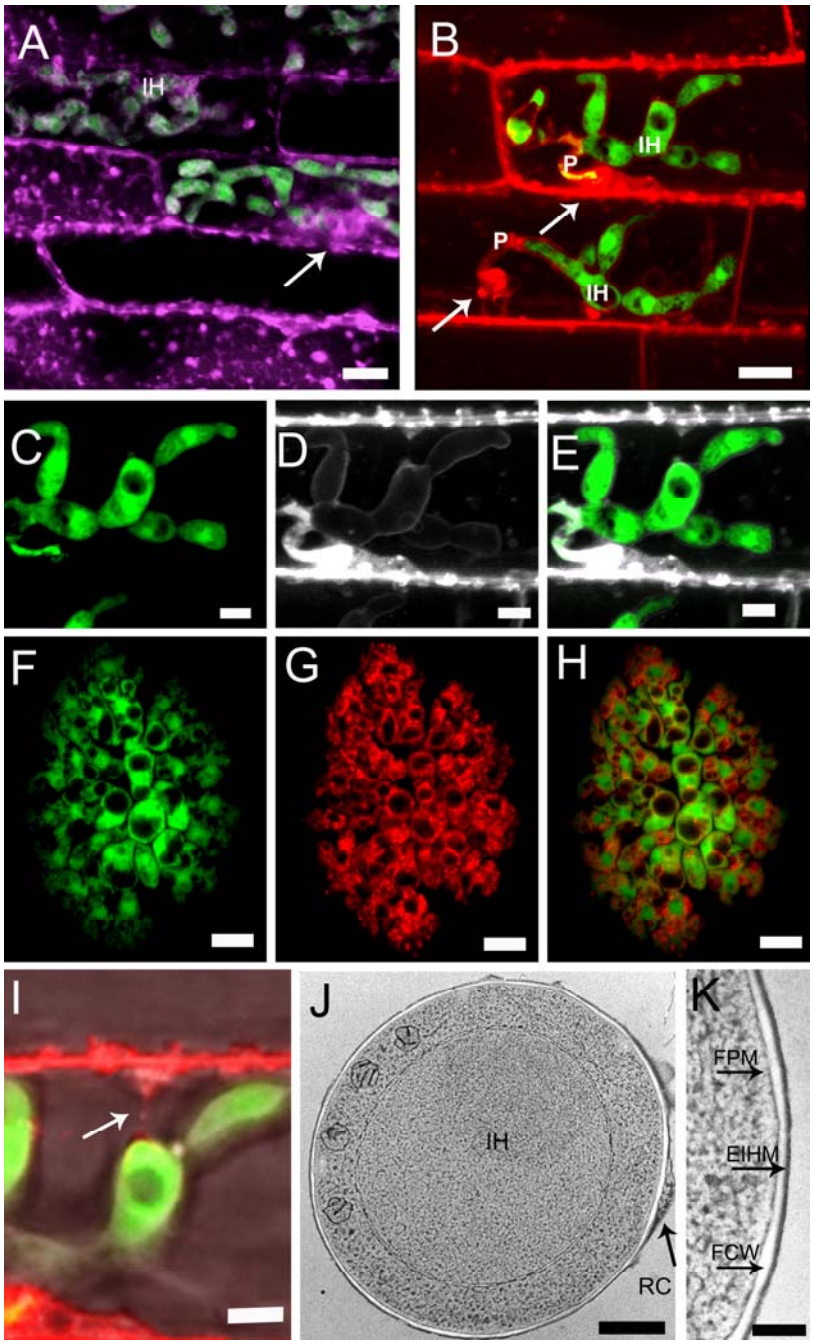

(A-B) Differential staining patterns with Hexyl-Rhodamine B (RB) and FM4-64 in rice sheath epidermal cells invaded by EYFP-labeled fungal strain KV1 (green). Arrows indicate sites where appressoria had penetrated into host cells. **(A)** RB dye (purple) stained the

endoplasmic reticulum inside rice cells and fungal IH at 36 hpi. Bar = 10 μm. **(B)** Plasma membrane and endocytotic membranes in rice cells were stained to saturation with FM4-64 (red). Narrow primary hyphae (P) extending from the penetration site differentiated into bulbous IH inside two invaded rice cells at 27 hpi. This image is a 3-dimensional projection of 20 optical sections acquired with a z-interval of 0.44 μm. Bar = 10 μm.

(C-E) FM4-64 outlines IH, but is not internalized by them. These images show separate and merged fluorescence channels for the upper rice cell in Figure 1B. **(C)** EYFP fluorescence; **(D)** FM4-64 fluorescence (white in this image), and **(E)** merged channels. Bars = 5 μm.

(F-H) Invasive-like hyphae formed *in vitro* on dialysis membrane internalize FM4-64. **(F)** EYFP fluorescence; **(G)** FM4-64 fluorescence (red) and **(H)** merged channels. Bars = 10 μm.

(I) Membrane encasing the IH had an FM4-64-stained connection (arrow) to rice membrane at the cell periphery. This is an enlarged view of a single optical section from the infection site in Figure 1C-E. The brightfield channel is included in this view (grey scale). Bar = 5 μm.

(J-K) TEM micrographs showed EIHM surrounding an IH inside an epidermal cell. **(J)** Transverse section of an IH at 26 hpi. The arrow indicates a fibrillar inclusion inside the generally close-fitting EIHM. RC = Rice cell. Bar = 500 nm. **(K)** High magnification view of the IH-host interface from the cell in (J). FPM = Fungal plasma membrane, FCW = Fungal cell wall, EIHM = Extra-Invasive Hyphal Membrane. Bar = 150 nm.

Figure 2.2 Rice membrane dynamics and fungal nuclear movement.

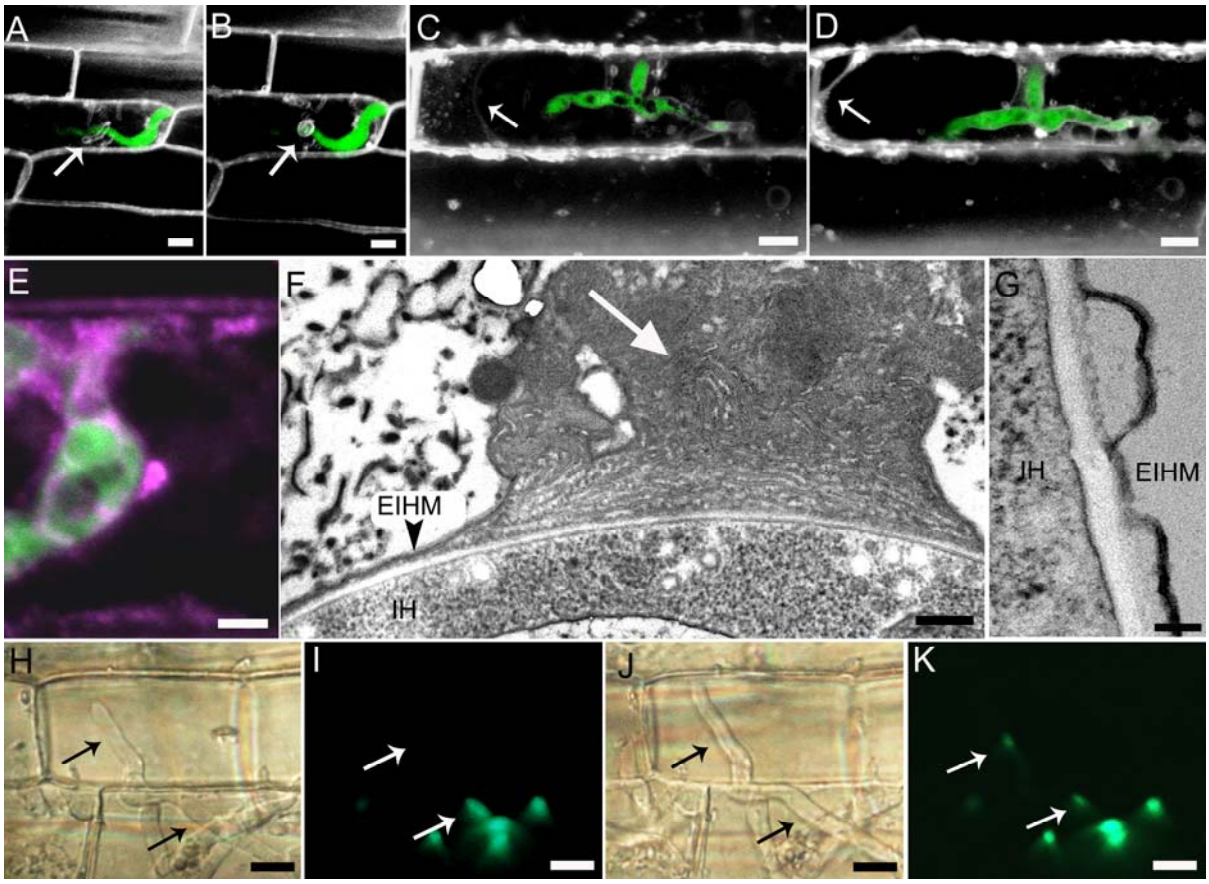

(A-B) Numerous membrane tubules occur around an IH (green) in an epidermal cell during early stages of FM4-64 (white) uptake. Arrows indicate a membrane tubule in (**A)** that appeared to be rounding up in (**B)** 4 minutes later. Note that (A) is imaged at a slightly lower magnification than (B). Each image is a projection of four optical sections taken at 0.5 µm z-intervals. The complete z-series are shown in Supplemental Movies 1 and 2. Bar = 10 µm.

(C-D) Shifting of internal rice membranes (white) around an IH (green) after loading to saturation with FM4-64. Arrows indicate a shift in the rice vacuolar membrane position from **(C)** to **(D)** 90 min later. Numerous connections are seen between the EIHM and peripheral rice membranes. Both images are projections of 4 optical sections taken at a 0.5 µm z-interval. Complete z-series are shown in Supplemental Movies 3 and 4. Bar = 10 µm.

(E) Endoplasmic reticulum (purple) in an RB-stained epidermal cell aggregated around the IH (green) at 36 hpi. Bar = 5 µm.

(F) TEM image of a complex aggregation (white arrow) of endoplasmic reticulum-like membrane and vesicles internalized between the EIHM (black arrowhead) and the IH cell wall. Bar = 150 nm.

(G) TEM image of EIHM elaborations containing electron transparent material between the membrane and the IH wall. Bar = 75 nm.

(H-K) Fungal nuclear movement to IH growing in neighboring cells. Infected cells were visualized using DIC optics **(H**, **J).** IH nuclei were visualized by fluorescence from a histone::GFP fusion protein expressed by the fungus **(I**, **K)**. Ten min elapsed between (H,I) and (J,K). Arrows mark equivalent cellular positions for localization of nuclear fluorescence relative to the developing IH. The lower arrow indicates fading nuclear fluorescence in (K) relative to (I) and the upper arrow indicates appearance of nuclear fluorescence in (K) relative to (I). Bars = 10 µm.

Figure 2.3 Blast hyphal types *in planta*

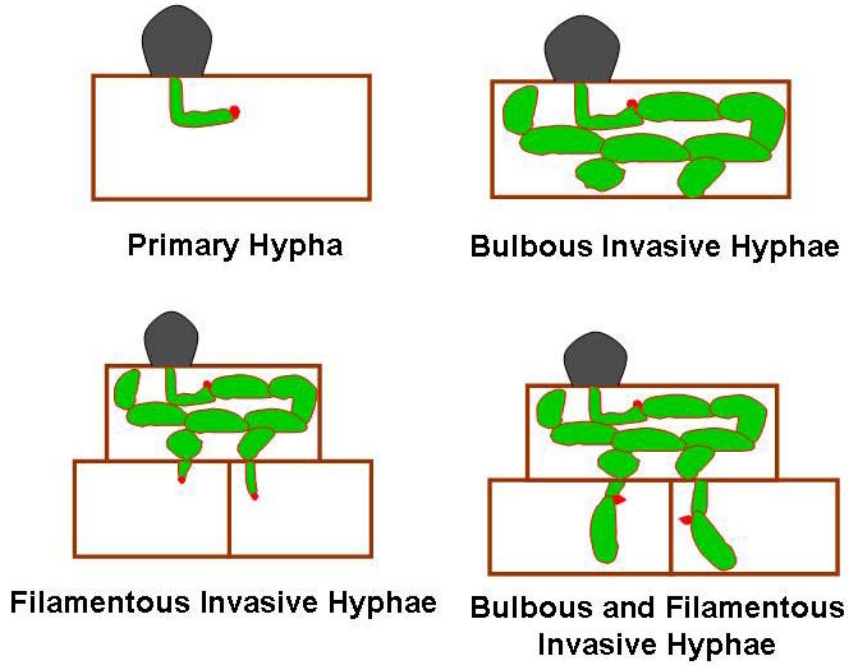

Figure 2.4 Biotrophic invasion continues in neighboring rice cells.

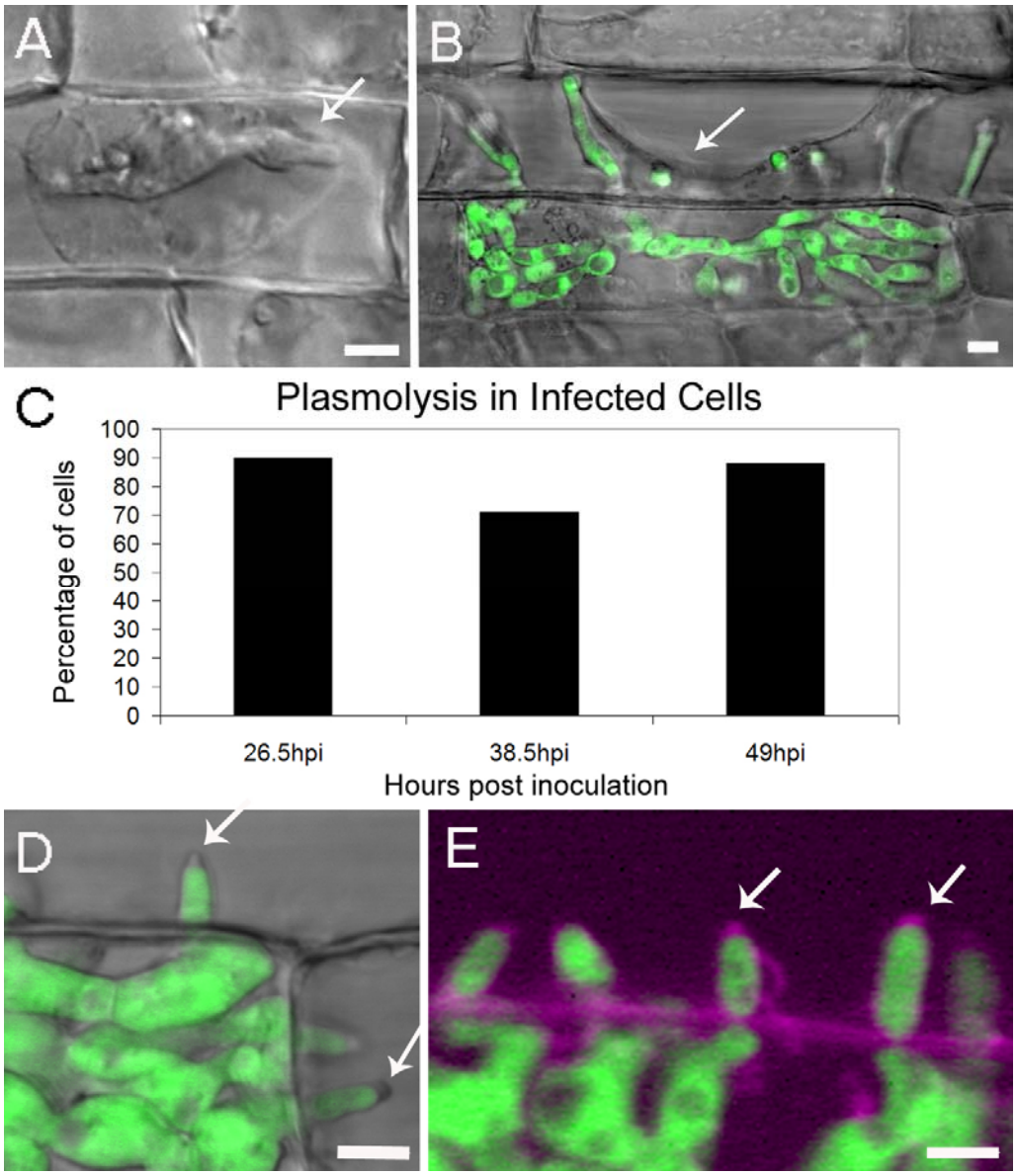

(A) An IH was surrounded by the shrinking protoplast (arrow) after plasmolysis in 0.75 M sucrose solution. These cells were visualized at 27 hpi using DIC optics. Bar = 5 µm.

(B) A rice cell at 48 hpi still plasmolyzes even though 7 IH have invaded it from the first-invaded cell. This image shows the green hyphal fluorescence merged with brightfield (grey

scale) of the plasmolyzed plant PM (arrow). Note that all IH expressed strong EYFP fluorescence. Some IH in this view do not appear green because they were below the focal plane. Bar = 5 μm.

(C) Quantification of plasmolysis in successively-invaded rice cells. Percentage plasmolysis was measured in first-invaded cells at 26.5 hpi, in second-invaded cells at 38.5 hpi, and in third- or fourth-invaded cells at 49 hpi. This experiment was performed independently from the experiment in Table 1.

(D-E) Filamentous IH growing in rice epidermal cells were sheathed in EIHM with prominent membrane caps at their tips (arrows). The membrane caps visible by DIC microscopy **(D)** stained with FM4-64 dye, shown as purple **(E)**. Bars = 5 μm.

Figure 2.5 Live-cell imaging suggested cell-to-cell movement involves plasmodesmata.

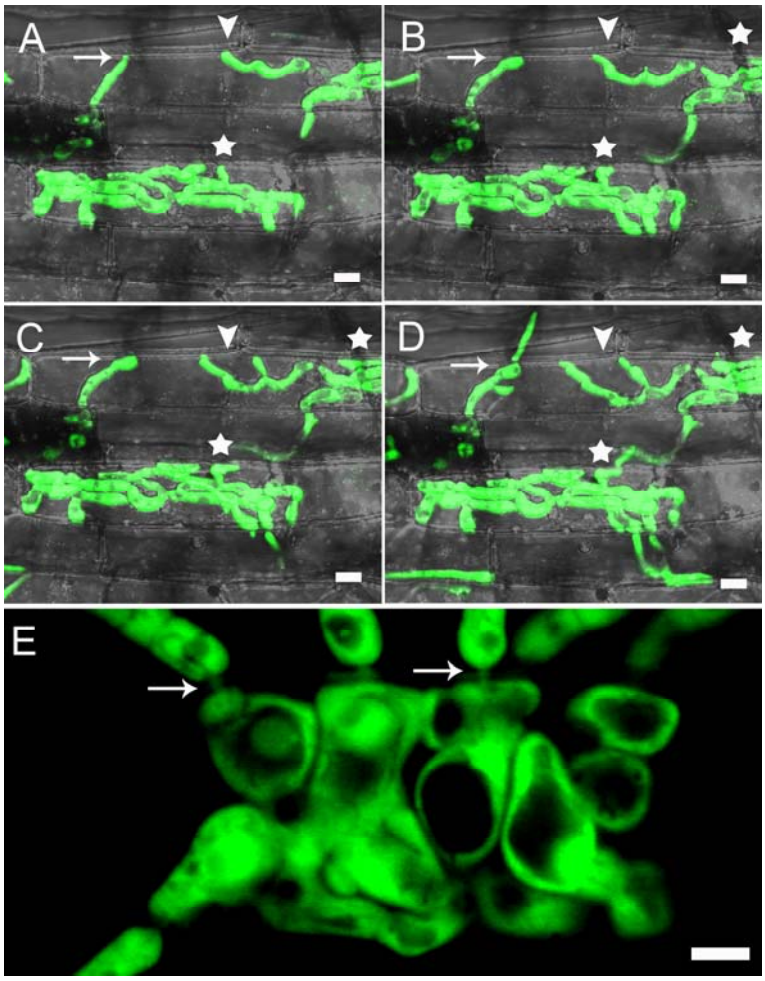

(A–D) IH seek out specific locations to cross rice cell walls. Four still images from Supplemental Movie 5 show IH growing in epidermal cells. Image (A) was obtained at 36 hpi. During the 2.5 hr period recorded, an IH (arrow) reached the cell wall and swelled slightly before crossing. The arrowhead indicates a fixed point in the cell and shows an IH developing by pseudohyphal budding and moving over time. Stars indicate IH that had each moved along rice cell wall for ~5 µm before swelling and crossing. The IH in the upper right corner was not visible in (A). Other examples can be seen in the movie, in addition to IH growing along the cell wall and not crossing. Bars = 5 µm.

(E) IH at 32 hpi exhibit extreme constriction (arrow) as they cross the rice cell wall. Only EYFP fluorescence is shown. Bar = 5 µm.

Figure 2.6 TEM images show IH associated with plasmodesmata.

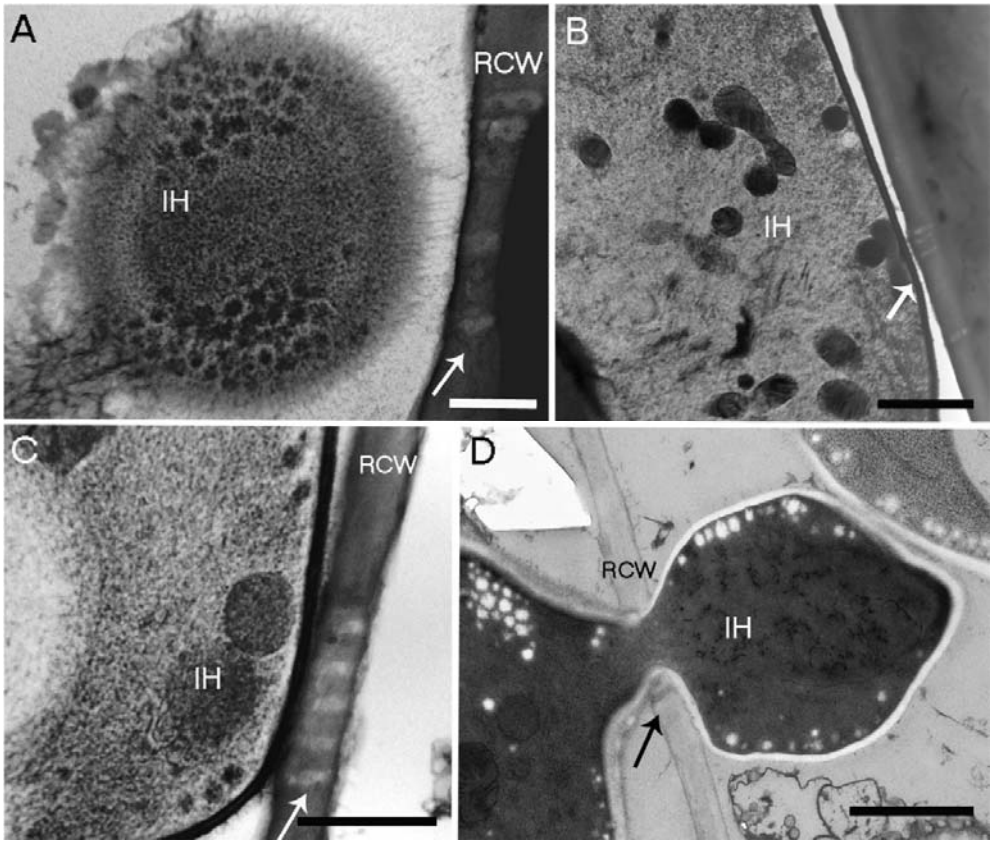

(A-C) IH associated with rice cell walls (RCW) at pit fields. Arrows indicate plasmodesmata. Semi-thick sections (250 nm) were used to visualize fine connections between IH and pit fields. Therefore, resolution of individual plasmodesma was reduced. **(A,B)** Two views of IH with fibrillar extensions towards pit fields. Note that the section just grazed the tip of the hypha in (A). Bar = 300 nm (A), 800 nm (B). **(C)** An IH pressed against the cell wall at a pit field. Bar = 500 nm.

(D) Ultra-thin section (80nm) of an IH that had traversed the host cell wall beside a plasmodesma (arrow). Bar = 1 μm.

Figure 2.7 Images relating to plasmodesmata and cell-to-cell movement.

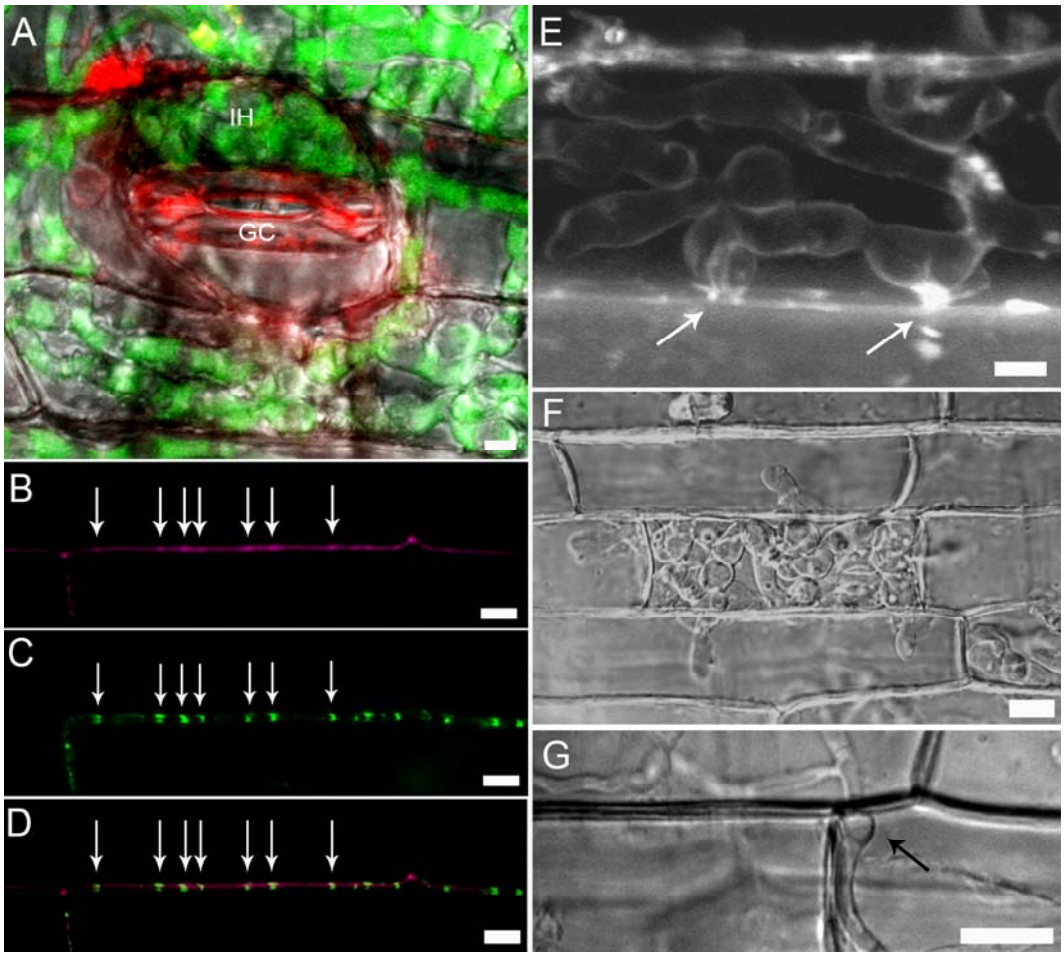

(A) IH (green) packed into a subsidiary cell failed to invade the neighboring guard cell. Plant membranes were stained with FM4-64 at 48 hpi. This image is a projection of 10 optical sections, each 1 µm thick. GC = guard cell. Bar = 5 µm.

(B-D) Co-localization of GFP-labeled TMV movement protein and FM4-64 spots identify pit fields (arrows) in epidermal walls. **(B)** FM4-64 fluorescence (purple); **(C)** MP-GFP fluorescence (green); and **(D)** merged channels. Bars = 10 µm.

(E) FM4-64 staining (white) of an IH at 36 hpi showed EIHM that appeared continuous with the membranes in pit field regions. EYFP and bright field channels are not shown in order to highlight the FM4-64 pattern. The left arrow indicates an IH with two adjacent membrane

connections, and the right arrow indicates an example where the EIHM appeared continuous with membrane in the adjacent cell. Bar = 5 μm.

(F-G) An *alb*$^{-}$ mutant that fails to produce the high pressure needed for appressorial penetration crosses internal walls normally. DIC images **(F)** and **(G)** show infection at 38 and 42 hpi, respectively. Arrow indicates swelling before movement. Bars = 10 μm.

Figure 2.8 PCR or genomic DNA from fungal transformants with TMV-MP fragment.

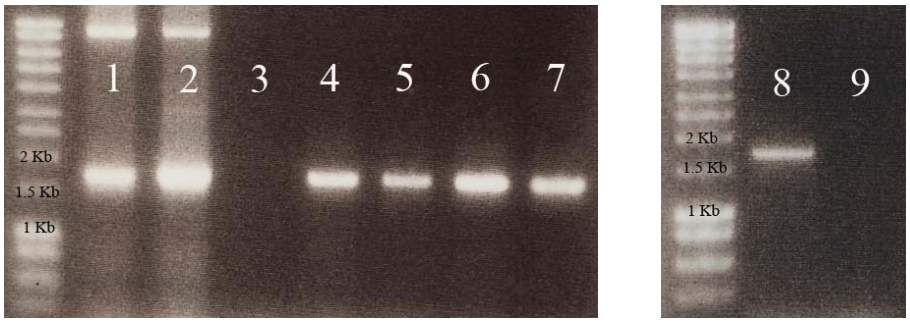

(1) pBV158, **(2)** pBV159, **(3)** empty well, **(4-6)** transformants with pBV158, **(7-8)** transformants with pBV159, **(9)** wildtype. The expected band size in the positive transitive transformants is ~ 1.6 kb (TMV_MP::GFP::Terminaotr). All the transformants had the expected band. The positive controls were the vectors and the negative control was the wildtype strain. The controls behaved as expected. The band sizes of the ladder are indicated.

Figure 2.9 Viability and morphology of IH in invaded rice sheath cells.

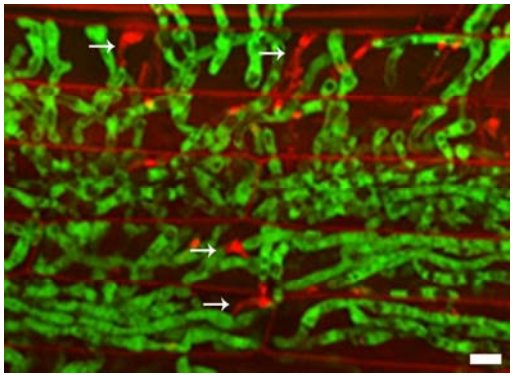

Propidium Iodide staining (red) identifies dead IH (arrows) among EYFP-expressing IH (green) in infected leaf sheath cells at 55 hpi. Bar = 10 µm.

Figure 2.10 Lead colonization at later stages of infection.

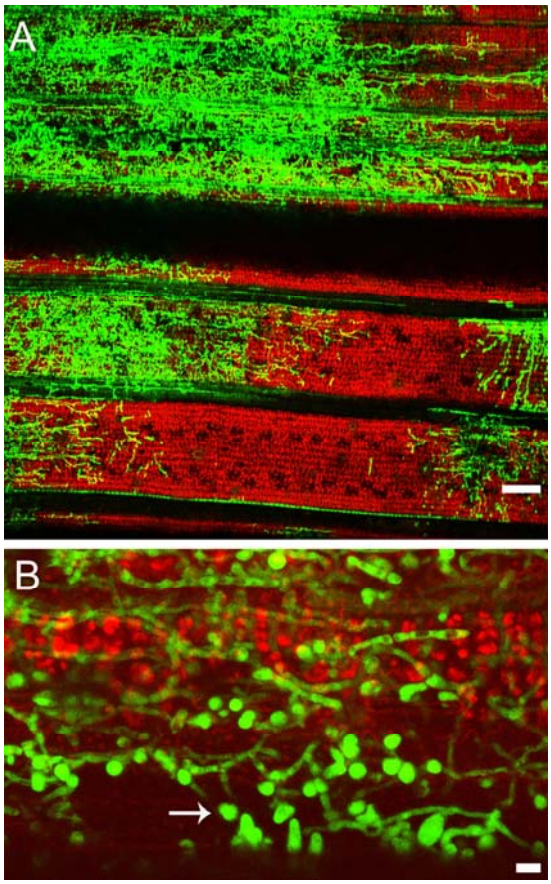

Swelling (arrow) of IH (green) indicates biotrophic invasion in rice leaves at 75 hpi. **(A)** 5x magnification of a drop-inoculated leaf and **(B)** 40x magnification of an area in (A). Image (A) is a projection of 24 optical sections of 3 µm intervals, and image (B) is a projection of 13 optical sections of 1 µm intervals. The red color is chloroplast autofluorescence. Bars = 50 µm and 10 µm respectively.

Figure 2.11 Excised leaf sheath infection assay inoculation and processing of sections.

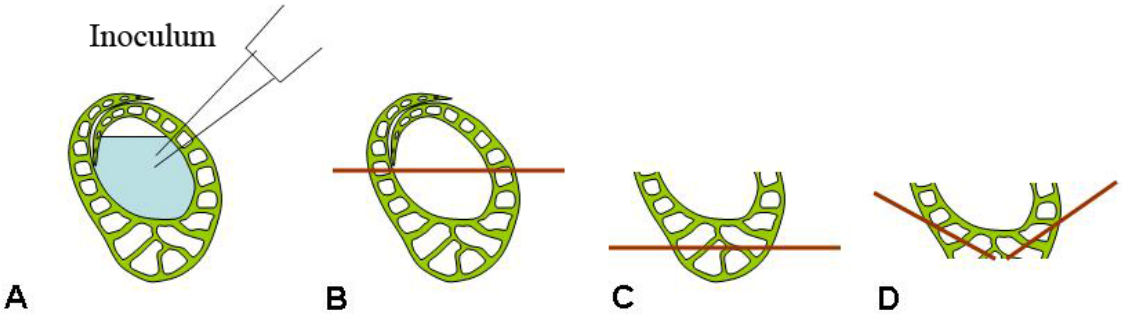

(A) Transverse view of a leaf sheath indicating the method of inoculation with fungal spores.

(B-D) The brown lines indicate the cuts for hand trimming the leaf sheaths for microscopic observation.

Table 2.1 Viability of rice cells invaded by the *AVR-Pita*-containing rice pathogen KV1 in compatible and incompatible interactions.

Rice variety	Plasmolysis[a]	No Plasmolysis[a]
YT-16 (*pi-ta*)	**120 (100%)**	**0**
Yashiro-mochi (*Pi-ta*)	**2 (100%)**	**98**

[a] Number of first-invaded epidermal cells (at 27 hpi) that plasmolyzed in 0.75 M sucrose. For all rice cells that plasmolyzed, the percentage of cells in which the IH were included within the shrinking protoplast is shown in parentheses.

Table 2.2 Comparison of blast hyphal types involved in biotrophic invasion of rice

Biological Features	Primary Hypha[a]	Bulbous IH[a]	Filamentous IH[a]
Growth Style:	Filamentous	Pseudohyphal and Filamentous	Filamentous
Hyphal Diameter:	3 to 5 μm	>5 μm	3 to 5 μm
Differentiates From:	Appressorial penetration peg	Primary hypha or filamentous IH	IH peg that crosses internal walls
Internalizes FM4-64:	YES	NO	NO
Has Membrane Cap:	YES	NO	YES
Viability Maintained During Lesion Formation:	NO	YES	YES

[a] Primary hyphae differentiate into bulbous IH as described by Heath et al. (1990). Bulbous IH include the pseudohyphal forms in the first-invaded cell and the enlarged filamentous to pseudohyphal forms in subsequently-invaded cells. Filamentous IH are the thin transient hyphae that grow in cells directly following crossing of internal walls.

CHAPTER 3 - Gene Expression Profiling of the Blast Biotrophic Hyphae using Laser Microdissection Technology

Abstract:

Magnaporthe oryzae is a hemibiotrophic fungus that causes rice blast disease. The fungus enters the host and initially forms a primary hypha that differentiates into biotrophic bulbous invasive hypha (IH) and grows intracellularly. This differentiation is critical for disease, but the molecular basis for this event remains unknown. Our attempts to study the gene expression profiles in the primary hyphae was challenging due to the low abundance of primary hyphal RNA in hand-trimmed and cryosectioned sheath tissue. In order to enrich fungal RNA at the early biotrophic stages, we optimized Laser Microdissection (LM) technology. We employed P.A.L.M. (Positioning Ablation Laser Microdissections) technology to isolate and purify biotrophic hyphae at 34 hours post inoculation (hpi). Using LM technology, we developed methods to extract good quality RNA that could be used for gene expression profiling after two rounds of linear amplification. Gene expression profiling with whole genome *M. oryzae* microarrays identified 1,720 genes that were up-regulated in IH relative to mycelium, and 2,493 genes that were down-regulated. *AVR-Pita* and *PWL2*, the two previously known infection specific genes, were up-regulated in our data set. The up-regulated genes were enriched for predicted secreted proteins which might play a role in controlling the plant processes during infection. We confirmed that several up-regulated genes were infection-specific. Mutational analyses with two of these did not yield a visible pathogenicity phenotype. The genes identified in our analysis overlap with the genes identified previously using hand-trimmed leaf sheath samples at 36 hpi. Our results indicate that LM can be used to produce reliable data in the rice blast pathosystem. Thus, LM technology can be used to understand the fungal and plant processes and their interactions during pathogenesis.

Introduction:

Rice Blast disease continues to pose a threat for rice production globally. The causal agent, *Magnaporthe oryzae*, is a filamentous ascomycetous fungus. Fungicides are used to control the disease in several parts of Asia with Japan being the largest user. The current available fungicides act as melanin biosynthesis inhibitors, as protein biosyntheis inhibitors and act on membrane phospholipids (Froyd and Froeliger, 1994). However fungicide control is not the most efficient disease management strategy in most rice growing areas for several reasons such as the higher chemical value compared to the rice crop itself, variable disease severity and lack of technical support. In addition this method is not preferred due to the environmental issues involved (Froyd and Froeliger, 1994). The other common strategy for disease control is to deploy blast resistant rice varieties with major resistance (*R*) genes as well as minor genes / QTL's (Quantitative Trait Loci) (Ou, 1980). Achieving durable blast resistance has been a challenge for blast researchers because the fungus is highly variable in the field (Kim et al., 2001). Thus, it has been a continuous battle for the breeders to find more sources of resistance for this disease. To date approximately 50 rice blast resistance genes have been identified. Extensive searches for fungal avirulence genes / effectors has so far resulted in cloning only five of them. They are *PWL1* (Kang et al., 1995), *PWL2* (Sweigard et al., 1995), *AVR1-CO39* (Farman and Leong, 1998), *AVR-Pita* (Orbach et al., 2000), and *ACE1* (Böhnert et al., 2004). *AVR-Pita* encodes a secreted 223-amino acid protein, a putative zinc metalloproease, and it has been shown to directly interact with its corresponding *R* gene, *Pi-ta* (Jia et al., 2000). *ACE1* corresponds to the *Pi33 R* gene in rice and encodes a polyketide synthase - non ribosomal peptide synthetase (Böhnert *et al*. 2004). *PWL2* and *AVR-CO39* encode unknown small proteins with signal peptides. Of the five known *AVR* genes only *AVR-Pita* is known to behave like a fungal effector protein that is secreted into the host cell.

To advance the field of blast research towards efficient disease control strategies, it is important to understand and integrate all the aspects of the disease – host, pathogen and environment. The pathogen's strategy for causing disease is an important aspect that will lead to understanding of critical host-pathogen interaction mechanisms. The cell biological aspects

revealed important pathogen mechanisms for host penetration and cell-to-cell movement. The appressorium generates a melanin layer in its cell wall to generate the enormous turgor pressure to penetrate the host cell wall (Howard and Valent, 1996; Talbot, 2003). Recently, we discovered that the blast IH appear to co-opt plant plasmodesmata to facilitate cell-to-cell movement (Chapter 2; Kankanala et al., 2007). The former finding led to the discovery of fungicides that efficiently block melanin biosynthesis, which renders the fungus incapable of invading the host. The later finding has opened a new dimension of research for plant-microbe interactions that could some day lead to novel control mechanisms. Mutational analysis studies have identified several genes that block appressorial structure and function (Talbot, 2003). Search for *M. oryzae* genes involved in the switch from biotrophy to necrotrophy has been futile to date. Kankanala et al. (2007) reported that the sequential rice cell colonization is biotrophic. The predicted switch from biotrophic to necrotrophic switch was not detected. Studying the molecular basis of the biotrophic growth phase will give better insights into the disease colonization strategies.

The recent release of the genome sequence of the fungus (Dean et al., 2005) as well as rice (Project, 2005), has made gene expression profiling studies with microarrays feasible. Microarray analyses of infected whole plants have identified few fungal genes (Chapter 1). Recently Mosquera et al. (2007) developed a leaf sheath assay method enriching the biotrophic hyphae up to 20% enabling efficient microarray analysis. They reported several highly induced genes which are hypothetical proteins with predicted signal peptides. These are potential candidates for effectors. It has been hypothesized that the blast fungus secretes effectors into the host cell (Jia et al., 2000). Kankanala et al. (2007) suggested that the fungus secretes effectors into the host cell and 'prepares' it for invasion. In order to study the gene expression temporally and spatially, it is essential to purify the RNA from the specific hyphal and host cells separately for expression analysis. Laser microdissections (LM) have been used in plant-pathogen systems recently to study the molecular basis of disease (Tang et al., 2006; Ithal et al., 2007). LM technology can be utilized to isolate and purify IH in infected rice cells from the rest of the rice tissue for gene expression analyses. It is also possible to isolate the rice cells surrounding the infected cells and study the changes in gene expression. This will give valuable insights into the mechanisms and strategies that the fungus employs to manipulate and control host cells.

In this work we attempted to study the gene expression analysis at very early stage of infection (26 hpi) when the penetration peg grows into the primary hyphae with prominent membrane caps and differentiates into bulbous IH. We also applied the P.A.L.M. (Position Ablation Laser Microdissection) technology to purify the fungus at 34 hpi in the leaf sheath tissue. This corresponds to the biotrophic stage of the fungus in the first invaded cell. Kankanala et al. (2007) reported that the IH exhibit a time dependent switch in its growth pattern between 32 – 34 hpi. Using LMs we purified the fungus to ~ 95% as opposed to ~ 20 % in the previous analysis by Mosquera et al. (2007). We optimized the various steps in the protocol for implementing the LM technology. These include the fixation method, orientation of the sample for optimal cryosections, processing the slides for laser cutting and catapulting, RNA extraction kits, and RNA linear amplification. The two infection specific genes *AVR-Pita* and *PWL2* were up-regulated under infection. This served as good internal control for the experiment. The results from this experiment were consistent with the results obtained in the previous study (Mosquera et al., 2007), which demonstrated the efficiency of this technology in studying the rice blast pathosystem. We validated the expression of several genes that were identified in this study. These results are detailed in the chapter along with functional analyses of two of the biotrophic IH-specific pathogen genes.

Results:

Gene expression analysis studies of primary hyphae in leaf sheaths at 26 hpi:

The penetration peg enters the host and forms the primary hyphae by 26 hpi. These primary hyphae must differentiate into bulbous IH for successful infection. The AVR-Pita and PWL2 proteins are secreted into the membrane caps formed at the tip of the primary hyphae (Berruyer et al., Unpublished results). Therefore it is likely that gene expression profiling at this stage will potentially identify secreted effector proteins. Although Mosquera et al. (2007) were able to perform microarray analysis with IH at 34 hpi in trimmed sheath tissue, these contain

biotrophic IH RNA rather than primary hyphal RNA. Therefore, we further purified epidermal cell layer with growing primary hyphae by cryosectioning sheath samples. The protocol for this sampling is indicated in the flow chart (Figure 1). Infected leaf sheaths were viewed under the microscope for good infection around 26 hpi and the spores, germ tubes and appressoria on the surface of the leaf sheath were removed using q-tips. We tested the effect of fixatives and sucrose infiltrations on the quality of RNA. We used ethanol:acetic acid (3:1) and 100% acetone as the fixatives. The EYFP in the fungus quenched very rapidly with the ethanol:acetic acid fixative. With 100% acetone, the EYFP intensity was reduced, but it was still possible to identify the fungus *in planta*. Retaining EYFP was important for the future laser microdissection experiments. For this reason and because acetone was previously used as a fixative to successfully extract RNA for gene expression profiling (Asano et al., 2002; Tang et al., 2006), we used acetone as the fixative for all the experiments. Sucrose infiltrations maintain better morphology with coagulative fixatives (Nakazono et al., 2003). We studied the effect of sucrose infiltrations together with the acetone fixative on the quality and quantity of RNA. Leaf sheaths were trimmed one piece at a time immediately followed by fixation and sucrose infiltrations. One set of hand-trimmed sections was fixed in acetone for 45 seconds. The other set of samples, was fixed in acetone for 45 seconds and immediately infiltrated with 10% ice cold sucrose made with 1x PBS in DEPC water for 15 minutes. The samples were then transferred to 20% and finally to 30% ice cold sucrose solutions for 15 minute infiltrations in each. All the samples were embedded in TFM and quick frozen in liquid nitrogen. Twenty micron thick cryosections of the epidermal layer were collected in 1.5 ml tubes. These were frozen in liquid nitrogen and stored at -80^{o}C until RNA extraction. Cryosections were smoother and the morphological features were better preserved in samples with sucrose infiltration when compared with the other samples. Before RNA extraction we homogenized the tissue using different methods as indicated in the flowchart (Figure 2). We used sterilized 0.5 mm zirconia/silicon beads (Cat # 11079105z; Biospec Products) for one set of samples and RNase free pestles for another set of samples to compare the two methods. We also studied the effect of heat treatment for homogenizing the tissues in combination with the above two methods. The beads were sterilized in 1% bleach solution and washed with DEPC water three times before use. Samples were vortexed with beads for a minute and centrifuged for 5 minutes at 13,000 rpm. The supernatant was collected in fresh tubes and incubated at 42^{o}C for 30 minutes before RNA extraction. The second set of samples

was homogenized with pestle for about a minute and centrifuged as above. The supernatant was heat treated for 30 min at 42^{o}C prior to RNA extraction. The third set of samples was homogenized with pestle without heat treatment. The samples were centrifuged as mentioned above and the supernatant was used for RNA extraction with the Ambion RNAqueous®-Micro kit.

The RNA yields were higher with the acetone and sucrose infiltration combination compared to acetone alone (Figure 3). The pestle method of homogenization proved to yield higher quantities of RNA than the beads. To check the quality of the RNA, we obtained Bioanalyser profiles using a nanochip (Figure 3). The profiles indicated that the heat treatment damaged the RNA. The combination of acetone with pestle and heat treatment yielded higher amounts of RNA than the same treatment with sucrose infiltration. This could be an artifact of the heat treatment or sample variability. The best quality RNA was obtained with Acetone fixation followed by sucrose infiltrations and pestle homogenization without heat treatment. We used this combination for further experiments.

The RNA samples were shipped to Agilent technologies (Delaware) for linear amplification and microarray hybridization experiments. The RNA samples were subjected to two rounds of linear amplification using the Epicenter TargetAmp^{TM} 2-Round Aminoallyl-aRNA Amplification Kit 1.0. The control RNA samples for this experiment were RNA from mycelia grown in 3-3-3 media and RNA from mock inoculated rice leaf sheath samples. The controls were also amplified to avoid any bias due to linear amplification. A starting of 100 pg total RNA was used yielding several micrograms of RNA (Table 1).

In order to have the appropriate ratios of fungal to plant RNA in the control samples, we used RT-PCRs to semi-quantify the amount of fungal to plant RNA in the infected samples. We initially determined the optimal number of cycles for the PCR by amplifying the fungal actin transcript with different numbers of cycles. As indicated in Figure 4A, after 25 cycles a faint band appeared which became brighter after 28 cycles. Thus, we decided 26 cycles would be optimal to run the reaction for determining the fungal to plant ratios in the infected samples. We used standard mixtures of fungal RNA to plant RNA ratios corresponding to 5:95, 10:90, 15:85

and 20:80 to estimate the ratio of fungal to plant RNA in the 26 hpi aRNA samples. After 26 cycles the fungal actin band in all the standards appeared with similar intensity (Figure 4B). The band in the infected sample was much fainter than the standards (Figure 4B). The plant actin band in the infected samples was much brighter than the standards (Figure 4C). The band pattern in the infected samples showed more plant compared to fungal RNA, which was expected. However, in the standard samples we expected the fungal actin band to get brighter as the fungal RNA concentration increased and the plant actin band to get fainter as the plant RNA concentration decreased. We did not observe this pattern (Figure 4B and 4C) suggesting 26 cycles were too many for the standards. Therefore, we set up another PCR with 23 cycles to amplify fungal actin in the standards and the infected sample. This time we saw the expected banding pattern in the standards with the increasing band intensity with the increasing fungal RNA concentration (Figure 4D). However we did not observe any band amplify in the infected sample with 23 cycles. When this reaction was continued to 26 cycles we saw the expected band in the infected sample (Figure 4D). These results suggested that the amount of fungus in the 26 hpi samples was less than 5%.

RT-PCR with the 26 hpi samples to check for fungal *AVR-Pita* expression as the positive control failed several times (Figures 4A, 5A). The possibilities for the failure could be a bias in the linear amplification process where low abundance transcripts did not amplify properly, or RNA degradation during shipping or freeze thaw cycles, or variability in the sampling. We used RT-PCR to amplify *AVR-Pita* and *PWL2* in the RNA samples before linear amplification, but did not detect the expected band (Figure 5B). The actin band amplified in these samples indicating the presence of fungal RNA. Therefore, failure due to bias in the linear amplification process as well as shipping and handling issues was less likely. We extracted RNA from two other biological replicates and did RT-PCR to amplify *PWL2* and *AVR-Pita* genes. In both the replicates, *PWL2* gene amplified as a faint band, but *AVR-Pita* gene failed to amplify (Figure 5C-D). Previous work done with *AVR-Pita*::GFP and *PWL2*::GFP translation fusion constructs showed that this gene was expressed at this early time point (Berruyer et al., Unpublished results). Since we did not see the transcripts for *AVR-Pita* and *PWL2* amplify satisfactorily in the RT-PCR with the three biological replicates, we concluded that the samples had very little fungal RNA to conduct microarray experiments for gene expression profiling. Our attempts to enrich

primary hyphal RNA in cryosectioned samples, thus proved challenging. Therefore, LM technology was most appropriate to achieve this goal.

Laser Pressure Catapulting Microdissections (LPC):

We used the P.A.L.M. (Positioning Ablation Laser Microdissections) from Carl Zeiss (Germany), which utilizes LPC (Laser Pressure Catapulting) technology for isolating individual cut cells (Figure 6). The critical steps in optimizing the LPC technology for the leaf sheath samples included ability to obtain cryosections that retain considerable morphology, a fixation method that retains EYFP expression in the IH to identify the infected cells, slides with good adhesion properties that retain the cryosections during washing, an efficient method to collect and pool the isolated cells and a successful RNA linear amplification process. In order to standardize the system, we used infected leaf sheath samples at 34 hpi when the first infected rice cell is filled with IH, because the amount of fungal RNA is higher. In the previous experiments we optimized the fixation and sucrose infiltrations steps to acquire cryosections that maintain good morphology and retain good EYFP in the IH.

Cryosection / Cryojane Tape Transfer System:

We used the inner epidermal layer of rice leaf sheaths for our experiments to describe the biology of IH (Kankanala et al., 2007). We adapted the cryo-preservation technique for our samples based on the earlier reports that the cryo-preservation was superior to the paraffin embedding method for generating RNA (Asano et al., 2002; Ramsay et al., 2004; personal communication with technical experts at P.A.L.M. Zeiss, Germany). Rice tissues have abundant silica in their cell walls and the epidermis has a waxy cuticle coating on the outside making it a brittle layer. These features posed challenges for mounting the sections smoothly onto the slides. We mounted the sections on different kinds of slides, for example, charged slides and superfrost slides (Fisher Scientific). In the downstream washing steps prior to laser microdissections, 80% of the samples detached from the slides and washed away. Among the sections that remained on

the slide, several of them were compressed or wrinkled. This happened because, as the sample came closer to the epidermal layer while sectioning, the waxy coating on the epidermis caused sections of uneven thickness. Additionally the epidermal leaf sheath layer is curved in nature. Thus in the sections, there was a combination of epidermal and underlying mesophyll layers. The mesophyll layer often has air spaces. While mounting the sections onto the slides these two features, wax and air spaces, caused the wrinkled mounting. The unevenness rendered proper laser cutting difficult. We adapted the cryojane tape transfer system (Instrumedics Inc, Cat# 475205) to retrieve flat, wrinkle free and uncompressed sections. The adhesive slides in this system had enhanced ability to retain the samples during the downstream washing steps. This system works by sectioning the sample on to flat adhesive tapes, followed by transfer of the sections from the tape to adhesive slides by UV pulse treatment. The key to obtaining good sections is to maintain the slides and the tape window at -20^{o}C. Care must be taken to avoid thawing the samples when working with gloved hands.

The adhesive slides are available in 1x, ½ x and 4x thickness. The difference in these three kinds is the amount of adhesive on the slide as indicated by the numbers. Usually slides with more adhesive are used for brittle tissues like bone, hair, etc. We tried mounting infected rice leaf tissues onto all the three types of slides. The transfer was not very efficient with 4x slides. The ½ x slides worked better for transfer over 4x slides. However, several sections still remained on the adhesive tape window after transfer on to ½ x slides. The 1x slides proved to be the best for our tissues. Typically, the transfer rate with 1x slides was 100%. The cryojane tape transfer system is designed to use one adhesive tape window per slide. To make the process cost efficient we cut each adhesive tape window into two. We transferred 3 to 4 sections onto each slide. The Robo mover on the P.A.L.M. machine used for laser catapulting is designed to access the central region of the slide. The extreme ends of the slides are out of the range for the system. Thus the sections were transferred onto the slides avoiding the ends of the slide as shown in Figure 7.

Loading the sample onto the cryostat chuck for cryosections:

The TFM is made into a base on the cryostat sample holder before loading the sample by placing some TFM on the sample holder and freezing it. The tisuetek block is trimmed with the cryostat blade to make a flat base. This base must be larger than the sample that will be loaded on to it. The sample is loaded onto the holder such that the tissue is at an angle to the knife as shown in figure 8. The block is trimmed into a trapezoid to allow smooth sectioning. We examined the efficiency of sectioning when the samples were loaded with the epidermal layer facing the sample holder as well as facing away from the sample holder. When the epidermal layer faced away from the sample holder, the first sheath layer that the blade hits was the epidermal layer. The probability of missing the first couple of sections, which contained our desired fungal material was high. Therefore, we loaded the sample with epidermal side facing the sample holder for sectioning. In this position, sometimes the sections have the epidermal layer continuous with the underlying mesophyll layer. Nevertheless, it was much easier to retrieve the epidermal layer with the desired fungal cells. The efficiency of transferring the sections from the adhesive tape windows to the slides was lower when the epidermal layer was facing away from the sample holder when compared to epidermal layer facing the sample holder. This could have been due to the differential properties of the outside (has waxy cuticle layer on the outside) and inside of the epidermal layer.

RNA extraction from the cryosections:

We checked the quality of RNA from cryosections processed by the methods we planned to use for LCM. Four to five cryosections of 18 µ thickness were collected into 1.5 ml tubes. The tubes were frozen in liquid nitrogen and stored at -80^{o}C until RNA extraction. We used sterilized beads for RNA homogenization due to the unavailability of the pestle at the time of this experiment. The sections were vortexed with the beads in lysis buffer for a minute. The samples were centrifuged and the supernatant was transferred to fresh 1.5 ml tubes. RNA extractions were done using Qiagen RNeasy Micro kit (Catalog # 74004; Qiagen) and PicoPure™ RNA Isolation Kit Catalog no # KIT0204; Arcturus) as per the manufacturers' instructions. The RNA concentration obtained with the RNeasy Micro kit was 3.4 ng/µl and with the PicoPure kit was 3.0 ng/µl. The quality of the RNA was checked by running the samples on the Agilent 2100

Bioanalyser using a pico chip (Figure 9). The quality of the RNA samples extracted with Qiagen kit was more satisfactory than that with Picopure kit. Since the quality of RNA was satisfactory, we proceeded with laser catapulting.

RNA extraction from LCM samples:

Several micrograms (5 to 7 µg) of RNA is required to conduct microarray hybridizations. In order to generate such high amounts, RNA obtained from the laser catapulted cells is subjected to two rounds of linear amplification. The infected rice leaf sheath cells at 34 hpi were visualized using a EYFP filter and marked using PALM Robo software (Figure 10). The cells were cut with a focused laser and catapulted with a defocused laser into two adhesive caps. One cap had 115 cells catapulted over a time period of 3.5 hours and the other had 75 cells catapulted over 3 hours. The RNA was extracted and taken through the first round of linear amplification using the TargetAmp 2-Round Aminoallyl-aRNA Amplification Kit 1.0. The aRNA (amplified RNA) was quantified using the Nanodrop Spectrophotometer to check the efficiency of the linear amplification process. We used mycelial RNA diluted to 200 pg as the control for linear amplification as well as the HeLa RNA provided with the kit. The HeLa RNA amplified from 200 pg to 548 ng. The mycelial RNA amplified from 200 pg to 1.7 µg. The two LCM samples had 84 ng and 104 ng RNA in the samples. Since the first round did not work efficiently with the LCM samples, we did not do the second round amplification. We checked if the amplification failed due to lack of initial RNA or due to poor quality RNA. We generated cDNA from the aRNA generated from first round of linear amplification and did PCR to amplify fungal actin and fungal *AVR-Pita* genes. The LCM samples amplified both the bands indicating the presence of RNA (Figure 11) in the samples. However, the bioanalyzer profiles indicated poor quality RNA (Figure 12). Bioanalyzer uses the microfluidics technology combining electrophoreses and flow cytometry. The components are separated based on size and the cellular components are detected by their fluorescence.

RNA for microarray hybridizations:

To improve the quality of RNA we reduced the amount of time spent for catapulting cells into each cap. We processed one slide at a time (as described in the materials and methods section) and catapulted cells into adhesive caps for no more than 60 min. The cells were suspended in lysis buffer and centrifuged to collect them at the bottom of the tube. These were immediately quick frozen in liquid nitrogen and stored at -80^{o}C until ready for RNA extraction. We catapulted two sets of 140 cells and did RNA extraction in two batches. Based on the suggestions from colleagues doing similar experiments, we used the Ambion RNAqueous®-Micro kit for RNA extractions. In comparison to other kits the quality of RNA extracted with Ambion kit was known to be better (Personal communication with Epicentre Biotechnologies Inc.). The RNA was eluted in 20 µl elution buffer provided with the kit. This was reduced to 4 µl by speed vacuuming and split into two sets of 2 µl each, which were used for linear amplification. The RNA yields after two rounds of linear amplification ranged from 9 µg to 39 µg total. The quality of this RNA was analyzed to be satisfactory on the Agilent bioanalyser nano chip (Figure 13). This RNA was used at Agilent for microarray hybridizations.

Microarray Hybridizations and Data Analysis:

The *M. oryzae* oligonucleotide microarray (Agilent Technologies) was used to hybridize the PALM sample. This array represents 15,170 *M. oryzae* genes and 6,325 rice genes. This is a DNA oligo chip with 60 base pair oligo probes. The complementary RNA samples were labeled with Cy3 and Cy5 dyes and hybridized to the chip (Figure 14). The control for this experiment was linear amplified RNA from mycelia grown in 3-3-3 medium in liquid cultures. The data was analyzed with Rosetta Resolver® (Figure 15). Four technical replicates were done with dye swaps for this experiment. In IH, 1,740 genes were >3-fold up-regulated and 2,493 genes were >3 fold repressed when compared with mycelial samples. The 50 most up-regulated and 50 most down-regulated genes are listed in tables 2 and 3 respectively. In order to validate the results, we picked up 10 genes with a varying range of fold change (28- to 126- fold up-regulated) to do RT-PCRs. We picked up genes expressing hypothetical as well putative proteins (Table 4). *AVR-Pita* and actin were included as positive controls. All the genes we tested were infection specific (Figure 16).

Up-regulated genes:

At 34 hpi several genes were up-regulated in IH indicating they were infection specific. The known *in planta* infection specific avirulence genes *PWL2* and *AVR-Pita* were up-regulated 62-fold and 34-fold respectively in our samples. The other known avirulence gene *AVR-CO39* was not included on this microarray. Among the 1,740 genes that were up-regulated 3-fold and above, 63 % of the genes encoded hypothetical proteins and 9%, predicted proteins. The appressorium specific gene, *ACE1*, was not identified in this gene set. *ACE1* encodes a polyketide synthase/non-ribosomal ribosomal peptide synthetase (PKS/NRPS). The *M. oryzae* genome has 8 predicted PKS-NRPS genes (Dean et al., 2005). We identified another putative PKS-NRPS, AMG13133 that was highly up-regulated (62 fold). Only 5% of >50-fold up-regulated genes had EST hits in the genome databases compared to 30% of >50-fold down-regulated genes (Table 6). Similarly, when we compared the percentage of genes with ESTs among the >10 fold up-regulated and >10-fold down-regulated genes, the number of EST hits were higher in the down-regulated gene set. Among the >50-fold repressed genes, 80% encoded hypothetical proteins and among the 10- to 50-fold repressed genes 79% encoded hypothetical proteins. Although a high number of these genes were hypothetical proteins, 30% of these genes had EST data. This was three times higher than the percentage of genes with EST's in >10 fold up-regulated set (9.6%; Table 5). This indicated that the induced genes were highly specific for the early biotrophic growth stage and weren't identified in earlier studies.

M. oryzae has a large secretome with 796 predicted secreted proteins in the genome (Dean et al., 2005). As reported in Mosquera et al., (2007), we have observed that a large number of the up-regulated genes had the predicted signal peptide indicating they were secreted into the host cells. In the >50-fold up-regulated gene set, 24% were secreted proteins. Among the 10- to 50-fold up-regulated genes, 16% were predicted secreted proteins and among the 3- to 10- fold up-regulated genes 6% were predicted secreted proteins (Table 5). Thus, there were significantly higher secreted proteins among the highly induced genes. Among the total 166 predicted secreted proteins, very few had a predicted function. *AVR-Pita* and *PWL2*, the two known avirulence

genes with predicted signal peptides were identified in the 10-fold and above induced gene set. Among the other genes in this group were predicted laccase, serine protease, endochitinase, β-xylosidase, cellulase, carboxy peptidase, alkaline phosphatase and β-1,3-endoglucanase. The secreted proteins with putative functions in the 3- to 10-fold induced genes included predicted ribonuclease, Est A, Endo 1,4 – β xylanase, extracellular chitinase, cyclosporine synthase, acid phosphatase, K12H4.7 protein, β-1,3 – exoglucanase and secretory aspartyl protease. Thus, among the total 166 predicted secreted proteins only 19 had predicted functions. This indicated that a large number of these predicted secreted proteins were very specific to this fungus. The location of the secreted proteins did not have any specific pattern nor were they in clusters in the genome. Among the >50-fold up-regulated genes the location varied among chromosomes I, II, III, IV,V, VI, VII, and UNK (Table 3).

Regulation of previously known pathogenicity genes:

Earlier studies have identified genes that played a role in pathogenicity although most of these genes were expressed outside the host. The *BUF1, RSY1* and *4HNR* genes involved in the melanin biosynthetic pathway, were expressed in appressoria during host invasion (Talbot, 2003). Our cell biology studies indicated that the melanin biosynthetic mutants were fully capable of IH growth (Chapter 2). Hence, we predicted that these genes would be down-regulated. All three genes were down-regulated in the IH (Table 3, 6). The other genes involved in appressorium structure and function, such as *PTH11*, *MPG1*, *MAGA*, *CALM* and *ACL1* were also down-regulated (Table 6). *PMK1*, encoding a MAP kinase, and the *MST12*, a transcription factor downstream of *PMK1*, were not changed significantly. The vacuolar serine protease, *SMP1*, also did not change its expression significantly. The alternate oxidase gene, *AOX1*, involved in oxidative stress with a potential role in appressoria was down-regulated in IH (Avila-Adame and Koller, 2002).

Gene Knockout Experiments:

The highly up-regulated genes in IH were mostly hypothetical proteins with predicted signal peptides suggesting that these might be secreted into the host cell. These are high probability candidates for effectors in the rice blast system. Recent gene replacement studies done with three of the most highly up-regulated hypothetical proteins with signal peptides (Mosquera et al) did not show any phenotypes either in pathogenicity or in axenic cultures. Thus we selected two genes with putative functions for gene replacement studies. AMG05133, a gene predicted to encode a laccase, was 62-fold up-regulated. This gene was confirmed to be infection specific at 34 hpi in RT-PCR experiments (data not shown). The other gene, AMG08210, with protein homology to Bilurubin Oxidase was 78-fold up-regulated. The predicted laccase had a signal peptide prediction indicating that it might be a secreted protein, while the putative bilurubin oxidase did not have a predicted signal peptide. We used a homologous recombination-based gene replacement strategy to characterize these genes (Figure 17).

Putative Laccase Knockout: We cloned 1065 bp upstream of the laccase coding sequence and 1038 bp sequence including 542 bp encoding C-terminal amino acids from the protein and 496 bp downstream from the stop codon separately into pGEMT. A restriction/ligation strategy was used to develop the gene replacement construct consisting of the hygromycin resistance gene flanked by upstream and downstream fragments. The hygromycin gene was under the control of the TrpC promoter from *Aspergillus nidulans*. The gene replacement construct was moved into the pGKO2 binary vector flanked by the left and right borders of the T-DNA. This was transformed into agrobacterium strain, Agl1. Two positive agrobacterium clones BV159 and BV160 were selected to transform the spores of O-137 fungal strain to generate gene knockouts. A total of 125 hygromycin resistant colonies were obtained using the strain BV159 in the second round selection. After 3 days, 108 colonies out of the 125 were selected for further analysis. These were allowed to sporulate on V8 media plates. Two monoconidials were isolated for each of the 108 fungal cultures. The purified cultures were used to screen for knockout strains by PCR using laccase and hygromycin primers (Table 7).

This same procedure was used to transform the O-391 fungal strain with the BV160 agrobacterium strain. The fungus was allowed to grow for 7 days on the co-cultivation plates

before removing the filter papers. Sixty colonies were transferred to second selection plates after 10 days. Three days later 44 of the 60 colonies were selected for sporulation and downstream analysis. DNA was extracted from mycelial mats and PCRs were done with a total of 156 fungal colonies. One positive clone was identified in the PCR (Figure 18) and was confirmed through southern analysis (Figure 19). We did leaf sheath inoculations to assay for any phenotype associated with the mutation. No significant differences were seen when the mutants were compared with ectopic and wildtype strains (Figure 20). The same result was observed in whole plant spray assays where there was no significant difference in the pathogenicity or lesion sizes and shapes in the knockout strain when compared with wild type and ectopic transformants (Figure 21).

Putative Bilurubin Oxidase Knockout: The gene replacement construct was generated by cloning a 897 bp sequence at the 5' end of the gene and a 816 bp sequence downstream from the stop codon flanking the hygromycin resistance gene into the pGEMT vector. The entire fragment consisting of upstream sequence, hygromycin resistance gene and downstream sequence was amplified by PCR and used to transform O-391 protoplasts. After second round of selection on hygromycin, 95 colonies were picked for downstream analysis. These were purified through single spores on 4% water agar plates and grown on oatmeal agar plates. DNA was extracted from mycleial mats for PCR. None of the 95 colonies were identified as positives containing gene replacement mutations.

Discussion:

Our goal was to study fungal gene expression at very early stages of biotrophic infection in the rice blast system. In the previous chapter we described the critical features of the biology of biotrophic IH. The penetration peg develops into primary hypha with a prominent membrane cap at its tip. The primary hypha differentiates into bulbous IH which fills the first-invaded cell. This differentiation is critical for the fungus to establish the disease cycle. The host cells in which the fungus fails to differentiate into IH generally cannot grow much beyond the first-

invaded cell. We predicted that the primary hyphae with membrane caps are enriched in secreted proteins because the AVR-Pita and PWL2 translational fusions with GFP, localized the proteins to the membrane caps (Chapter 1; Kankanala et al., 2007; Berruyer et al., Unpublished results). At 26 hpi, the first-invaded cells have one primary hyphal cell and 1 to 2 IH cells. We developed methods to obtain good quality RNA material at 26 hpi in the leaf sheath assays. However, we had very little fungal RNA represented (< 5%) after two rounds of linear amplification making gene expression profiling difficult. In our sampling protocol, we were not able to check the number of infection sites we were harvesting in the cryosections. Thus, it was possible that we did not have substantial number of infection sites to enrich for the primary hyphal RNA. Our semi-quantitative experiments have shown that these samples have more than 95% plant RNA. RNA generated through this method can used to study the plant responses during the early stages of fungal host interactions.

Due to the challenges in enriching primary hyphal RNA with conventional methods like hand-trimming and cryosectioning, we optimized LPC using the P.A.L.M. Zeiss technology. For establishing this technology we used 34 hpi samples which typically have 30 to 40 IH cells per leaf sheath epidermal cell. This high amount of fungal material would allow us to optimize the system, which could then be used to sample and study earlier infection time points where the fungal RNA is less abundant. We successfully developed methods to obtain high amounts (several micrograms) of good quality RNA after two rounds of linear amplification suitable for microarray hybridizations. We have proven that this technology can be used efficiently with the rice leaf sheath assay system to isolate cells and conduct gene expression profiling studies.

Laser Microdissection technology has been used to isolate cells and study several plant processes successfully (Nelson et al., 2006). However, only two reports are available so far where this technology was successfully applied to study host-pathogen interactions using microarrays. Tang et al. (2006) generated 10 µg aRNA after two rounds of linear amplification from the samples containing 1mm^2 area of tissue, which approximately contained 800 maize stalk sclerenchyma cells. In another study of transcript profiling of soyabean cyst nematode feeding cells in soybean roots, 7 µg aRNA was generated after two rounds of linear amplification from a 1 mm^2 area of plant tissue (Ithal et al., 2007). In our study we generated ~ 25 µg of RNA

from 1.5 mm^2 area of infected tissue which included approximately 140 individually catapulted infected rice leaf sheath cells. These contained approximately 5000 fungal cells.

Mosquera et al. (2007) enriched for IH RNA up to ~ 20 % in infected leaf sheath tissues by hand-trimming and did microarray analyses after one round of linear amplification. With LCM we isolated individual infected cells at the same infection time point. The data set obtained with the LCM samples is consistent with the one generated by Mosquera et al. (2007). This validates the reliability of the laser cutting, RNA extraction and the two round linear amplification processes. This is the first report where IH RNA at 34 hpi was highly purified. We expected to identify a large number of *in planta*-specific fungal genes. The controls for this sample were RNA from mycelia grown in axenic cultures. We did not include any plant RNA in our control samples for microarray hybridizations because we purified the IH RNA and there was very little plant material. As expected, we identified a higher number of genes that were up-regulated 3-fold and above (1,720) when compared with the previous studies (1079; Mosquera et al., 2007). Similarly we identified 2,493 genes 3-fold and above down-regulated as compared to 614 in the other study. Tang et al. (2006) used this technology to study the *Colletotrichum graminicola* – maize interactions. They identified 437 and 370 significantly up-regulated and down-regulated genes respectively. Developmental transcript profiling of cyst nematode syncytial cells in the soybean roots identified 1,116 and 649 differentially up-regulated and down-regulated respectively (Ithal et al., 2007). While Tang et al., used a 2-fold change and Ithal et al., used a 1.5-fold change as the threshold to study the differential expression, we used 3-fold change as the threshold to do the analysis. We have identified a larger set of genes when compared to the two other pathosystems discussed above.

The distribution of hypothetical genes among the up-regulated genes was very similar when compared with the analysis done by Mosquera et al. (2007). The percentage of genes with known EST's remained similar in >10-fold induced genes, but in the range of 3- to 10-fold up-regulated gene set, there were only 19% genes in LCM data set versus 38% in the other study. We were able to efficiently capture genes that had lower levels of differential expression under infection (3- to10-fold). The predicted secreted proteins were 24 % in >50-fold, 16% in 10- to 50-fold and 6% in 3- to 10-fold up-regulated genes. This distribution is also similar to the

previous study except for the >50-fold up-regulated genes, which was 50% in Mosquera et al. (2007). We identified a higher number of genes in this range of up-regulation than identified in the previous study, which may account for the lower percentage of predicted secreted proteins in the LCM data set. It was interesting to observe that a large percentage of these genes were hypothetical/putative proteins. In the down-regulated gene set we identified a total of 2,493 genes that were 3-fold and above down-regulated. A high percentage of these genes had corresponding EST data in contrast with the up-regulated gene set. These results have indicated that we highly enriched the fungal biomass in the samples by using P.A.L.M. microdissections.

We examined relative expression levels of the previously characterized pathogenicity genes (Table 6). Most of these genes either did not change significantly or were down-regulated. Most of these genes were involved in surface sensing, appressorium formation and pre-penetration stages of the disease. We removed all the appressoria and germ tubes on the surface of the leaf sheaths to avoid any contamination from genes of these cell types in our samples. A similar set of genes was identified in work done by Mosquera et al. (2007). The other pathogenicity genes previously identified in the hand-trimmed leaf sheath assays, *MgATP2, ABC1, ABC3, MAGB, MGB1,* and *ACE1*, were not detected in the data set in this study. However we identified *MAGA*, which was not identified previously and as expected was not changed significantly.

Melanin plays a significant role in appressorium maturation and host surface penetration (Talbot et al., 1993; Howard and Valent, 1996). We previously reported that melanin-deficient mutants can form IH that grow from cell-to-cell like wild type fungus (Chapter 2; Kankanala et al., 2007). The melanin biosynthesis genes were down-regulated in our microarray data supporting this conclusion. In another study, gene expression analysis done under nitrogen starvation conditions identified *PTH11, MPG1* and melanin biosynthetic genes (Donofrio et al., 2006). The *SPM1*, serine vacuolar protease was up-regulated in their studies. This suggests that the condition of nitrogen starvation might represent more of the pre-penetration and penetration phases of infection. The transcriptome of IH is very different from the fungus grown under nitrogen starvation conditions. We haven't observed a very high up-regulation of cell wall degrading enzymes. It has been suggested that cell wall degrading enzymes might play a

significant role during colonization of plant tissue (Wu et al., 1995; Wu et al., 2006). We hypothesize that the cell wall degrading enzymes might play a role in later stages of infection in the necrotrophic hyphae growing in regions with macroscopic symptoms.

Another interesting feature was the high occurrence of secreted proteins in the >50-fold induced data set. The over all percentile of secreted proteins in the 3-fold and above induced genes was greater than in the 3-fold and below repressed genes. This suggests that the fungus secretes a large number of proteins into the host cytoplasm to promote the disease. These secreted proteins are potential candidates for effectors in this system. Previous studies done to characterize three of the highly up-regulated genes, AMG8261, AMG8541, and AMG12560 failed to identify any phenotype on the rice cultivar YT-16 (Mosquera et al., 2007). Thus, in this study we did gene replacement experiments to study two genes with a putative function.

Gene replacement studies with the predicted laccase (AMG05133) did not yield any pathogenicity phenotype on YT-16 rice cultivar. The mutant did not have any significant phenotype in conidia and mycelia either. *M. oryzae* has 9 putative laccase encoding genes with copper oxidase domains. Only one of these was up-regulated in the up-regulated gene set. Laccases generally act as oxidoreductases on phenolic substrates. They catalyze one electron oxidations of a wide range of substrates. Laccases are predicted to play a role in fungal morphogenesis as well as host-pathogen interactions (Baldrian, 2006). AMG05133 in *M. oryzae* has a predicted signal peptide. This laccase could be a secreted protein with a potential role in turning down the host defense responses, which usually include phenolic compounds. However, the high level of redundancy of these multicopper oxidase domains in the *M.oryzae* genome, it could explain the lack of significant phenotype in the knockout mutant.

Bilurubin oxidases have been identified in fungi, mammals and bacteria. This group of enzymes has a multicopper oxidase domain like laccase and catalyses the conversion of bilurubin to biluverdin in mammals. The bilurubin oxidase genes of the fungi *Myothecium verrucaria* and *Trachyderma tsunodae* have been well studied. This enzyme has higher affinity towards substrates containing tetrapyrole structures (Tanaka and Murao, 1982; Sakasegawa et al., 2006). Among the compounds having tetrapyrole ring structures are hemin and chlorophyllin (Tanaka

and Murao, 1982). In photosynthetic organisms, chlorophylls contain cyclic tetrapyrrole structures. Interestingly, in our data only one putative bilurubin oxidase precursor was significantly induced. We hypothesized that this enzyme might play a role in degrading the tetrapyrrole ring structures of chlorophyll in the plants. Although there was no predicted signal peptide for this gene, it could be secreted through non-conventional secretion system. Our studies failed to isolate a mutant for this gene. It is possible that this is an essential gene for the fungus. The other possibility could be the position in the genomic location that could make it difficult for recombination.

In a susceptible reaction, generally the appressorium fails to infect the cell in 5 to 20% of the cases (Heath et al., 1990). Thus, whole leaf sheath assays might represent a heterogeneous population of fungal and plant cells. A robust method to isolate homogeneous plant and fungal cells is necessary to understand the susceptible reaction. With our method we successfully isolated homogeneous cells from tissues and produced reliable data. In our work on the biology of the rice blast fungus, the primary hypha looks very similar to the filamentous IH that first enter neighboring cells. Both these hyphal types are anucleated initially (Chapter 1; Kankanala et al., 2007). They accumulate the prominent membrane caps at their growing tips and both of these differentiate into bulbous invasive hyphae. The membrane caps are predicted to be enriched for secreted proteins (Berruyer et al., unpublished data, Giraldo et al., unpublished data). LM technology can be further used to purify these fungal types and study the genes expressed in these hyphae and secreted into the membrane caps. We had earlier hypothesized that the fungus might be controlling the plant processes before its invasion (Chapter 1; Kankanala et al., 2007). In our continuing attempts to understand the molecular basis of this disease we are preparing to isolate the rice cells surrounding the first invaded cell at 36 hpi and study the changes in gene expression. We also propose to isolate the infected host cells at ~ 26 hpi to study the gene expression changes. These will generate critical data to study fungal-host interactions.

Although, we have been successful in generating excellent gene expression profiling at 34 hpi, we had considerable challenges in replicating this experiment. The RNA linear amplification kit has been a major limiting factor thus far. At the time when we did these experiments, only one kit (Epicenter Biotechnologies Inc.) was available in the market that could

generate micrograms of aRNA from picograms of starting material, after two rounds of linear amplification. We successfully used this kit to produce micrograms of aRNA. However, we couldn't reproduce the linear amplification with the same success rate every time. With the rapid increase in the use of LM technology in the recent years, a couple of other RNA linear amplification kits are currently available. We will work to develop a robust and reliable linear amplification process to proceed with our experimental plans. In spite of the current challenges, we believe LM technology is a powerful tool at hand to dissect the molecular plant microbe interactions in the future.

Materials and methods:

Laser Microdissection experiments:

Sample preparation for PALM microdissections:

Leaf sheath inoculations were done as described in the materials and methods section of chapter 2. At 34 hpi the leaf sheaths were scanned for good spread of infection sites using a fluorescent stereomicroscope. Selected samples were hand-trimmed to give 3 to 4 layered sections. The germination tubes and the appressoria were scraped off from the surface of the leaf sheath. The samples were then fixed in 100% acetone for 45 seconds followed by 15 minute infiltrations in 10%, 20%, and 30% sucrose solutions, with each at ice cold conditions. The sucrose solutions were made with 1xPBS in DEPC water. The sucrose solution was removed and individual samples were embedded in Tissue Freezing Medium™ (TFM) (Cat # H-TFM, Triangle Biomedical Sciences, Durham, NC) followed by quick freezing in liquid nitrogen. The samples were then stored at -80^{o}C.

Cryosectioning:

A Leica 3050 S cryotome was used for cryosectioning the samples at -20^{o}C. The embedded samples were mounted on the sample holder by placing a drop of TFM on it and then quick freezing the TFM by spraying cytocool™ II rapid freezing aerosol (Cat # 8323, Ricard-Allan Scientific). The samples were first trimmed using 50 µ sections until the leaf sheath was visible. Once the sample was visible, sectioning was done at 20 µ thickness. The sections were mounted onto cryojane slides (Cat # 475209, Instrumedics Inc.) using the cryojane tape transfer system. The slides were stored in mailer boxes at -80^{o}C until ready for laser catapulting.

Laser Pressure Catapulting:

The laser cutting and catapulting was done with the Zeiss P.A.L.M. (Positioning Ablation Laser Microdissection) microscope. The rice leaf sheath cells containing invasive hyphae were identified by GFP fluorescence and selected using the PALM Robo software. The selected cells were cut using the laser and catapulted into the PALM® adhesive caps (Cat # 1440-0250, P.A.L.M. Micolaser Technologies AG, Germany) with the defocused laser (Figure 7). The UV focus ranged from 70 to 72, the cut energy varied between 60 and 75. More energy was needed to cut the cross walls of the host cells. We used maximum cutting and catapulting speed.

RNA extractions for PALM experiments:

RNA extractions from the PALM samples were done using the RNAqueous®-Micro kit (Cat # 1931, Ambion Inc, Texas). The laser catapulted samples in the lysis buffer were retrieved from -80^{o}C freezer and incubated at 42^{o}C for 30 minutes after adding the LCM additive (provided with the kit). Following the incubation, RNA extraction was done as per the instructions from the manufacturer. RNA was eluted 2 X in 10 µl of elution buffer provided with the kit.

RNA linear amplification:

RNA linear amplification was done with TargetAmp^{TM} 2-Round Aminoallyl-aRNA Amplification Kit 1.0 (Cat # TAA2R4910; Epicenter Biotechnologies Inc, Madison, WI). The instructions from the manufacturer's protocol were followed for the amplification. RNA from the PALM sample was eluted in 20 µl of elution buffer. This was concentrated to 2 ul to use for the amplification step. For the control sample (mycelial RNA), 400 pg was used as the starting material. Every time either a reagent or a mixture of reagents were added to the tube, we mixed it by finger flicking and collected the contents at the bottom of the tube by spinning them in the table top centrifuge (cat # C1200/DW41; Labnet International Inc). Qiagen RNeasy Mini Kit (Cat # 74104, QIAGEN, CA) was used to purify the aRNA as per the instructions in the TargetAmp^{TM} 2-Round Aminoallyl-aRNA Amplification Kit 1.0.

Total RNA extractions for P.A.L.M. controls and gene validations:

Fungal samples were ground in liquid nitrogen and the powder was transferred to 1.5 ml tubes till the 0.1 ml mark. RNA extraction was done using a TRIZOL method. One ml of trizol (Cat # 15596-026, Invitrogen) was added to the tubes and incubated at room temperature for 5 minutes. To each tube, 0.2 ml chloroform was added and the tubes were shaken vigorously for 15 seconds before incubation for 3 minutes at room temperature. The tubes were centrifuged at 9,000 rpm in the cold room (4^{o}C) for 10 minutes. The upper clear aqueous layer was transferred to a fresh tube and 0.25 ml sodium acetate (3M) and 0.25 ml isopropyl alcohol were added in that order. The tubes were mixed by inversion and incubated at room temperature for 10 minutes. The tubes were centrifuged at 9,000 rpm for 10 minutes in the cold room. The supernatant was removed and the RNA pellet was washed twice with 1 ml ice cold 75% ethanol. The tubes were centrifuged for 5 min at maximum speed in the cold room (4^{o}C). The ethanol was removed and the pellet was air dried for 15 to 20 minutes. RNA was dissolved in 20 µl DEPC water and quantified using a nanodrop spectrophotometer (ND-1000, Nanodrop Technologies, Delaware). The quality of the RNA was assessed based on the bioanalyzer profiles (Agilent Technologies).

First strand cDNA synthesis:

Complementary DNA (cDNA) synthesis was done using the Invitrogen™ first strand cDNA synthesis kit (cat # 11904-018). Each RNA sample was mixed with the dNTP mix and random hexamers in a total volume of 10 µL. Samples were incubated at 65°C for 5 minutes and chilled on ice for at least 1 minute. A reaction mix composed of RT buffer, $MgCl_2$, DTT, and RNaseOUT recombinant ribonuclease inhibitor was made and 9 µl of this was added to tube. Samples were mixed, centrifuged, and incubated at 25°C for 2 minutes. One micro-liter of the SuperScript™ II reverse transcriptase was added to each tube except the negative controls. Samples were incubated at 25°C and after 10 minutes, they were incubated at 42°C for 50 minutes, chilled on ice, and centrifuged. One micro-liter of RNase H was added to each sample. Finally, they were incubated at 37°C for 20 minutes and stored at -20°C.

Reverse Transcriptase - Polymerase Chain Reaction (RT-PCR) for microarray gene expression validations:

RT- PCR reactions were done using the DNA Taq polymerase (Cat # M8291, Promega). The reactions were performed in a 25 µL reaction mixture containing 2µl cDNA / genomic DNA, 2 µl 10x buffer, 1.5 µl MgCl2, 1 µl of 10 mM dNTP's, 0.5 µl of each primer (10mM), and 0.2 µl taq polymerase. The thermocycler program was set up to do an initial denaturation of 1 minute. The lid temperature was set up to 95°C. The program had denaturation at 95°C for 30 seconds, primer annealing at 55°C for 30 to 45 sec, extension at 72°C (time 1 minute/kb). This cycle was repeated 30 times followed by a final extension of 5 minutes. Following PCR, 10 µl of the products were run on a 0.8% agarose gel and the DNA bands were stained with ethiduim bromide for 15 minutes and visualized under a UV transiluminator.

Gene replacement experiments:

Gene Knockout Constructs:

Gene replacement constructs were made by a restriction/ligation method in pGEM®-T (Cat # A3600, Promega) cloning vector. Approximately 1 Kb of upstream sequence, or the 5' end of the gene and 1 Kb of downstream sequence, or 3' end of the gene were PCR amplified. The primers were designed to insert the required restriction sites to allow for the cloning. The PCR products were cloned into pGEMT vector. A restriction/ligation method was used to build the upstream::hygromycin cassette::downstream construct. For the laccase gene replacement experiment, the knockout construct was moved to the binary vector pGKO2 (Khang et al., 2005) using a restriction/ligation method.

Polymerase Chain Reactions for Gene Replacement constructs:

PCR reactions were done with the Takara Ex-Taq™ Polymerase (Product # TAK RR001A,B,C Takara, WI). The reaction mixture contained 5 µl of 10X buffer, 4 µl dNTP mixture, 0.25 µl Ex-Taq, 2 µl template, and 1 µl of each primer at a concentration of 10 mM in a reaction volume of 50 µl. The thermocycler program was set to an initial denaturation of 1 min. The lid temperature was set to 95^{o}C. The cycle with denaturation at 95^{o}C for 30 sec, annealing for 1 min, extension at 72^{o}C was repeated 30 times followed by a final extension of 2 minutes.

Agrobacterium Mediated Fungal Transformations:

The agrobacterium clones BV159 and BV160 (containing the knock-out vector pBV155) were grown in minimal media for 44 hrs. Later, 100 µl of these cultures were used to inoculate 100 µl of induction media containing acetosyringone and kanamycin. Acetosyringone is the inducer to transfer the T-DNA into fungal spores. The agrobacterium cultures were induced for 6 hrs at 28^{o}C at 250 rpm. A spore suspension from the fungal strain O-137 was prepared at a concentration of 10^{6} spores/ml. 100µl of this spore suspension was mixed with 100 µl of the induced agrobacterium cultures and spread onto the Whatman® sterile membrane filters (Cat # 7141 104, 0.45µm pore size) on the cocultivation medium plates. The plates were kept in dark at 28^{o}C for 36 hrs. The filters were then moved to TB3 (3 g yeast extract, 3 g casaminoacids, 20%

sucrose) plates with cefatoxim (200 µg/ml) and hygromycin (200µg/ml). Cefatoxim is toxic to agrobacterium and kills the bacteria to give pure fungal cultures. This is added to clean the fungal cultures from bacterial growth. These plates were wrapped in aluminum foil and placed in the fungal growth chamber at 24^{o}C. After two days, a significant amount of agrobacterium was seen growing on the filter papers. With the aid of a pipet tip, the cultures were spread onto the plate. On the fifth day the plates were observed under the stereomicroscope for fungal growth. Mycelia were growing out of the edges of the filter paper. The filter papers were discarded and the plates were returned to the 24^{o}C fungal chamber. Distinct fungal colonies were seen growing on the plates. On the seventh day the colonies were moved to the second round of selection plates with the negative selection. These plates were made with V8 media (80 ml V8 juice per 1 liter distilled water, 310 ul 10N NaOH, pH 6.8) with cefatoxim, hygromycin and 5-fluoro-2'-deoxyuridine (F2dU). F2dU is the negative selection marker to increase the efficiency of selecting positive transformants and reduce the ectopic transformants (Khang et al., 2005). This same procedure was used to transform fungal strain O-391 with the BV160 agrobacterium strain.

Protoplast mediated fungal transformation:

The PCR amplicon from the bilurubin oxidase gene replacement construct (pBV281) was used to transform protoplasts of the fungal strain O-391 (Protoplasts were obtained from Valdovinos-Ponce, G.). The PCR product was purified using the QIAquick® PCR Purification Kit (cat # 28104). Ten microliters amplicon (total concentration 2.3 µg) was added to 140 µl protoplasts. The negative control for this experiment was done by adding 10 µl of water to 140 µl protoplasts. The mixture was incubated at room temperature for 20 min. To each tube, 1ml PTC [40% PEG in STC (20% sucrose, 50 mM Tris-Cl, pH 8.0, 20 mM $CaCl_2$)] was added and incubated at room temperature for 20 min. Later 5 ml of TB3 medium was added to each tube to allow cell wall generation and growth during incubation at 26^{o}C for 8 hrs with shaking at 250 rpm. The fungus was pelleted by centrifuging for 5 min at 24^{o}C and 10, 000 rpm. The supernatant was discarded leaving approximately 500 µl of medium inside the tube. The fungal pellet was resuspended in it and spread on selection plates (TB3 with Hygromycin). The plates were wrapped in aluminum foil and kept in the fungal growth chamber at 24^{o}C.

DNA extractions for screening gene knockouts:

Fungal mycelia were scrapped from 1cm^2 cultures growing either on oatmeal or V8 plates with the flat end of sterile wooden tooth picks. Care was taken to avoid agar in the scrape. This mycelial mat was suspended in 500 µl of extraction buffer (100 mM Tris – HCl - pH 8.0, 10 mM EDTA - pH 8.0, 1 M KCl) in 1.5 ml tubes. Mycelia were ground using WING2 (a hand-held grinder with a pestle at its tip for macerating the tissue). The WING2 was set to high and ground for 30 seconds. The tubes were centrifuged at 5,000 rpm at room temperature for 10 minutes. The supernatant was transferred into fresh 1.5 ml tubes containing 300 µl isopropyl alcohol (Cat # A416-500, Fisher Scientific) at -20^oC. The tubes were inverted several times to allow the alcohol precipitation of the DNA and centrifuged at 4^oC for 15 minutes at 13,000 rpm to pellet the DNA. The pellet was washed with 800 µl of 70% ethanol (-20^oC) and centrifuged at 4^oC for 5 min at 13,000 rpm. Ethanol was discarded taking care that the DNA pellet remained at the bottom of the tube. The tubes were air dried for 15 to 20 minutes and the DNA pellet was resuspended in 20 µl double distilled water.

Genomic DNA extractions for Southern analyses:

Mycelial samples were ground in liquid nitrogen into fine powder using a mortar and pestle. The mycelial powder was transferred into 1.5 ml tubes till the 0.5 ml mark. 700 µl of pre-heated (65^oC) 2% CTAB (NaCl 1.4 M, Tris – HCl 0.1 M, $Na_4EDTA.2H_2O$ 20 mM, CTAB 10g) buffer was added to these tubes followed by 7 µl of beta mercaptoethanol (Cat # M-7154, Sigma Aldrich). The tubes were vortexed for 20 seconds and placed in a 6^oC incubator for 10 minutes. The tubes were vortexed again to release any clumps and reincubated at 65^oC for another 20 minutes. To each tube, 300 µl of chloroform: isoamyl alcohol (24:1 v/v) (Cat # C-0549, Sigma Aldrich) was added. The tubes were vortexed for 15 seconds and mixed by inverting for 2 to 3 minutes. These were centrifuged at 12,000 rpm for 5 minutes at room temperature to separate the organic (lower) and the aqueous (upper) phases. The upper aqueous phase was very carefully transferred to a fresh 1.5 ml tube. This was again mixed with 300 µl of chloroform: isoamyl alcohol (24:1 v/v) and thoroughly mixed first with brief vortexing and then by inverting the tubes for 2 to 3 minutes. The tubes were centrifuged at 12,000 rpm for 5 min and the upper aqueous

phase was transferred to fresh tubes. DNA was pelleted in these tubes by adding 500 µl of isopropyl alcohol and setting them on bench top for 5 minutes. The tubes were then centrifuged at 13,000 rpm for 5 minutes. The supernatant was discarded and the pellet was washed with 70% ethanol. The tubes were centrifuged for an additional 2 minutes and the ethanol was decanted. The tubes were air dried by inverting them on to fresh paper towels for 15 minutes. The DNA pellet was resuspended in 150 µl of elution buffer from the QIAprep® Miniprep kit (Cat # 27104) with RNase (provided with the kit) added at a concentration of 20 µg/ml.

Southern Hybridizations:

Genomic DNA from the wildtype O-137, LKO-1 and an ectopic transformant were digested with *Hind*III (Cat # R6041, Promega Corporation) and *Sph*1 (Cat # R6261, Promega Corporation) enzymes at 37^{o}C overnight. The digested DNAs were electophoresed on 1% agarose gels at 25 V for 3 hrs and the bands were visualized under UV light before transferring them to the positively charged nylon membrane (Hybond™-N+; Amersham Pharmacia Biotech Inc, NJ). The transfer apparatus was set up according to the manufacturer's instructions. We used the AlkaPhos DIRECT kit for labeling (Cat # RPN3680 Amersham Pharmacia Biotech Inc, NJ) and detection (Cat # RPN2132, Amerxham Biosciences Corporation, NJ). After overnight transfer the membranes were prehybridised with the hybridization buffer for 15 minutes at 55^{o}C. The hygromycin cassette from knockout vector pBV155 and the laccase coding sequence from the genomic DNA were amplified using the corresponding primers (Table 7). The PCR products were gel purified from a 1% agarose gel run at 50 V for 30 min. Probe labeling was done according to the instructions from the manufacturer. Following labeling, the probe was added to the membranes and hybridized overnight at 55^{o}C. The membranes were then washed in primary wash buffer twice at 55^{o}C and in secondary wash buffer twice at room temperature. The membranes were incubated with detection reagent for 5 minutes and wrapped in a layer of saran wrap. The film was exposed to the membranes for 3 hrs before developing it.

Fungal growth media:

Fungal strains were grown on oatmeal agar plates in a 24^{o}C incubator under continuous light to allow sporulation. For DNA and RNA extractions, a 3cm^{2} piece of the mycelial mat was cut from the oatmeal agar plates. Care was taken to avoid the oatmeal agar as much as possible. The mycelial mat was ground in complete media (6g yeast extract, 6g casamino acids, 10g glucose in 1 liter) for 5 seconds thrice and was grown overnight in complete media. The cultures were filtered through sterilized milk filters and ground in complete media thrice again. This was grown overnight and the cultures were filtered through sterile milk filters and dried in paper towels. The mycelial mat was stored at -80^{o}C. The mycelia were ground in liquid nitrogen into fine powder and used for the DNA / RNA extractions as described. The fungal mycelia for microarray hybridization experiments were grown in 3-3-3- media (3 g yeast extract, 3 g casamino acids, 3 g glucose in 1 liter water).

Rice Blast spray inoculation assays:

Spore suspensions of 5x10^{4} spores/ml were made in sterile 0.25 % gelatin. Three week old rice plants were used for this assay. Two pots were placed in a plastic bag and 5 ml of spores were sprayed using an artist's air brush (Paasche H, No. 1) attached to compressed air tank at 20 psi. The control plants were sprayed with 0.25% gelatin. The bags were closed and left in the lab for 24 hrs. Later the pots were removed from the bags and moved to the growth chamber. After 7 days, the youngest leaf was used to score the assay for number of lesions, lesion size and shape.

References:

Asano, T., Masumura, T., Kusano, H., Kikuchi, S., Kurita, A., Shimada, H., and Kadowaki, K.-i. (2002). Construction of a specialized cDNA library from plant cells isolated by laser capture microdissection: toward comprehensive analysis of the genes expressed in the rice phloem. The Plant Journal **32,** 401-408.

Avila-Adame, C., and Koller, W. (2002). Disruption of the alternative oxidase gene in *Magnaporthe grisea* and its impact on host infection. Molecular Plant-Microbe Interactions **15,** 493-500.

Baldrian, P. (2006). Fungal laccases - occurance and properties. FEMS Microbiology reviews **30,** 215-242.

Berruyer, R., Khang, C.H., Kankanala, P., Kang, S., and Valent, B. (Unpublished results).

Böhnert, H.U., Fudal, I., Dioh, W., Tharreau, D., Notteghem, J.-L., and Lebrun, M.-H. (2004). A putative polyketide synthase/peptide synthetase from *Magnaporthe grisea* signals pathogen attack to resistant rice. Plant Cell **16,** 2499-2513.p

Dean, R.A., Talbot, N.J., Ebbole, D.J., Farman, M.L., Mitchell, T.K., Orbach, M.J., Thon, M., Kulkarni, R., Xu, J.-R., Pan, H., Read, N.D., Lee, Y.-H., Carbone, I., Brown, D., Oh, Y.Y., Donofrio, N., Jeong, J.S., Soanes, D.M., Djonovic, S., Kolomiets, E., Renmeyer, C., Li, W., Harding, M., Kim, S., Lebrun, M.H., Bohnert, H., Coughlan, S., Butler, J., Calvo, S., Li-Jun, M., Nicol, R., Purcell, S., Nusbaum, C., Galagan, J.E., and Birren, B.W. (2005). The genome sequence of the rice blast fungus *Magnaporthe grisea*. Nature **434,** 980-986.

Donofrio, N.M., Oh, Y., Lundy, R., Pan, H., Brown, D.E., Jeong, J.S., Coughlan, S., Mitchell, T.K., and Dean, R.A. (2006). Global gene expression during nitrogen starvation in the rice blast fungus, *Magnaporthe grisea*. Fungal Genetics and Biology **43,** 605-617.

Farman, M.L., and Leong, S.A. (1998). Chromosome walking to the *AVR1-CO39* avirulence gene of *Magnaporthe grisea*. Discrepancy between the physical and genetic maps. Genetics **150,** 1049-1058.

Froyd, J.D., and Froeliger, E.H. (1994). Strategies for the discovery of rice blast fungicides. In rice blast disease, R.S. Zeigler, S.A. Leong, and P.S. Teng, eds (Wallingford, Oxon, UK: CAB International / IRRI), pp. 501-520.

Heath, M.C., Valent, B., Howard, R.J., and Chumley, F.G. (1990). Correlations between cytologically detected plant - fungal interactions and pathogenicity of *Magnaporthe grisea* toward weeping lovegrass. Phytopathology **80,** 1382-1386.

Howard, R.J., and Valent, B. (1996). Breaking and Entering: Host penetration by the fungal rice blast pathogen *Magnaporthe grisea*. Annual Review of Microbiology **50,** 491-512.

Ithal, N., Recknor, J., Nettleton, D., Maier, T., Baum, T.J., and Mitchum, M.G. (2007). Developmental transcript profiling of cyst nematode feeding cells in Soybean roots. Molecular Plant Microbe Interactions **20,** 510-525.

Jia, Y., McAdams, S.A., Bryan, G.T., Hershey, H.P., and Valent, B. (2000). Direct interaction of resistance gene and avirulence gene products confers rice blast resistance. The EMBO Journal **19,** 4004-4014.

Kang, S., Sweigard, J.A., and Valent, B. (1995). The *PWL* host specificity gene family in the blast fungus *Magnaporthe grisea*. Molecular Plant-Microbe Interactions **8,** 939-948.

Kankanala, P., Czymmek, K., and Valent, B. (2007). Roles for rice membrane dynamics and plasmodesmata during biotrophic invasion by the blast fungus. The Plant Cell **19,** 706-724.

Khang, C.H., Park, S.-Y., Lee, Y.-H., and Kang, S. (2005). A dual selection based, targeted gene replacement tool for *Magnaporthe grisea* and *Fusarium oxysporum*. Fungal Genetics and Biology **42,** 483-492.

Kim, S., Il-Pyung, A., and Lee, Y.-H. (2001). Analysis of genes expressed during Rice-*Magnaporthe grisea* interactions. Molecular Plant-Microbe Interactions **14,** 1340-1346.

Mosquera, G., Coughlan, S., and Valent, B. (2007). Analysis of the interaction transcriptome of biotrophic invasion by the rice blast fungus, *Magnaporthe oryzae*. Submitted.

Nakazono, M., Qiu, F., Borsuk, L.A., and Schnable, P.S. (2003). Laser-capture microdissection, a tool for the global analysis of gene expression in specific plant cell types: identification of genes expressed differentially in epidermal cells or cascular tissues of Maize. Plant Cell **15,** 583-596.

Nelson, T., Tausta, S.L., Gandotra, N., and Liu, T. (2006). Laser microdissection of plant tissue: What you see is what you get. Annual Review of Plant Biology **57,** 181-201.

Orbach, M.J., Farrall, L., Sweigard, J.A., Chumley, F.G., and Valent, B. (2000). A telomeric avirulence gene determines efficacy for the rice blast resistance gene Pi-ta. The Plant Cell **12,** 14.

Ou, S.H. (1980). Pathogen variability and host resistance in rice blast disease. Annual Review of Phytopathology **18,** 167-187.

Project, T.I.R.G.S. (2005). The map-based sequence of the rice genome. Nature **436,** 793-800.

Ramsay, K., Wang, Z., and Jones, M.G.K. (2004). Using laser capture microdissection to study gene expression in early stages of giant cells induced by root-knot nematodes. Molecular Plant Pathology **5,** 587-592.

Sakasegawa, S.-i., Ishikawa, H., Imamura, S., Sakuraba, H., Goda, S., and Ohshima, T. (2006). Bilirubin oxidase activity of *Bacillus subtilis CotA*. Applied and Environmental Microbiology **72,** 972-975.

Sweigard, J.A., Carroll, A.M., Kang, S., Farrall, L., Chumley, F.G., and Valent, B. (1995). Identification, cloning, and characterization of *PWL2*, a gene for host species specificity in the rice blast fungus. The Plant Cell **7,** 1221-1233.

Talbot, N.J. (2003). On the trail of a cereal killer: exploring the biology of *Magnaporthe grisea*. Annual Review of Microbiology **57,** 177-202.

Talbot, N.J., Ebbole, D.J., and Hamer, J.E. (1993). Identification and characterization of *MPG1*, a gene involved in pathogenicity from the rice blast fungus *Magnaporthe grisea*. The Plant Cell **5,** 1575-1590.

Tanaka, N., and Murao, S. (1982). Purification and some properties of bilirubin oxidase of *Myrothecium verrucaria MT-1*. Agriculture and Biological Chemistry **46,** 2499-2503.

Tang, W., Coughlan, S., Crane, E., Beatty, M., and Duvick, J. (2006). The application of laser capture microdissection to i*n planta* gene expression profiling of the maize anthracnose stalk rot fungus *Colletotrichum graminicola*. Molecular Plant-Microbe Interactions **19,** 1240-1250.

Wu, S.-C., Kauffmann, S., Darvill, A.G., and Albersheim, P. (1995). Purification, cloning and characterization of two xylanases from *Magnaporthe grisea*, the rice blast fungus. Molecular Plant Microbe Interactions **8,** 506-514.

Wu, S.-C., Halley, J.E., Luttig, C., Fernekes, L.M., Gutiérrez-Sanchez, G., Darvill, A.G., and Albersheim, P. (2006). Identification of an *endo*-beta-1,4-D-xylanase from *Magnaporthe grisea* by gene knockout analysis, purification and heterologous expression. Applied and Environmental Microbiology **72,** 986-993.

Table 3.1 aRNA quantities measure with Nanodrop Spectrophotometer after two rounds of linear amplification

Sample	Quantity (Micrograms)
Inf 26 hpi	11.5
Mycelium	18.0
Mock inoculated rice	4.7

Table 3.2 List of 50 most up-regulated invasive hyphal genes at 34 hpi (early biotrophic state)

MGOS probe[a]	Putative Function	Fold change	cDNA Libraries[b]	Predicted Secreted Proteins	Chromosome Location
AMG08263	Hypothetical protein	253.01	-	SP[c]	IV
AMG08261	Hypothetical protein	178.02	-	SP	IV
AMG08417.2	Hypothetical protein	173.51	-	SP	IV
AMG15604	Hypothetical protein	170.35	-	-	
AMG03682.1	Hypothetical protein	169.82	mk	SP	
AMG02439	Hypothetical protein	148.64	-	SP	I
AMG07462	Hypothetical protein	133.62	-	-	
AMG15980	Hypothetical protein	125.78	-	SP	UNK
AMG13025	Hypothetical protein	123.9	-	SP	VI
AMG06650	Hypothetical protein	112.16	-	SP	III
AMG03682.2	Hypothetical protein	108.68	-	-	
AMG08508	Hypothetical protein	106.92	-	-	
AMG03019	Hypothetical protein	105.64	-	SP	II
AMG06765	Hypothetical protein	102.48	-	SP	III
AMG07077	Hypothetical protein	98.61	-	-	
AMG13187	Hypothetical protein	97.54	-	SP	VII
AMG14713	Hypothetical protein	95.09	-	-	
AMG02908	NTR [Herpesvirus papio]	94.83	-	-	
AMG13138	3-phytase A precursor [Thielavia heterothallica]	91.47	-	-	
AMG13082	monosaccharide transporter [Aspergillus niger]	90.37	-	-	
AMG04213	Hypothetical protein	90.05	-	-	
AMG16197	Hypothetical protein	85.56	my	SP	II
AMG13593.2	Hypothetical protein	85.46	-	SP	VII
AMG15428	Hypothetical protein	83.99	-	-	

AMG08327	Hypothetical protein	83.63	-	-	
AMG08238	Hypothetical protein	82.88	-	-	
AMG10399	Hypothetical protein	82.03	-	-	
AMG15373	flocculin [Saccharomyces cerevisiae]	81.67	-	-	
AMG04886	Hypothetical protein	79.63	-	-	
AMG00161	Hypothetical protein	79.30	-	-	
AMG02143	Hypothetical protein	79.04	-	-	
AMG01935	Hypothetical protein	78.40	-	-	
AMG08210	Bilirubin oxidase [Myrothecium verrucaria]	78.10	-	-	
AMG02432	Hypothetical protein	77.13	-	-	
AMG15989	Hypothetical protein	75.29	-	-	
AMG13251	Hypothetical protein	74.52	-	SP	VII
AMG02155	Hypothetical protein	72.16	-	-	
AMG13016	Hypothetical protein	69.61	-	-	
AMG02197	Hypothetical protein	69.58	-	-	
AMG00026	Hypothetical protein	67.86	-	-	
AMG11615	Hypothetical protein	67.69	-	-	
AMG02483	Hypothetical protein	67.24	-	-	
AMG07056	Hypothetical protein	66.57	-	SP	V
AMG13616	Hypothetical protein	66.35	-	-	
AMG04095	Hypothetical protein	65.99	-	-	
AMG04082	Hypothetical protein	65.70	-	-	
AMG08812	Hypothetical protein	65.20	-	-	
AMG10347	NADP-dependent leukotriene b4 12-hydroxydehydrogenase; [Botryotinia fuckelian	63.86	-	-	
AMG13014	Hypothetical protein	62.99	-	SP	VI

a. MGOS probes correspond to Agilent *M. oryzae* version 2 micrroarray. The corresponding Broad Database gene names can be retrieved from www.mgosdb.org

"-" indicated either no EST hits or no predicted signal peptide

b. Library abbreviations: mk = *pmk1*$^{-}$ mutant and my = mycelium from minimal medium

c. SP = signal peptide

Table 3.3 List of 50 most down-regulated invasive hyphal genes at 34 hpi (early biotrophic phase)

MGOS probe	Putative Function	Fold Change	cDNA Libraries[a]	Predicted secreted Proteins	Chromosome Location
AMG13341	Hypothetical protein	-975.57	-	-	
AMG14000.1	Hypothetical protein	-814.41	-	SP	VII
AMG10496	metalloprotease 1 precursor [Coccidioides posadasii]	-740.89	-	SP	IV
AMG04896.2	Hypothetical protein	-688.30	-	SP	III
AMG09891	Hypothetical protein	-541.45	cs, cw, mk, mt	-	
AMG00941.1	Hypothetical protein	-497.78	mt, ns, su	SP	I
AMG12539	Hypothetical protein	-467.37	-	-	
AMG13001	Hypothetical protein	-445.95	-	-	
AMG06174	alternative terminal oxidase [Magnaporthe grisea]	-441.11	cm, cs, cw. mk. mt. ns, su	-	
AMG04491.2	Hypothetical protein	-421.54	cs, mk, mt	-	
AMG06063.1	Hypothetical protein	-385.77	-	-	
AMG12697.2	Hypothetical protein	-380.16	ns	-	
AMG06337	Hypothetical protein	-356.13	-	-	
AMG11243	cytochrome P450 monooxygenase [Botryotinia fuckeliana]	-339.99	-	-	
AMG13759.1	Hypothetical protein	-332.18	cm	-	
AMG00195	Hypothetical protein	-322.42	-	SP	I
AMG14969	Hypothetical protein	-321.35	-	-	
AMG07838.2	Hypothetical protein	-316.89	cs	-	
AMG05150	Hypothetical protein	-311.01	-	-	
AMG14037.1	Putative oxidoreductase [Sinorhizobium meliloti]	-310.65	ns	-	

AMG04953	acidic amino acid permease [Penicillium chrysogenum]	-266.54	cm, cw, mt	-	
AMG05149	Hypothetical protein	-266.06	-	-	
AMG06063.2	Hypothetical protein	-265.81	-	-	
AMG07092	Hypothetical protein	-256.40	-	-	
AMG11426	Hypothetical protein	-249.93	su	-	
AMG15478	potential allantoate permease [Candida albicans]	-248.88	-	-	
AMG15600	Het-eN [Nectria haematococca]	-247.65	-	-	
AMG05096	laccase [Gaeumannomyces graminis var. tritici]	-241.54	-	-	
AMG00656	Hypothetical protein	-240.95	cm, cw, mk, mt, my, su	-	
AMG12211	Hypothetical protein	-238.96	cw	-	
AMG07022	Hypothetical protein	-226.49	-	-	
AMG06697	Hypothetical protein	-218.90	-	-	
AMG15576	Hypothetical protein	-210.22	-	-	
AMG12371.1	Hypothetical protein	-208.63	-	-	
AMG06018	likely beta alanine synthase [Candida albicans]	-207.33	-	-	
AMG07563	Hypothetical protein	-199.94	-	-	
AMG13340	Hypothetical protein	-196.71	cw	-	
AMG09517	Hypothetical protein	-187.94	-	-	
AMG10412	Hypothetical protein	-186.84	-	SP	IV
AMG13844	Hypothetical protein	-185.98	my, ns	-	
AMG11634.3	Hypothetical protein	-181.83	cs, mk, mt	-	
AMG12820	esterase [Aspergillus terreus]	-180.12	-	-	
AMG01829.1	Hypothetical protein	-177.13	cm, cw, my, ns	-	

AMG02679	Hypothetical protein	-175.05	-	-	
AMG12697.1	clock-controlled gene-9 protein [Neurospora crassa]	-172.63	cw, mt, ns	-	
AMG09892	Hypothetical protein	-172.39	cs, cw, mk, mt	-	
AMG06993.2	Hypothetical protein	-171.81	-	-	
AMG05773	Hypothetical protein	-168.27	-	SP	III
AMG11762	Hypothetical protein	-166.92	-	-	
AMG05270	Hypothetical protein	-165.90	cm, cs, cw, mt, my, ns, su	-	

a. Library abbreviations: cm = mycelium from complete medium, cs = conidiospores, cw = mycelium grown on rice cell walls, mk = *pmk1*$^{-}$ mutant, mt = mating type, my = mycelium from minimal medium, ns = nitrogen starved mycelium and su = subtracted library (Ebbole et al., 2004)

Table 3.4 List of the up-regulated genes validated with RT-PCR

MGOS code	Putative function	Fold change
AMG13025	Hypothetical protein	124
AMG13187	Hypothetical protein	97
AMG13138	Phytase A precursor	91
AMG10399	Hypothetical protein	82
AMG08210	Bilurubin Oxidase precursor	78
AMG08787	Hypothetical protein	57
AMG08524	Probable Sugar Transporter	54
AMG02511	G-protein coupled receptor	29
AMG16216	Hypothetical protein	28

Table 3.5 Properties of genes that are up- and down- regulated in IH

Features	Number of up-regulated genes and percentages		
	> 50 fold	10 to 50 fold	3 to 10 fold
Total	78	420	1242
Hypothetical Protein	65 (83%)	293 (70 %)	745 (60%)
Putative Proteins	2 (2.5%)	33 (7.8%)	127 (10.2%)
EST's	4 (5%)	44 (10%)	248 (19%)
Secreted Proteins	19 (24%)	70 (16%)	77 (6%)

Features	Number of down-regulated genes and percentages		
	> -50 fold	-10 to -50 fold	-3 to -10 fold
Total	262	680	1552
Hypothetical Proteins	208 (80%)	536 (79 %)	1173 (75%)
Putative Proteins	7 (2.6%)	40 (5.8%)	112 (7.2%)
EST's	80 (30%)	164 (24%)	320 (21%)
Secreted Proteins	34 (13%)	33 (5%)	76 (5%)

Table 3.6 Expression data for previously studied pathogenicity genes identified in microarray data

MGOS probe	Fold change	Gene name/function	Role[a]	P-Value
AMG06174	-441.1	*AOX1*, alternative oxidase	INF	0
AMG06064	-108.4	*RSY1*, Syclatone dehydratase	P	0
AMG01944	-108.3	*4HNR,* Tetrahydroxynaphthalene Reductase	P	0
AMG05260	-125.7	*PTH11*, integral membrane protein	A	0
AMG02948	-108.2	*BUF1*, trihydroxy naphthalene reductase	P	0
AMG14765	-17.3	*MPG1*, hydrophobin	A	2.74E-13
AMG01183	-4.4	*MAGA,* Alpha subunit of heteromeric G protein	A	0
AMG03758.1	-1.7	*CALM*, calmodulin	A	8.28E-15
AMG07015	1.8	*PMK1*, pathogenicity MAP kinase	A,INF	5.82E-16
AMG10289	1.9	*SPM1*, vacuolar subtilisin-like Serine protease	C,A,INF	2.06E-35
AMG06876	2.8	*NTH1 (PTH9),* neutral trehalase	INF	6.00E-34
AMG04255	2.8	*ACI1, MAC1* (adenylate Cyclase)- interacting protein 1	C,A	0
AMG05982	3.0	*MST12*, transcription	P,INF	0

		factor downstream of *PMK1*		

a. Pathogenicity traits affected: C= conidiation, A = appressorium formation, P = penetration, INF = infectious growth (usually defined as inability to infect wounded tissue), AVR = avirulence activity in rice containing the corresponding *R* gene

Table 3.7 Primer table

Primer Name	5' – 3' Sequences
AMG13025 F	CCTTGTGTCTGCAATCATCG
AMG13025 R	CACAGTCACCGTCTCCTTGA
AMG13187 F	AGCTTCCATAACCCAGCCCACTTA
AMG13187 R	ATACTGGTCATTGTCCGTGTGCCT
AMG13138 F	GGCAATCGTAGCCAATGCTCAAGT
AMG13188 R	ACATTGATCCCAACGCCCTCCATT
AMG10399 F	TACGCTAGTAAGCAGCGTTGCAGT
AMG10399 R	CGGTTGAATAACTGTGTCCTCCCA
AMG08210 F	AAGCTCAAGAACCAGATCAGCGGT
AMG08210 R	TTGTTGACGTCGGCAAAGGTG
AMG08787 F	AATTGGAGTCGCTGTCATCTTGGC
AMG08787 R	AGGGTCTGACCACCTTCTTT
AMG08524 F	TGGTTTCGACAATGGCCTCA
AMG08524 R	AATGCGCCCTGAAACACGAA
AMG16216 F	TGCAGATCAAGACTTTCGCCGCTA
AMG16216 R	ACTTGGCCTCGTAGATGCAC
AMG02511 F	TCGATCAACGGCACTCTTGT
AMG02511 R	ATGCCGATCCACATTGTTGCCT
AVR-Pita F	GCACCTTTTCACACCCAGTT
AVR-Pita R	CTCGGACGCACGTATAAACA

Fungal Actin F	TCCCATGTCACCACTTTCAA
Fungal Actin R	TTCGAGATCCACATCTGCTG
PWL2 F	GTGGCGGGTGGAACTAACAAACAAT
PWL2 R	AAACTCGCCTGGCGGTCCATAATA
Rice Actin F	GAAGATCACTGCCTTGCTCC
Rice Actin R	CGATAACAGCTCCTCTTGGC
Hyg F	AGCGGATCCGGCTTGGCTGGCGCTAGTGGAGG
Hyg R	AGCACTAGTAACCCGCGGTCGGCATCTACTCTA
Laccase F	TGGCATCCGACAGAACTACACCAA
Laccase R	TCAAGCGAGAACTTCCACTGAGTA

Figure 3.1 Flow chart with the protocol for RNA extractions for gene expression profiling

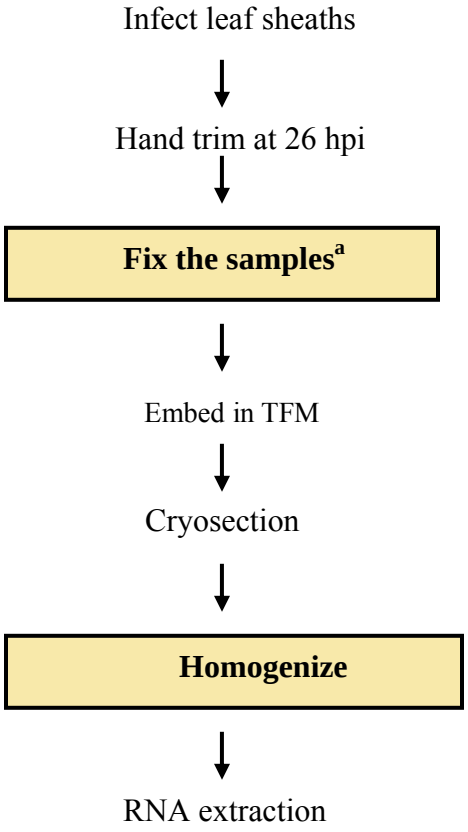

[a] The critical steps that needed standardization

Figure 3.2 Flow chart indicating the different fixatives and homogenization methods and the combinations used

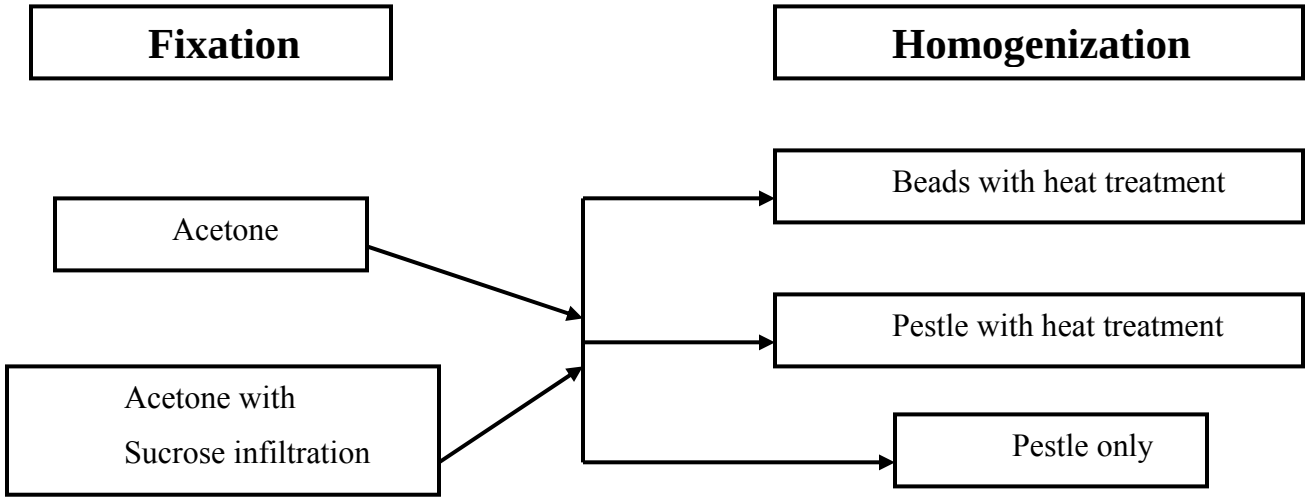

Figure 3.3 Quantification and bioanalyzer profiles indicating the quality of RNA extracted with different fixatives and homogenization methods

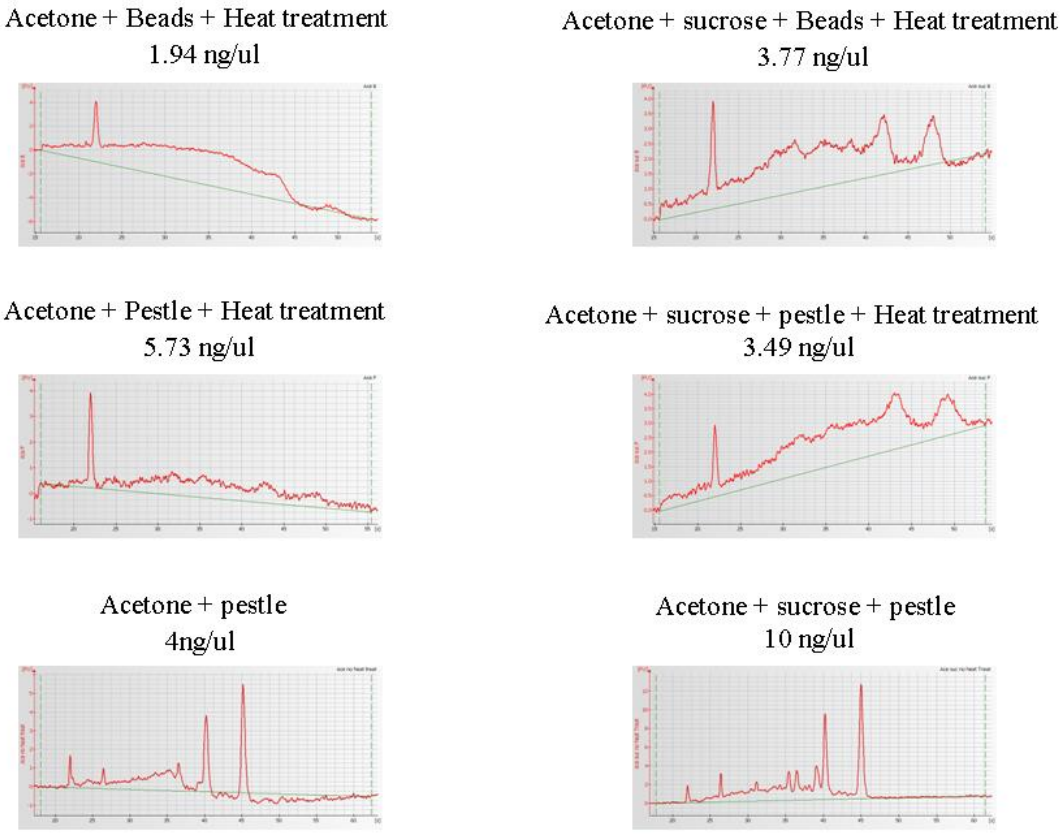

The Bioanalyser profiles of the total RNA from eukaryotic cells indicates the ribosomal RNA peaks corresponding to 18S and 28S subunits. A good quality RNA sample is identified by sharp ribosomal peaks with a good base line. In plant tissues the chloroplast ribosomal RNA is also detected as minor peaks. In the profiles shown above the Acetone + sucrose + pestle gave the best quality RNA. The base lines in all the heat-treated samples were poor compared to the non heat-treated samples indicating that the heat treatment damaged the RNA.

Figure 3.4 Semi-quantitaive curve indicating the fungal to plant ratios in the infected samples and standards.

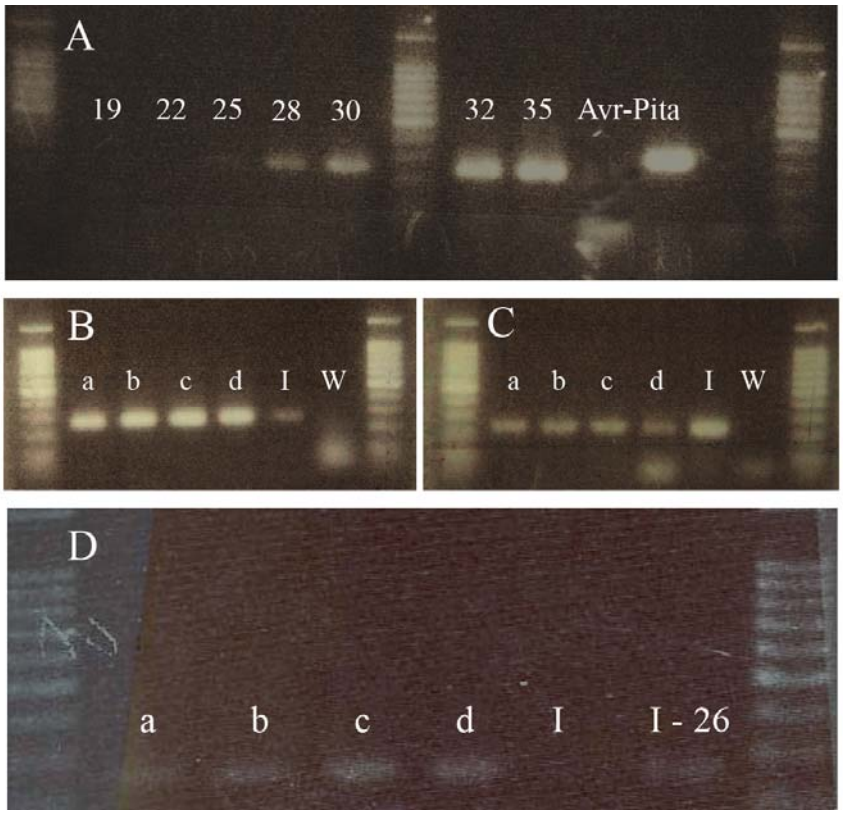

(A) The numbers indicate the number of PCR cycles used to amplify the fungal actin band from 26 hpi RNA samples. The two lanes labeled *AVR-Pita* are 26 hpi RNA and KV1 DNA samples respectively amplified for *AVR-Pita* transcript for 35 cycles. The 26 hpi samples did not have the band while the positive control KV1 amplified the band. **(B-D)** Standards with fungal:plant ratios (a) 5:95, (b) 10:90, (c) 15:95, (d) 20:80, (I) 26 hpi samples, (w) water controls. **(B)** Fungal actin band amplified with 26 PCR cycles. **(C)** Rice actin band amplified with 26 PCR cycles. **(D)** Fungal actin amplified with 23 PCR cycles in the standards and 26 hpi samples except I-26 which was amplified for 26 cycles.

Figure 3.5 Checking for infection specific genes in 26 hpi samples

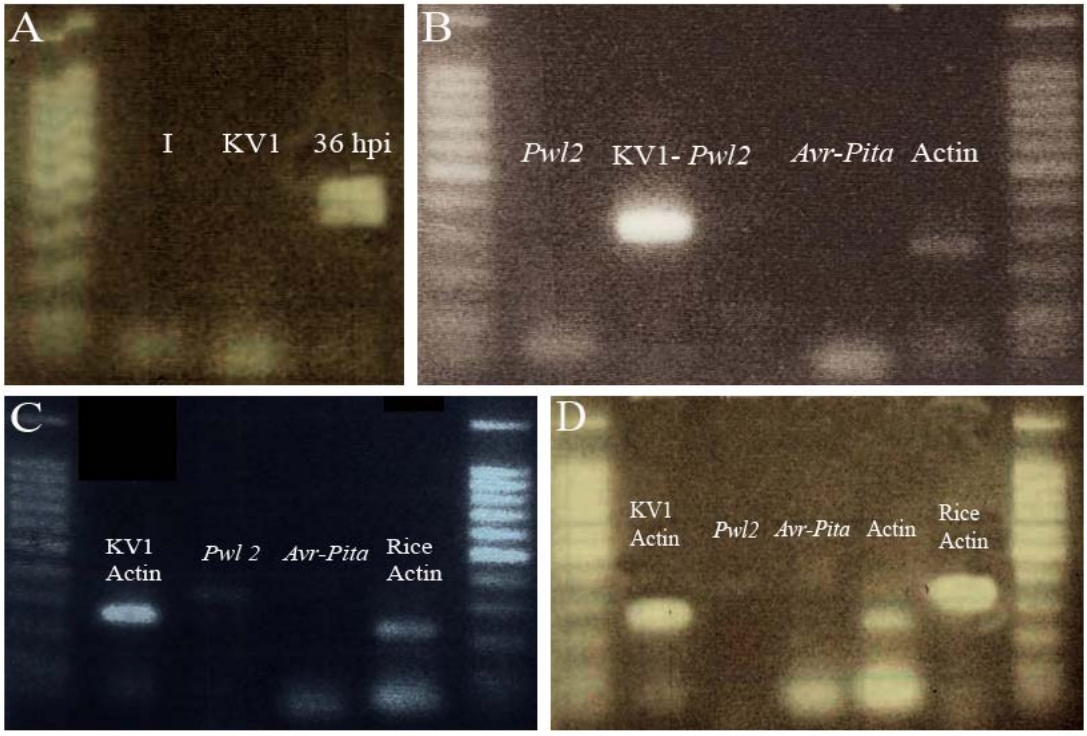

(A) I- 26 hpi samples, KV1 RNA and 36 hpi RNA samples amplified for *AVR-Pita* with 35 PCR cycles. The 36 hpi sample amplified with two bands indicating some genomic DNA contamination. The 26 hpi lacked the band. **(B)** All the lanes indicate 26 hpi RNA except KV1-*PWL2*. The *PWL2* and *AVR-Pita* failed to amplify from the 26 hpi infected samples. A faint actin band amplified indicating the presence of fungal RNA. The KV1 genomic DNA amplified *PWL2*. **(C-D)** 26 hpi infected sample replicates 2 and 3 respectively. The rice actin amplified in both of them. The *PWL2* has a very faint band in replicate 2. The *AVR-Pita* failed to amplify in both the replicates. KV1 RNA amplified the fungal actin transcript. All amplifications were done with 26 PCR cycles.

Figure 3.6 P.A.L.M. Microscope and the principle of the technology

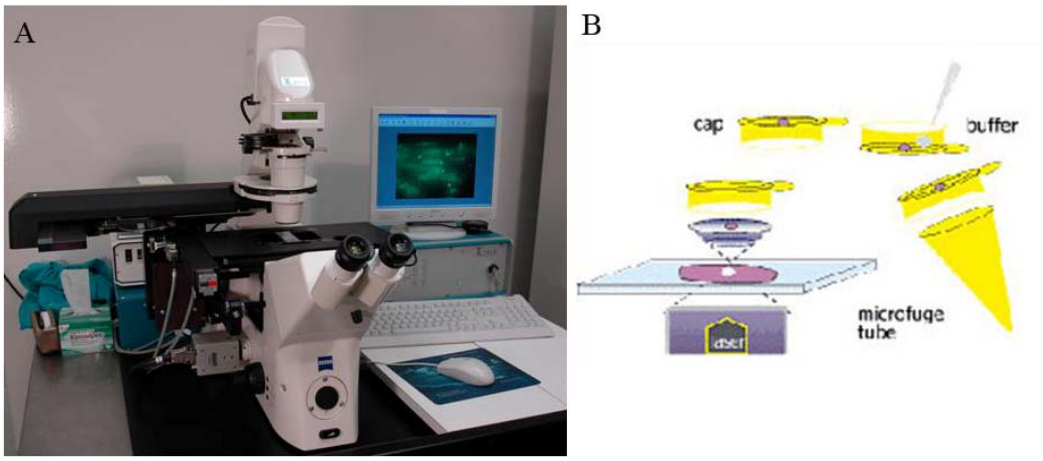

(A) The inverted P.A.L.M. laser Microdissection scope. (B) This figure depicts the principle of the P.A.L.M. technology. A laser from underneath the slide cuts the selected cells, defocuses and catapults the sample into the cap of a 0.5 ml eppendorf tube held above it with a robo mover. The cells are suspended in buffer and centrifuged to collect them at the bottom of the tube.

Figure 3.7 This figure indicates the region of the slide that can be used for LCM

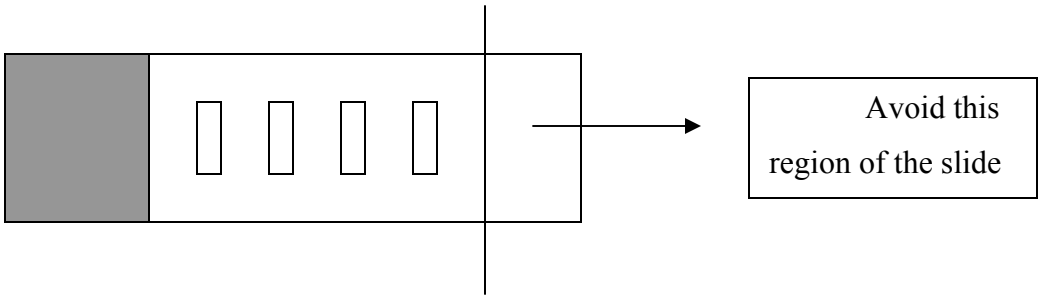

Figure 3.8 This figure indicates the angle to load the sample onto the sample holder in the cryostat and the cuts for trimming the block

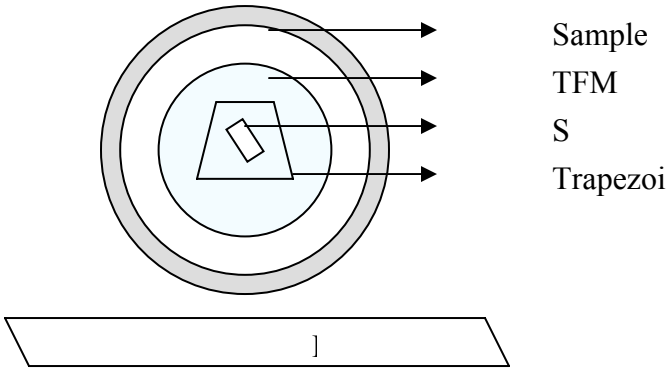

Figure 3.9 The bioanalyzer profiles indicating the RNA quality extracted with Qiagen kit and Picopure kit

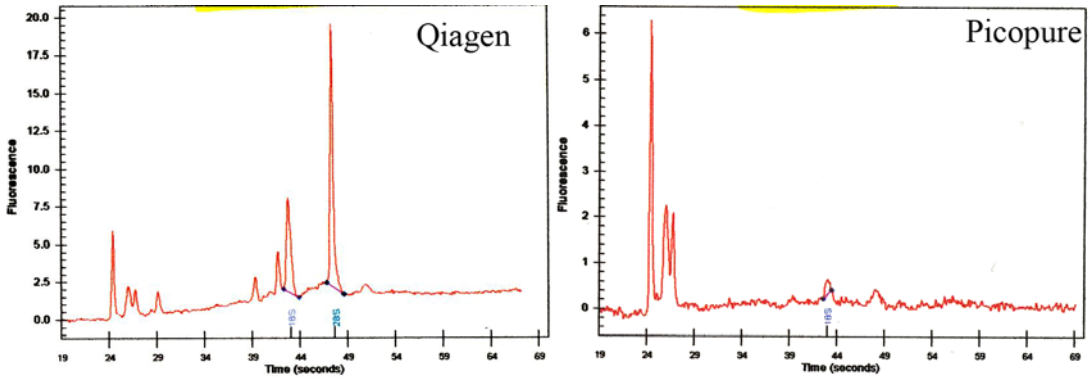

Figure 3.10 This figure shows selecting individual rice leaf sheath epidermal cells infected with *M. oryzae* for LPC

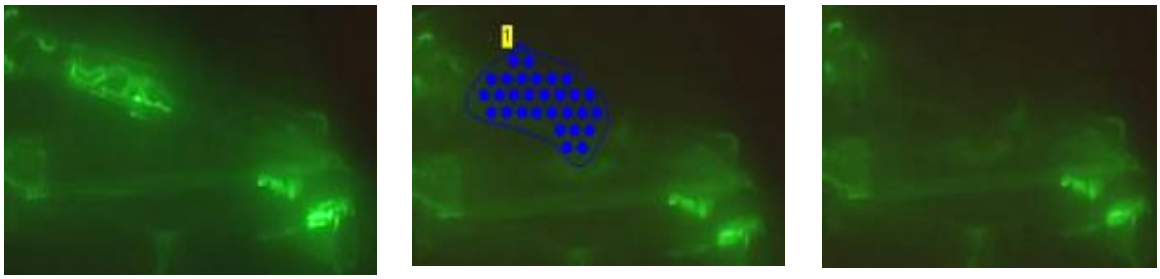

Fluorescent IH visualized before catapulting

Digital pulses marked for catapulting the IH

After

Figure 3.11 Validation of RNA in the laser microdissected samples after one round of linear amplification by RT-PCR

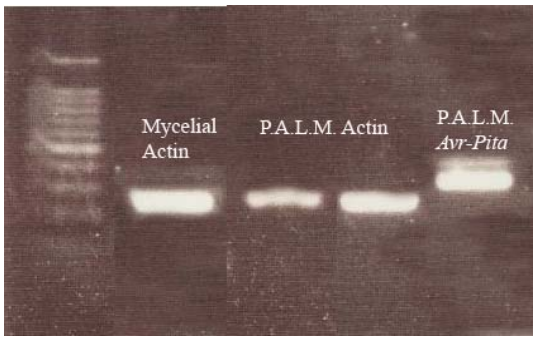

The P.A.L.M. samples amplified fungal actin and *AVR-Pita* genes with 35 amplification cycles indicating the presence of fungal RNA in these samples. *AVR-Pita* had a second faint band indicating some DNA contamination (The genomic copy contains introns and is thus indicated by a larger band size). The mycelial control is the KV1 mycelial RNA.

Figure 3.12 Bioanalyzer profiles of the P.A.L.M. aRNA generated from one round of linear amplification

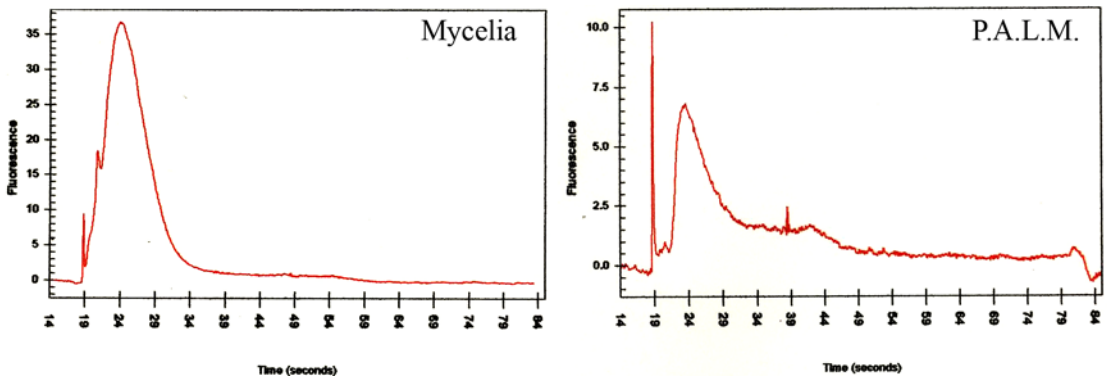

The aRNA has abundant mRNA compared to the other forms of RNA. The Bioanalyzer profiles of these samples shows the peak that corresponds to the sizes of the mRNA. The KV1 mycelial and P.A.L.M. aRNA had its peak at 25 seconds which corresponds to small fragments (200 to 500 bp). Small fragments indicate poor quality RNA.

Figure 3.13 Bioanalyzer profile of the P.A.L.M. aRNA used for microarray hybridizations

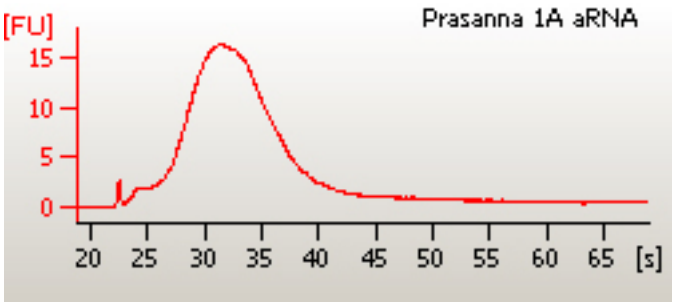

The peak corresponds to ~1000bp fragments of mRNA which corresponds to good quality mRNA.

Figure 3.14 The picture of the microarray slide that was hybridized with P.A.L.M. and KV1 mycelial RNA samples

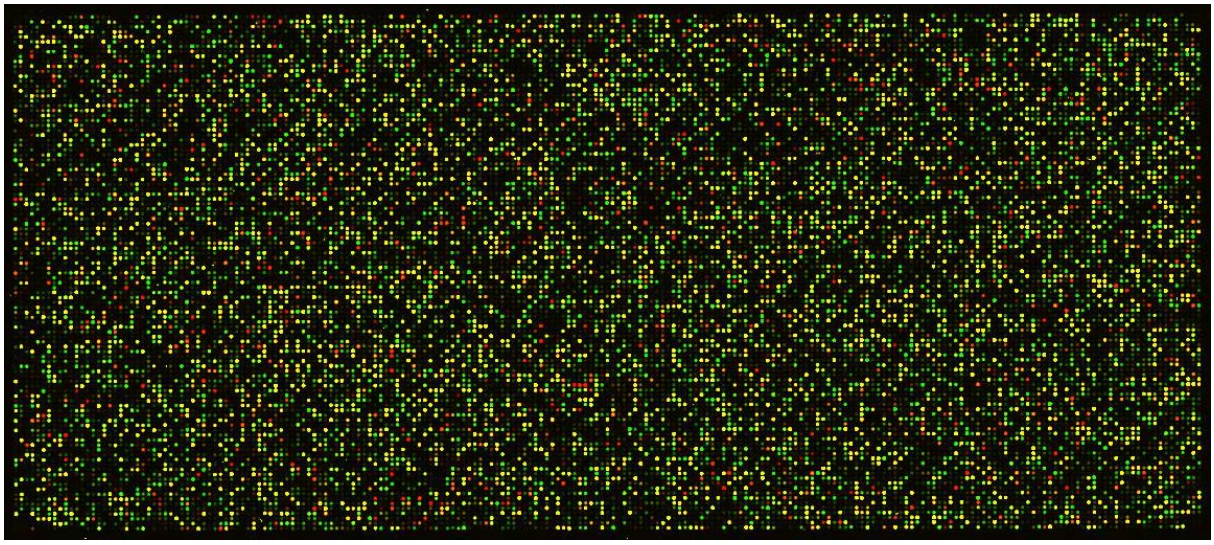

Figure 3.15 Data analysis with Rosetta Resolver®

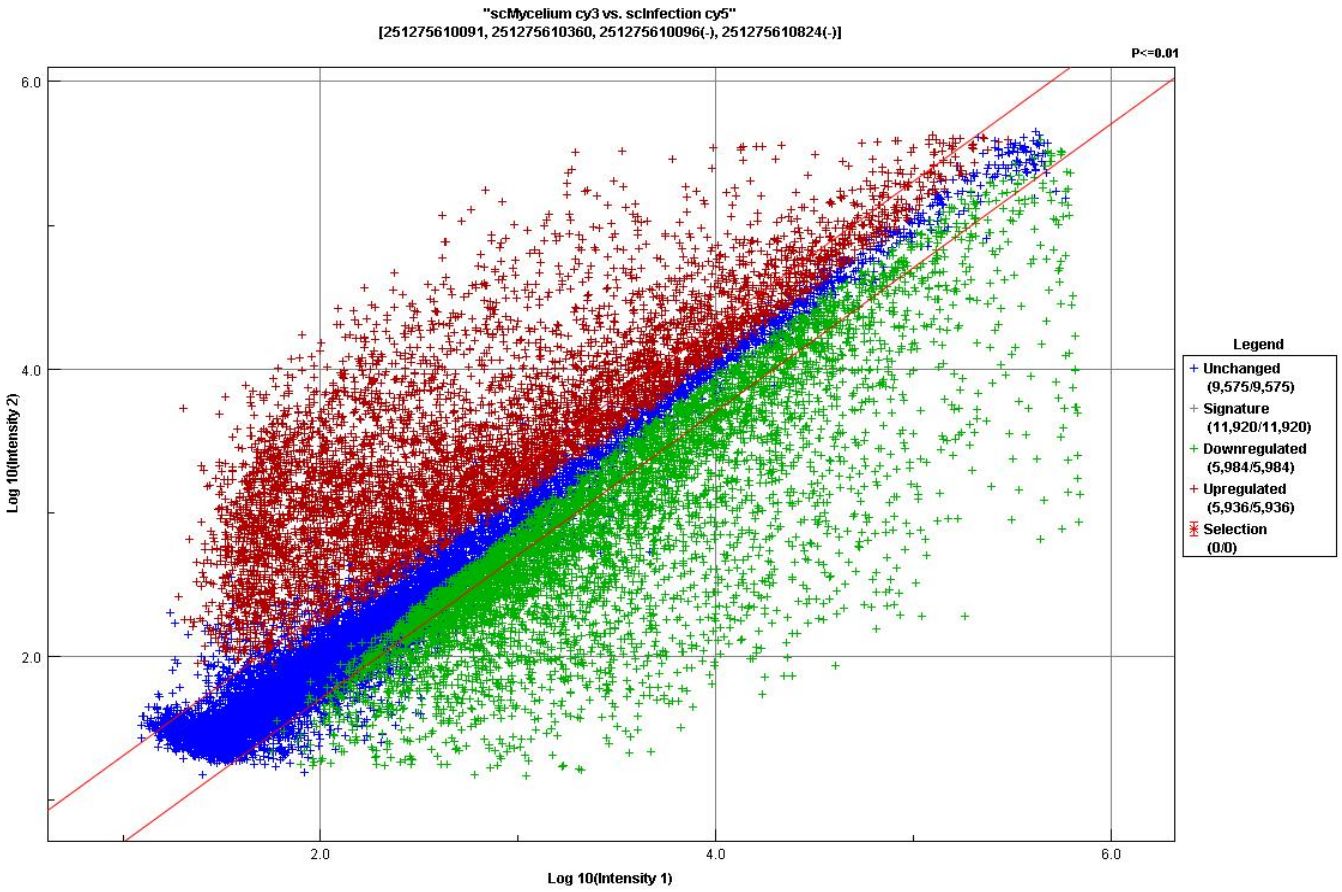

The graph indicated the changes in gene expression profiling in the 34 hpi infected samples compared to pure mycelial RNA. The red color is the up-regulated gene set, the green color is the down-regulated gene set and the blue color indicated the genes that were not significantly changed.

Figure 3.16 Gene validations with RT-PCR indicating the differential expression in the 34 hpi infected samples

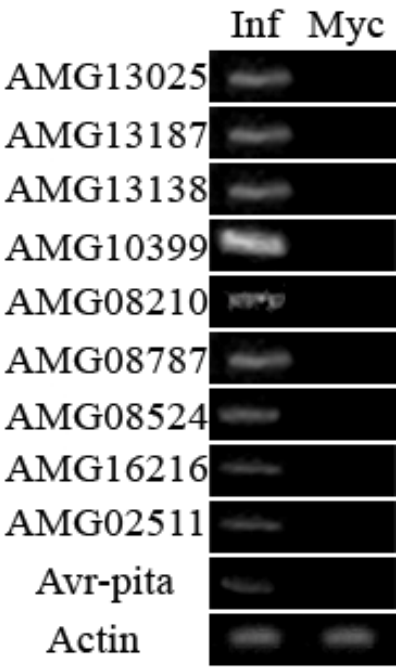

The Inf is 34 hpi infected leaf sheath samples. Myc is KV1 mycelial RNA. Amplification was done with 26 cycles. The mycelial sample amplified actin but not the others confirming the others as infection specific.

Figure 3.17 Gene replacement strategy

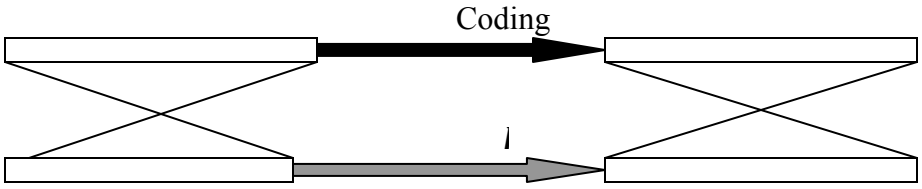

The knockout construct was made with approximately 1 kb fragments upsteam and downstream of the coding sequence flanking the hygromycin resistance gene (*hph*). In instances where the up-stream and down-stream sequences were part of the coding sequences of the other genes, we used part of the coding sequence to generate the knockout constructs.

Figure 3.18 Laccase knockout screening experiment

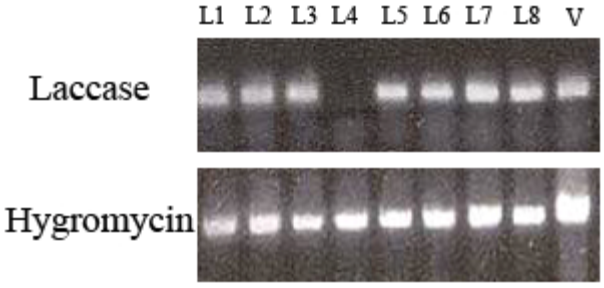

(L1-L8) Independent hygromycin resistant laccase knockout transformants. (V) Knock out vector. Only L4 did not amplify the laccase band indicating positive for gene replacement event.

Figure 3.19 Southern analysis with the laccase knockout strain

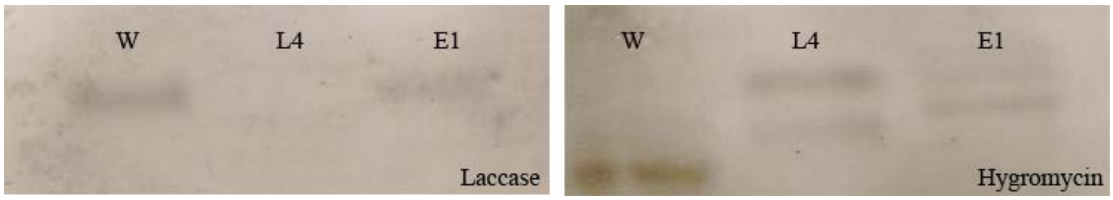

(w) Wildtype strain, (L4) Laccase knock out strain, (E1) ectopic transformant. The Wild type strain hybridized with the laccase probe and not with the hygromycin probe. The knockout strain did not hybridize with the laccase probe but did with the hygromycin probe. The ectopic transformant hybridized with both the probes.

Figure 3.20 Leaf sheath assays with the Laccase knockout strain

Leaf sheath assays at 44 hpi. There was no difference in the IH growth *in planta* in the knockout, ectopic and wildtype strains.

Figure 3.21 Whole plant spray assays with laccase knockout strain

YT-16 rice variety sprayed with 5 x 10^4 spore concentration in 0.25% gelatin. (W) Wild type fungal strain – o137. (L) Laccase knockout strain. (E) Ectopic transformant. (C) 0.25% gelatin control. There was no significant reduction in the pathogenicity in the knockout strain.